The Hong Kong Polytechnic University

Department of Building Services Engineering

A Systematic Fault Diagnosis Strategy for Building HVAC Systems

Zhou Qiang

A thesis submitted in partial fulfillment of the requirements for the Degree of Doctor of Philosophy

February 2009

CERTIFICATE OF ORIGINALITY

I hereby declare that this thesis is my own work and that, to the best of my knowledge and belief, it reproduces no material previously published or written, nor material that has been accepted for the award of any other degree or diploma, except where due acknowledgement has been made in the text.

Zhou Qiang

Department of Building Services Engineering

The Hong Kong Polytechnic University

Hong Kong, China

February 2009

ABSTRACT

Abstract of thesis entitled: A Systematic Fault Diagnosis Strategy for Building HVAC Systems

Submitted by : Zhou Qiang

For the degree of : Doctor of Philosophy

at The Hong Kong Polytechnic University in February, 2009.

The building energy use accounts for a large portion of energy end use of commercial sectors. The performance of HVAC systems is very important in terms of energy saving and energy efficiency. However, the HVAC systems may suffer various faults, such as fouling, pipe clog and improper control, etc. A great deal of research can be found on the performance evaluation and fault detection and diagnosis (FDD) for HVAC components. However, few researchers paid attention to the system-level FDD and the comprehensive structure of the building system diagnosis strategy. The thesis presents a three-level FDD strategy for the building HVAC systems, i.e. the building load estimation/forecast scheme for overall building performance, the system-level FDD scheme for the HVAC systems and the component-level scheme for the chiller.

The building-level diagnosis scheme adopts a simplified building load estimation model as the benchmark to characterize the overall performance of the entire building system. The basic model of the building load estimation/forecast scheme is the thermal network model in thermal resistance and capacitance pattern. The building envelopes including exterior walls and roofs are represented by a thermal network model with three resistances and two capacitances. The internal mass is represented by a thermal network model with two resistances and two capacitances. The building load estimation scheme using monitoring weather information (e.g. solar radiation, outdoor air temperature/relative humidity) via building management systems (BMS) as the input of the building thermal network

model is applied in the building-level diagnosis. The building load forecast scheme using the weather forecast information from the observatory as the input of the building thermal network model is applied in the optimal control strategies. In the forecast scheme, two weather prediction modules are incorporated into the thermal network model. One is the outdoor air temperature/relative humidity prediction module based on the grey dynamic model. The other is the solar radiation prediction module based on the cloud amount and temperature forecast from the observatory. Both weather prediction modules and the building load estimation/forecast scheme are validated using the field data.

The system-level FDD scheme for the HVAC systems has two steps. The first step is to detect, diagnose the sensor, and to estimate the fault (i.e. sensor fault detection, diagnosis and bias estimation (FDD&E)) prior to the use of the system FDD method. The second step is to diagnose the system (i.e., system FDD) by using the sensor FDD&E as the guarantee of measurement health. Principal component analysis (PCA) as the basis of the sensor FDD&E is capable of capturing the variance of a number of correlated sensor measurements based on the first law. Using the normal or corrected sensor measurements, one or more performance indices (PIs) are obtained to characterize the performance of the HVAC systems. An on-line adaptive threshold of the PI residuals, determined by the training data and measured data, is used to define the normal range. The sensitivity analysis of the sensor FDD&E to system faults and the validation of the system-level FDD scheme are conducted using simulation data.

As chillers take the largest part of the power consumption in HVAC systems, the component-level FDD scheme for the chiller is developed using fuzzy modeling and artificial neural network (ANN). Based on the sensitivity analysis tests, performance indices (PI) are selected to characterize the health status of the chiller. PI residual is defined as the difference between the PI model benchmark and PI measurement. All the PI residuals are fuzzified into a series of standardized quantitative PIs (SQPs) using membership functions. A SQP is an interval covering an operation range of PI residuals. All the SQPs cover the full operation range of PI residuals in the tests. SQP is very effective to distinguish the faults, even to the faults having the same qualitative rule patterns. Then, ANN is used to identify the chiller fault by matching the SQPs with the fault category. The scheme is validated using the laboratory data provided by the ASHRAE RP 1043.

The three-level building HVAC system diagnosis strategy is developed into a software package implemented on IBmanager, which is an open integration and management platform for intelligent building systems based on the middleware technologies. As a function module of IBmanager, the software package of the building HVAC system diagnosis strategy is supposed to report alarms, generate the diagnosis results and recommend improvements through an Intelligent Control and Diagnosis System for a commercial building. This system is a platform working in the foreground of the working station as an interface between IBmanager and end-users.

PUBLICATIONS ARISING FROM THIS STUDY

Journal Papers

Qiang Zhou, Shengwei Wang, Xinhua Xu and Fu Xiao. 2008. A Grey-Box Model of Next-day Building Thermal Load Prediction for Energy-Efficient Control, *International Journal of Energy Research*, Vol.32(15):1418-1431.

Qiang Zhou, Shengwei Wang and Fu Xiao. 2009. A Novel Strategy of Fault Detection and Diagnosis for Centrifugal Chiller Systems, *HVAC&R Research,* Vol.15(1):57-76.

Qiang Zhou, Shengwei Wang and Zhenjun Ma. 2009. A Model-based Fault Detection and Diagnosis Strategy for HVAC Systems. International Journal of Energy Research, DOI: 10.1002/er.1530.

Shengwei Wang, Qiang Zhou and Fu Xiao. A System-level Fault Detection and Diagnosis Strategy for HVAC Systems Involving Sensor Faults. Submitted to *Energy and Buildings.*

Journal Papers under Preparation

Qiang Zhou and Shengwei Wang. An On-line System-level Commissioning and Performance evaluation for the HVAC systems. Under preparation.

Qiang Zhou, Fu Xiao and Shengwei Wang. A Hierarchical Fault Detection and Diagnosis Strategy for the Central Chilling Systems. Under preparation.

Conference Papers

Qiang Zhou, Shengwei Wang, Fu Xiao and Xinhua Xu. 2008. A Gray-box Model of Next-day Building Thermal Load Prediction for Energy-efficient Control. *1st International Conference on Building Energy and Environment* (COBEE 2008), JUL 13-16, 2008 Dalian, PEOPLES R CHINA. PROCEEDINGS VOLS 1-3, Page: 108-115.

ACKNOWLEDGEMENTS

The thesis would not have been possible without the guidance, encouragement and support from the people who are gratefully acknowledged here.

Foremost, I would like to express my gratitude to my chief supervisor, Prof. Shengwei Wang for his inspiration, expertise and patience during the past three years. I would also like to thank my co-supervisors, Dr. Fu Xiao and Prof. Hongxing Yang for their encouragement and assistance.

Sincere thanks also go to all of my colleagues in the team, especially Dr. Xinhua Xu, Dr. Zhenjun Ma and Mr. Zhengyuan Xu. Their suggestions and good ideas help me a lot.

I would like to sincerely thank my parents, my younger sister. I owe my thanks to my wife, Jixia Hu for standing beside me and looking after my little son. It is to them I dedicate this thesis.

TABLE OF CONTENTS

LIST OF FIGURES

LIST OF TABLES

NOMENCLATURE

Symbols	Description
a,b,c,d	Regression coefficients
A,B,C,D	Matrix
$\mathbf{A},\mathbf{B},\mathbf{C},\mathbf{D},\mathbf{G},\mathbf{H}$	Coefficient matrix
b	Bias of ANN
C	Thermal capacitance ($kJ/(kg$ ℃$)$) or cloud amount (Oktas)
C_{pw}	Water specific heat ($kJ/(kg$ ℃$)$)
c	Center of a fuzzy set
const	Constant
COP	Coefficient of performance
$\mathbf{e}$	Residual vector
Eff_{moter}	Motor efficiency
G	*s*-transfer function
I_0	Hourly extraterrestrial radiation incident on a horizontal surface (Whm^{-2})
J	Objective function
L	Thickness (m) or local latitude (degree)
LMTD	Logarithm mean temperature difference(F)
M	Mass flow rate (kg/s) or mean value
MBE	Mean bias error
$\mathbf{P}$	Loading matrix
P_{RC}	Pressure of refrigerant in condenser(PSIG)
Q	Cooling load (kW)

q	Heat flow (Wm^{-2})
R	Thermal resistance (m^2KW^{-1})
R^2	Coefficient of determination
$RMSE$	Root mean square error
s	Laplace variable or roots
S	Covariance matrix
t	Number of the fuzzy sets
T	Temperature (℃)
T_{CA}	Condenser approach temperature(F)
T_{CO}-T_{CI}	Temperature difference between inlet and outlet condenser water (F)
T_{EI}-T_{EO}	Temperature difference between inlet and outlet evaporator water(F)
Th	Threshold
TO_{feed}	Temperature of oil feed (F)
TO_{sump}	Temperature of oil in sump (F)
TRC_{sub}	Liquid line refrigerant subcooling form condenser (F)
$T_{approach}$	Approach temperature (℃)
U	Matrix of eigenvectors
UA	Conductance-area product
W	Power (kW)
w	Connecting weight in ANN
x	Input of fuzzy models
X,Y,Z	Vector

x_h, x_l	Forecasted maximum and minimum temperature (℃) or RH
y	Output of fuzzy models
z	Output of ANN

Greek

λ	Thermal conductivity ($Wm^{-1}K^{-1}$) or eigenvalue
ρ	Density (kgm^{-3})
ω	Frequency ($rad\ s^{-1}$)
δ	Scale factor
ε	Effectiveness
σ	Total uncertainty or standard deviation or width of a fuzzy set
$\mathbf{\Lambda}$	Diagonal matrix of non-negative real eigenvalues with decreasing magnitude

Subscript	**Description**
act	Actual
afhx	After heat exchanger
bfHX	Before heat exchanger
CD	Condenser
chws	Chilled water supply
conv	Convective heat
CT	Cooling tower
dryin	Inlet dry-bulb
ecw	Entering condenser water
equip	Equipments

est	Estimated
EV	Evaporator
fr	Fresh air
HX	Heat exchanger
in	Inside or indoor
m, avg	Average
occup	Occupants
out	Inside or outside
rf	Associated with roof
sol	Associated with solar air temperature
tot	Total
wb	Wet-bulb
wetin	Inlet wet-bulb
win	Inlet water or Windows
X,Y,Z	Associated with external, across and internal heat conduction

CHAPTER 1 INTRODUCTION

1.1 Motivation

According to DOE (2007), the energy use in commercial sectors accounted for 18% of the total energy consumption in United States in 2005. Space heating and cooling were the main consumers with 27.3% in terms of energy end use of commercial sectors. In ten years from 1993 to 2003 based on the Hong Kong energy end-use data (EMSD 2005), the building energy use increased very fast, by almost double. In Hong Kong of 2005, the commercial sectors accounted for 61% of the total energy consumed by residential, commercial, industrial and transport sectors, and the largest consuming portion was attributed to HVAC systems with 28% in energy end use of commercial sectors (EMSD 2007). 15% to 30% of the energy waste in commercial buildings is due to the performance degradation, improper control strategy and malfunctions of HVAC systems. The particular reasons may be inappropriate temperature set points, malfunctions of cooling towers, chillers, pumps, and sensor faults such as sensor bias. It is very essential to implement a fault detection and diagnosis (FDD) strategy to identify the real causes of the performance deterioration and abnormal energy use.

In modern office and commercial buildings, total building electricity consumption is usually the concern of the tenants and property management firms when the indoor environment requirement is met. In fact, the electricity consumption is seriously related to the cooling/heating energy consumption. In old buildings without building management systems (BMS), there are not enough sensors installed in building systems to monitor the operating performance and maintain the normal operating conditions. Therefore, it is very meaningful to monitor and evaluate the performance of building systems at the building level using the cooling/heating energy consumption. It can not only indicate the overall operating performance of building systems, but also demonstrate directly the economic benefits.

The excess energy consumption (usually indicated by electricity consumption) is detected at the building level by evaluating the cooling/heating energy consumption. The abnormal energy consumption must be due to some reasons, such as control failure, equipment performance degradation, blocked water pipe and so on. All these unexpectations can be attributed to malfunctions of building systems. A typical building HVAC system contains a number of cooling towers, chillers, pumps, heat exchangers, many air handling units (AHUs), and variable air volume (VAV) components, etc. To detect and diagnose the malfunctions of a building system at system level, more sensor measurements are needed to provide sufficient information for performance evaluation when compared with the diagnosis at the building level. For example, COP, which usually is calculated based on the measurements of water flow rate, supply and return chilled water temperatures, and the chiller power consumption, is a representative performance indicator for evaluating the operating performance of a chiller, although it can not tell the component fault (e.g. condenser fouling, refrigerant leakage) resulting in the performance degradation. The system performance monitoring and FDD are effective to detect and diagnose if the building system working at low efficiency.

If one goes further to find the possible reasons causing the system fault, the FDD at component level is necessary. For different HVAC systems, there are many specific faults which may cause the abnormal energy consumption and system efficiency degradation. There are so many categories of faults in each HVAC system so that one FDD strategy for one system is usually not capable of identifying all possible faults or find reasons why the performance degrades. However, for some typical faults which happen much more often than others, it is still meaningful to study how to characterize the performance behaviors when faults occur. Chiller system accounts for the largest portion of total electricity consumption of the building system and are responsible to satisfy the cooling demand in most cases. Therefore, FDD for chillers is essentially needed in practice to determine if they work properly for saving energy and prolonging equipment life.

Nowadays, building management systems (BMS) are widely used in commercial and office buildings, especially in new buildings. BMS is very helpful to monitor the operating performance of HVAC systems and components by basic on-line measurements, such as temperature, flow rate, pressure difference, power and so on. Sensors may also suffer various faults, such as drift, bias and complete failure, etc. Complete failure is easy to be detected by continuous monitoring and range limitation, while bias and drift are not easy to be detected but potentially harmful to performance evaluation and control, etc. Methods of performance evaluation and FDD for HVAC systems are strongly dependant on the reliability of sensor measurements. For HVAC systems with sensor performance and system performance considered simultaneously, sensor fault detection and diagnosis and estimation (FDD&E) is the first step to judge the health status of sensor measurements which are related to system FDD.

1.2 Literature Review

Some previous papers described the method of building system performance evaluation and FDD on the basis of systematic view. House and Kelly (1999) presented two approaches commonly used for diagnostic reasoning in the hierarchical structure of HVAC systems and sub-systems in buildings. The first one is the top-down approach. It uses high-level performance indicators to reason the possible low-level causes of degradation. Usually, whole building energy use is a high level indicator that provides useful information of building performance. If energy use exceeds the threshold of expected values, top-down reasoning would be used to navigate from building level, system level to component level and isolate the most probable reasons for the abnormal energy use. The second one is the bottom-up approach. It uses low-level performance indicators to isolate problems and propagate the problem up to determine its impact on the whole building performance. If the impact is large enough, then a high priority is given to the problem correcting.

FDD methods can also be roughly classified into two groups based on the Ref. (Gertler 1998), i.e. model-free methods and model-based methods. Model-free method does not need a mathematical or experiential model as the performance reference to be compared with the actual performance while model-base method needs a model as the performance benchmark as shown in Figure 1.1.

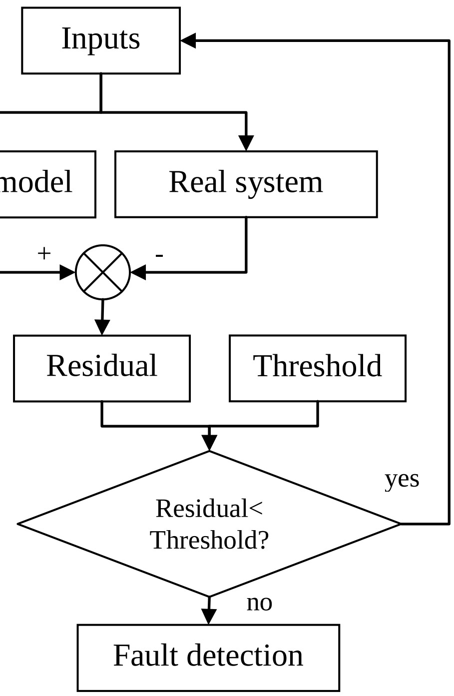

Figure 1.1 Flowchart of model-based FDD methods

Liu et al. (2002) presented three steps to fulfill the task of building diagnosis. The first step implemented before the building diagnosis is the evaluation of building performance. A quantitative evaluation of performance requires a baseline or reference. It can be derived from the previous, current performance of comparable buildings and the previous or intended performance of the building in question. The second step is to identify the faults in a building by comparing the reference performance with the actual performance. The actual performance can be the energy consumption (such as whole building electricity, and cooling energy consumption). The third step is to diagnose the problems if the measured performance differs from the expected or predicted performance. This can be accomplished by using specialized system models or component models, or calibrating baseline models to match the simulation output to currently measured energy performance data by adjusting input and operation parameters. The article also demonstrated two case studies. One is for dual duct air handling units, and the other for single duct air handling units.

By comparing the measured energy use with the baseline, the fault was isolated. Then diagnosis was implemented by calibrating the model with schedule adjustment to the current performance data. A system-level hierarchical fault detection and diagnostic (FDD) method for HVAC system was developed by Schein and Bushby (2006). It functions as an interface between multiple equipment-specific FDD tools and an operator. One advantage of the method is that it can prioritize conflicting fault reports from equipment-specific FDD tools, perform FDD at the system level, and present an integrated view of an HVAC system's fault status to an operator. The results showed that the primary diagnosis was correct for 57 of 60 simulation runs and it was effective to filter equipment-level fault reports and detect and diagnose system-level faults.

The specific literature review on the building system performance evaluation and FDD methods is presented accordingly as follows.

1.2.1 Building Energy Performance Evaluation and Diagnosis

Usually at the building level, the performance evaluation and diagnosis are implemented using a reference model to judge if the total building energy is in normally expected range. Therefore, accurate load prediction is essential to the building-level diagnosis and to many energy-efficient optimization strategies. For example, it is beneficial in deciding the proper amount of energy to be stored during off-peak hours in cool storage systems, and in deciding the proper starting time of cooling/heating systems for start-up load requirement and energy cost saving. Methods for building load estimation/forecast mainly include three categories, physical models, black-box models and grey-box models.

Physical models such as models used in EnergyPlus (Crawley et al., 2000), DOE-2 (Ed Kidd et al. 2001), HVACSIM+ (NTIS 1986), TRNSYS (Klein et al. 1990) and AIRMODEL (Giebler et al. 1998) are accomplished in detailed building energy analysis with multiple zones in buildings of complex design. Some of them are widely recognized as the industry standard by architectural engineers, energy consultants, etc. However, they have a large number of parameters to tune and need a lot of building and system information as inputs. The process for such information collection is time-consuming and not cost-effective.

There are a lot of “black box” models (or called data driven models) discussed in previous papers. Forrester and Wepfer (1984) applied multiple linear regressions using a 24-hour regressor to predict the electric load of a large commercial building. MacArthur et al. (1989) developed an on-line recursive estimation method for load profile prediction. It is based on an autoregressive moving average technique with exogenous inputs (ARMAX).

Dhar et al. (1999a) developed a generalized Fourier series model (GFS) to estimate the heating and cooling energy use in commercial buildings using ambient temperature, ambient specific humidity and global solar radiation. Based on GFS, Dhar et al. (1999b) developed temperature-based Fourier series models (TFS) with outdoor temperature as the only weather variable.

Seem and Braun (1991) split the time-series building load into deterministic part and stochastic part, and modeled the two parts separately. A cerebellar model articulation controller (CMAC) combined with exponential weighted moving average (EWMA) technique was utilized to model the deterministic trend. Autoregressive (AR) models were selected to model the stochastic part with a comparison with autoregressive moving average (ARMA) models. Four different models based on ARMA, EWMA, linear regression (LR) and artificial neural network (ANN) separately for thermal load prediction are compared quantitatively with the same data set by Kawashima et al. (1995). Mohandes (2002) applied support vector machines (SVM) in the short-term load forecasting and compared the performance with the AR model.

With regard to the weakness of physical and black-box models, some researchers attempted grey-box models to estimate or predict the building thermal load. Braun and Chaturvedi (2002) developed a thermal network model for transient building load prediction. This inverse grey-box model needs one week of data to train with rich zone temperature variations or two to three weeks of data to train with limited zone temperatures variations. The model error can be limited within 2% with simulation data and 9% with in-situ data. Wang and Xu (2006) simplified the building thermal load prediction using simplified dynamic thermal models of building envelope and internal mass. The parameters of building thermal network models for building envelope are determined by frequency characteristic analysis. The parameters of thermal network models for lumped internal mass are identified using monitoring operation data and generic algorithm.

1.2.2 FDD Methods for HVAC&R Systems

The HVAC&R systems installed in high-rise buildings can be divided into water-side systems and air-side systems. Katipamula and Brambley (2005a) summarized FDD methods for HVAC systems and categorized the methods as shown in Figure 1.2. The papers of FDD methods are reviewed as follows in terms of HVAC&R system categories. The papers on chillers FDD are not included because they are summarized in the next section.

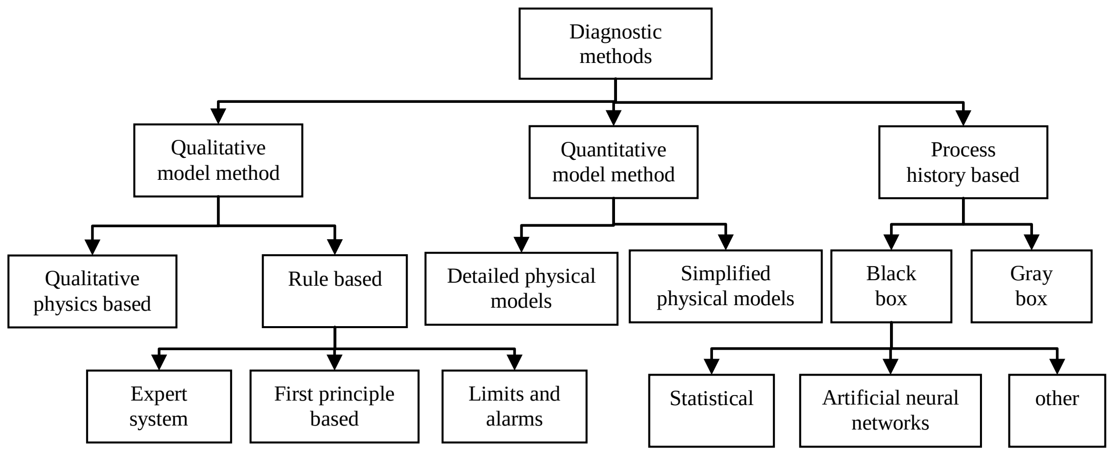

Figure 1.2 Category of diagnostic methods (Katipamula and Brambley 2005a)

For cooling towers, a temperature sensor fault, a condenser water pump fault and a cooling tower fan fault were simulated on TRNSYS platform, and diagnosed using the proposed performance indices based on Ahn et al. (2001). A fouling model was developed by Khan and Zubair (2004) to study the effect of fill fouling on performance characteristics of cooling towers.

For heat exchangers, fouling and leakage of the vessel are the typical faults to be considered in FDD strategy. Upadhyayaa and Eryurekb (2006) proposed a group method of data handling (GMDH) to diagnose the sensor fault and tube fouling on a tube-and-shell heat exchanger. Weyer et al. (2000) proposed a method based on a first principle model to track the heat transfer coefficient and diagnose the settled material breakage. Six faults were studied by Persin and Tovornik (2005) including four sensor faults, tube clog and vessel leakage. A velocity-based linearization and a linear observer based on the energy balance were proposed to detect and diagnose these faults. Transferable belief model (TBM) was developed to improve the inconsistency of data to make diagnosis more stable.

FDD methods for air handling units (AHUs) and variable air volume (VAV) terminals are a hot research area. Many papers can be found in publications. Yoshida et al. (1996) discussed some typical AHU faults i.e. outdoor air damper malfunction, fouling on cooling coils, air leakage through ductwork, fan motor malfunction and stuffing air filers. The autoregressive model with exogenous input (ARX) and extended Kalman Filter were compared to detect a sudden failure in AHU control loop. Yoshida and Kumar (1999) discussed the ARX model and adaptive forgetting through multiple models (AFMM). They were applied in the on-line FDD for real VAV systems. Compared with ARX models, AFMM models needed longer window length but more sensitive to the system change. The author concluded that ARX models were more robust. Lee et al. (1996a and 1996b) carried out the FDD for AHUs using autoregressive moving average with exogenous input (ARMX), ARX and ANN. The concerned faults were complete failure of the supply and return fans, failure of the chilled water circulation pump, stuck cooling coil valve, failure of temperature sensors, static pressure sensor, and air flow stations. Lee et al. (1997) extended the previous work in improving the ANN models for AHU FDD. More faults including several abrupt and performance degradation faults were considered in the AHU by Lee et al. (2004) using general regression neural-network (GRNN) models for FDD. Dexter and Ngo (2001) improved the previous work (Ngo and Dexter 1999) using a multi-step fuzzy model to detect and diagnose the AHU faults. Compared with the generic fuzzy reference models, the new approach could prevent false alarms and be able to isolate the valve leakage and fouling faults. As a part of ASHRAE research project (RP-1020), Norford et al. (2002) applied two FDD methods for AHU faults. One was first-principle model-based, and the other was semi-empirical polynomial regression-based. Wang and Xiao (2004) presented a FDD strategy for AHU sensor faults based on principal component analysis (PCA). Two PCA models were built based on the heat transfer balance and pressure-flow balance in air-handling process. For each PCA model, the related sensors with a fixed bias could be detected and diagnosed. Qin and Wang (2005) conducted a survey on the VAV faults, and found 20.9% of VAV terminals were ineffective and ten main faults existed in the VAV systems. A PCA-based method was used to detect the flow sensor and reconstruct it. The other faults were isolated by integration of recognition, expert rules and performance indices.

1.2.3 FDD Methods for Chillers

Chillers are concerned most in HVAC&R FDD study as they account for the largest portion of energy consumption. According to a survey conducted by Comstock and Braun (1999), approximately 60% of thirteen typical chiller faults could be detected using sensor measurements in real-time operation monitoring. These faults accounted for around 42% of the service resources and around 26% of repair costs. The papers are summarized as follows.

Model-free FDD methods are usually discussed in early applications in small or medium-size chillers, such as Yoshimura and Ito (1989), Inatsu et al. (1992) and McIntosh (1999).

The model-based FDD methods are widely used in application in chiller systems. Stylianou and Nikanpour (1996) proposed an FDD method including an off-cycle module, a start-up module and a steady-state module for reciprocating chillers. In the steady state module, the chiller performance was verified based on the universal chiller model developed by Gordon and Ng (1995). The residuals between the estimated variables by the linear regression models and the measured variables were matched to the known rule pattern to diagnose the chiller faults. The rule pattern is shown in Table 1.1. This work is similar to the Grimmelius et al. (1995).

Table 1.1 Rule patterns of FDD for chillers (Stylianou and Nikanpour 1996)

Fault	Discharge Temp.	Discharge pressure	High pressure liquid line Temp.	Low pressure liquid line Temp.	Suction line Temp.	Suction pressure	Condenser water Temp difference	Evaporator water Temp. difference
Liquid line restriction	▲	▼	▼	▼	▲	▼	▼	▲
Refrigerant leakage	▲	▼	▼	▼	▲	▼	▼	▲
Reduced condenser water flow rate	▲	▲	▲	▼	▼	▼	▲	▼
Reduced evaporator water flow rate	▲	▼	▼	▼	▼	▼	▼	▼

Notes: ▲ *means measurements increase when a fault happens;* ▼ *means measurements decrease when a fault happens.*

Stylianou (1997) used a statistical pattern recognition algorithm (SPRA) to replace the rule-based method to match the rule patterns for chiller FDD. Combinations of residuals between the prediction by linear regression models and the measurements were responsible for the fault patterns. The new proposed method was dependant on the training data both in normal conditions and faulty conditions.

Peitsman and Bakker (1996) developed black-box models using multiple-input/single output ARX and artificial neural network (ANN). The black-box models contain 14 system models for fault detection and 16 component models for fault diagnosis. The selected inputs from the current and previous time steps and outputs from two previous time steps were used in the ANN models. According to Peitsman and Bakker (1996), the data must have a fixed time step.

Rossi and Braun (1997) used a steady-state polynomial regression model to predict different temperatures in normal tests. These temperature predictions were compared with the corresponding measurements in faulty tests in order to generate the residuals for FDD analysis. A rule pattern table for diagnosing five faults in consideration was composed of different combinations of seven temperature residuals.

Comstock et al. (2001) presented eight common faults tested on a 90-ton centrifugal chiller at four levels of severity. The eight faults could be detected using a rule table composed of sensitive measurements deviation.

Both McIntosh et al. (2000) and Jia and Reddy (2003) implemented a FDD strategy by using the characteristic quantities (CQs) to characterize various chiller faults. The CQs are sensitive to some certain faults and not to the others.

Wang and Cui (2006) developed a strategy which consists of a model-based chiller FDD scheme and a sensor FDD and estimation (FDD&E) scheme. Six performance indices deduced from theoretical analysis were used to characterize the health condition of a centrifugal chiller, while the principal component analysis (PCA) method was used to handle sensor faults. The sensor FDD&E scheme for centrifugal chillers was enhanced by using wavelet analysis by Xu et al. (2007).

Li and Braun (2007) presented a physical decoupling methodology to diagnose the multiple simultaneous faults in vapor-compression air conditioners. This method using simplified mathematical and non-mathematical decoupling approaches could eliminate the requirement of high-cost measurements for modeling.

1.2.4 FDD Methods for Sensors

Accuracy of sensor measurements is an important factor for affecting the reliability of performance monitoring and FDD strategies. Many papers on sensor FDD can be found in engineering fields in recent ten years.

Roumeliotis et al. (1998) used a multiple model adaptive estimation (MMAE) based on Kalman to detect and diagnose sensor faults in a mobile robot. Both abrupt faults and soft faults of sensors were handled using this method.

A sensor FDD strategy base on multi-scale analysis and dynamic PCA was implemented by Luo et al. (1999) in five steps. The proposed strategy could detect the temperature sensor faults in a low detection ratio and false alarm ratio.

Two neural networks based on radial basis functions were used by Yu et al (1999) in sensor FDD for a chemical reactor. One neural network was used to generate the residuals. The other was used to identify the sensor fault using the residuals.

Hashimoto et al. (2001) proposed an interacting multiple-model (IMM) approach to detect and isolate sensor faults in the dead reckoning of mobile robots. Sixteen system modes of four internal sensors could be estimated using Kalman filters in the experiment.

Mehranbod et al. (2005) extended the instrument fault detection and identification (IFDI) method proposed by Mehranbod et al. (2003). The sensor FDD method was developed based on the Bayesian belief network (BBN) and applied in the processes operating at transient or steady state.

Sensor FDD in the HVAC&R field is also intensive in recent years. Wang and Wang (1999) proposed a sensor FDD method based on fundamental mass and energy conservation in air-conditioning systems. Flow meters and temperature sensors with soft biases were detected using this method. Wang and Wang (2002a, 2002b) improved the sensor biases evaluation by using genetic algorithm. The sensor estimate, confidence intervals and comparisons of the balance residuals before and after fault correction were helpful for the engineers to diagnose the possible sensor faults.

Wang and Xiao (2004) developed a sensor FDD strategy based on principal component analysis (PCA) for a typical air handling unit (AHU). The proposed strategy was verified using simulation data and site data of a real building. The effect of sensor faults on building energy efficiency was also evaluated.

Xiao et al. (2008) found the inefficiency of PCA methods in isolating faults due to the strong coupled multiple variables in air-handling process. A decoupling method based on expert knowledge was used to generate fault patterns of typical sensors in AHUs. The PCA method proposed by Wang and Xiao (2004) was enhanced by the expert knowledge.

Wang and Qin (2004) applied PCA method in detecting flow sensors of VAV terminals both in system level and terminal levels. The faulty sensor was reconstructed when it was diagnosed. An iteration of the FDD strategy carried on using the recovered sensor measurements until no fault was detected.

Wang and Cui (2005) focused the sensor FDD on the water-cooled centrifugal chillers. Q-statistic and Q-contribution plot based on PCA were used to detect and isolate the sensor faults.

The sensor fault detection, diagnosis and estimation (FDD&E) was validated using data from a real building system.

Hou et al. (2006) developed a sensor FDD strategy based on data mining (DM) for AHUs and fresh air handling units (FHUs). Fuzzy theory and ANN were used to reduce redundant information and pattern recognition respectively. Tests show the strategy using temperature and humidity measurements could distinguish the sensor faults of supply chilled water temperature and returned chilled water temperature.

Chen et al. (2006) found that the flow meter faults in the central chilling systems could not be diagnosed by PCA methods due to the fault collinearity. The wavelet transform having a good property of local time-frequency was used to enhance the diagnosis ability of PCA methods.

1.3 Objectives

Comprehensive performance evaluation and diagnosis for building HVAC systems are important in improving indoor environment quality, enhancing building energy efficiency and prolonging equipment life. However, most of previous papers are mainly focused on the performance evaluation and FDD at the component level and not sufficient in terms of systematic FDD strategy implemented at the building level, system level and component level. The objectives of this thesis are as follows.

The main objective is to develop a systematic fault diagnosis strategy for building HVAC systems at three levels, i.e. building level, system level and component level.

At the building level, the building load estimation/forecast scheme is proposed based on a building thermal network model using different weather input types. The building load estimation using the monitoring weather information on site via BMS as the input of the thermal network model is viewed as the benchmark to evaluate the performance of the whole building system. The building load forecast using the on-line weather forecast information from the observatory via an internet interface as the input of the thermal network model is used to decide the optimal setting of HVAC system control strategies.

At the system level, all the working HVAC components of the same category are viewed as one system to implement the fault detection and diagnosis scheme. There are total five HVAC sub-systems of concern. They are cooling tower system, chiller system, secondary pump system before heat exchangers, heat exchanger (HX) system and secondary pump system after heat exchangers. The system performance evaluation and FDD scheme is affected by the sensor accuracy. For the HVAC system with sensor faults and system faults existing simultaneously, sensor FDD&E is implemented to evaluate the sensor performance prior to the use of the system FDD.

At the component level, a FDD scheme is developed for chillers as they take the largest portion of chilling system energy consumption. This scheme can conquer the weakness of the traditional chiller FDD methods which are based on the symbolic pattern of rules. Usually the rule patterns are difficult to decide how sensitive the selected performance indices (PIs) are to the chiller faults of concern, especially in the situation that some faults have the same symbolic pattern of rules. These concerned faults are reduced condenser water flow, condenser fouling, refrigerant leakage, refrigerant overcharge, reduced evaporator water flow, non-condensables in refrigerant and excess oil.

1.4 Organization of The Thesis

This chapter firstly presents the motivation of the building system performance evaluation and diagnosis. Typical fault detection and diagnosis methods for the overall building systems and particular HVAC systems are critically reviewed. Then, the objective of the thesis is proposed. The organization of the other chapters is as follows.

Chapter 2 presents an overview of the building system diagnosis strategy. The structure of the diagnosis strategy for building systems and the relationship of the three level FDD schemes of this strategy are interpreted in detail. The building load estimation/forecast scheme based on a building thermal network model, system-level FDD scheme for the HVAC systems and component-level FDD scheme for chillers are also briefed.

Chapter 3 presents the building load estimation/forecast scheme for the building-level diagnosis of building systems. In this scheme, the simplified building thermal network model, outdoor temperature/relative humidity prediction module, and solar radiation prediction module are developed for building cooling load prediction. The outdoor temperature/relative humidity prediction module is established based on the grey dynamic model (GM), while the solar radiation prediction module takes advantage of the forecast of cloud amount and maximum/minimum outdoor air temperatures.

Chapter 4 presents the validation of the building load estimation/forecast scheme using the field data. The validation of T/RH prediction module and solar radiation prediction module are also presented.

Chapter 5 presents the system-level FDD scheme for HVAC systems. This scheme is implemented in two steps. The first step is to detect, diagnose the sensor fault, and to estimate the fault (i.e. sensor fault detection, diagnosis and bias estimation (FDD&E) module) prior to the use of the system-level FDD scheme. The second step is to diagnose the system (i.e., system FDD module) by using the sensor FDD&E as the guarantee of measurement health.

Chapter 6 presents the validation of the system-level diagnosis scheme using simulation data. The validations of the sensor FDD&E module and the system FDD module are presented individually. The sensitivity analysis of the sensor FDD&E module to system faults is seriously discussed. Then, the validation of HVAC system-level FDD scheme involving sensor faults is presented.

Chapter 7 presents a component-level FDD scheme for the chiller based on two artificial intelligence techniques. A quantitative fault diagnostic classifier is established based on fuzzy models. The fault identification is realized by matching the standardized quantitative performance indices (SQPs) with the fault categories using the artificial neural network (ANN).

Chapter 8 presents the validation of the component-level FDD scheme for the chiller using the laboratory data provided by the ASHRAE RP 1043. The validation of the chiller PI benchmark model is also presented.

Chapter 9 presents the in-situ implementation of the three-level building system diagnosis strategy. The strategy is developed into a software package as a function module of IBmanager working in the background of the working station. IBmanager is an open integration and management platform for intelligent building systems based on the middleware technologies. A platform named Intelligent Control and Diagnosis for a commercial building, working in the foreground, provides a user-friendly interface for convenient use.

Chapter 10 summaries the thesis and comes up with some recommendations for the future practical applications.

CHAPTER 2 OVERVIEW OF THE BUILDING SYSTEM DIAGNOSIS STRATEGY

The systematic methodology of the building HVAC system diagnosis is illustrated in this chapter. The strategy involves three function schemes, i.e., the building load estimation/forecast scheme, the system-level FDD scheme, the component-level FDD scheme, for evaluating the performance and diagnosing the faults of HVAC systems in a hierarchical way.

Section 2.1 briefs the strategy for building system diagnosis at three levels. The relationships between these three level schemes are also presented. Section 2.2 presents the building load estimation/forecast scheme briefly. Applications of the scheme are also briefed. Section 2.3 presents the system-level FDD scheme for the HVAC systems briefly. An introduction on sensor FDD&E and HVAC system FDD is also given. Section 2.4 presents briefly the component-level FDD scheme for the chiller including the quantification of PI residuals based on the fuzzy model and the fault identification based on ANN. Section 2.5 is the summary.

2.1 A Brief of the Three-level Diagnosis Strategy

The building system diagnosis strategy is implemented at three levels, namely building level, system level and component level. The building-level diagnosis scheme focuses on how to indicate the overall health status of the building system. The building system at this level is considered as a whole including HVAC systems and non-HVAC systems as shown in Figure 2.1. HVAC systems typically include chillers, cooling towers, heat exchangers, primary and secondary pumps, air handling units (AHUs), VAV terminals, etc. Non-HVAC systems related to the building energy consumption include lightings, appliances, etc.

The malfunctioning, performance degradation and control failure of these sub-systems or components may affect the whole building health in terms of building energy performance. Building system performance evaluation and diagnosis at the building level is an effective measure to detect the unhealthy conditions of some important system(s) or component(s). Once the building system performance degradation is detected at the building level, it must be due to some particular reasons, such as schedule problems in the lighting system, malfunction of pumps and malfunction of fresh air control methods. The building system diagnosis at the building level is not supposed to identify the particular faults, but to be helpful to remind the operators of potential faults, which are existing and severe enough to harm the whole building performance. Building energy data such as building cooling load are an effective indicator to evaluate the building system performance. The accurate estimation/forecast of the building cooling load is essential to the building system performance evaluation and some optimal control strategies for HVAC systems.

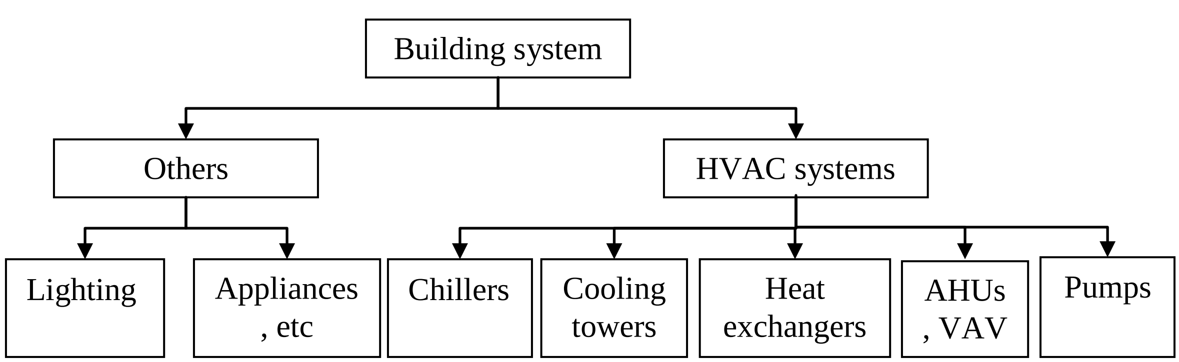

Figure 2.1 Composition of the typical building systems

Since the health status of some particular sub-system(s) and component(s) accounts for the main overall building system operating performance, it is necessary to implement the system-level and component-level fault detection and diagnosis to identify the faulty system(s) and faulty component(s). For non-HVAC systems such as the lighting system and appliances, the time schedule is usually fixed, so the monitoring and diagnosis for this part is easy to implement by referring to the schedule. If the electricity consumption of this part is abnormal, it may be due to the schedule rearrangement or control malfunctioning. The system-level FDD focuses on the HVAC sub-systems such as chiller system, cooling tower system, heat exchanger system, pumps system. One sub-system may include one or more components of the same class. They are aggregated as a system to perform the FDD rather than to evaluate the component performance one by one.

The component-level FDD is necessary to identify what fault causes the HVAC systems performance degradation. As the chiller accounts for the largest portion of the power consumption, FDD for this component is more meaningful. The proposed component-level FDD scheme is supposed to be valid to other components.

The relationships among these three level FDD schemes of the strategy are shown in Figure 2.2. The building level is the highest level covering the HVAC systems and non-HVAC systems. The system level focusing on the performance of HVAC systems is higher than the component level focusing on the chiller health. The other components at the component level can be the cooling towers, pumps, heat exchangers, AHUs, etc. These three level FDD schemes of the strategy are implemented separately. Further discussions and recommendations on the structure can be found in Chapter 9 and Chapter 10.

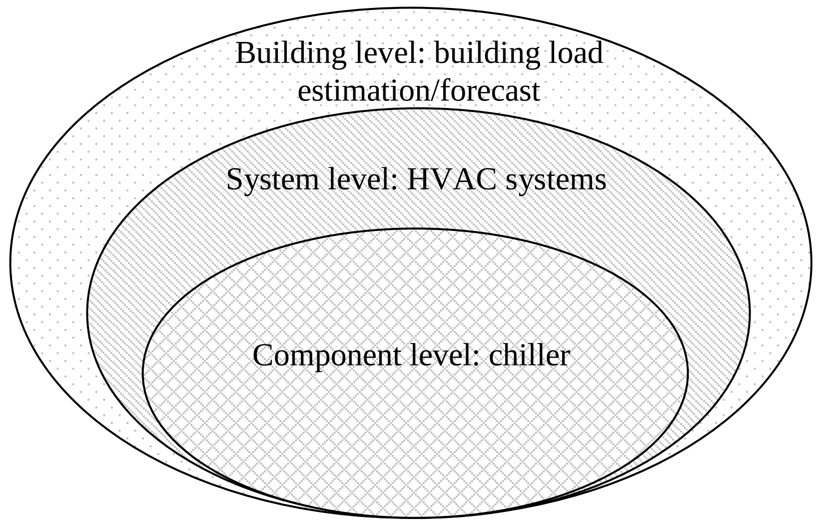

Figure 2.2 FDD structure and relationship among the three level FDD schemes levels

2.2 Building Load Estimation/Forecast Scheme

The building-level scheme is implemented based on building load estimation and forecast as shown in Figure 2.3. The load estimation scheme using the monitoring weather via BMS as the input of the building thermal network model is applied in the building-level diagnosis. The load forecast scheme using the on-line weather forecast from the observatory of the building thermal network model is applied in deciding the optimal settings of HVAC control strategies, such as peak demand control and chiller sequence control etc. The building thermal network model uses thermal resistances (R) and thermal capacitances (C) to represent the building envelope and building internal mass. The weather inputs include solar radiation, outdoor air temperature and relative humidity. The detailed description of the building-load estimation/forecast scheme can be found in Chapter 3 and Chapter 4.

Building performance evaluation and diagnosis is a model-based method as depicted in Figure 1.1. The reference model for the building-level diagnosis is a building thermal network model for building cooling load estimation. The real system performance is the building load measurement. The threshold is predetermined as the benchmark of the load residual. The load residual is defined as the difference between the load prediction and load measurement. If the residual violates the threshold, the fault is considered to occur. The building-level diagnosis depends on reliability of the building load estimation.

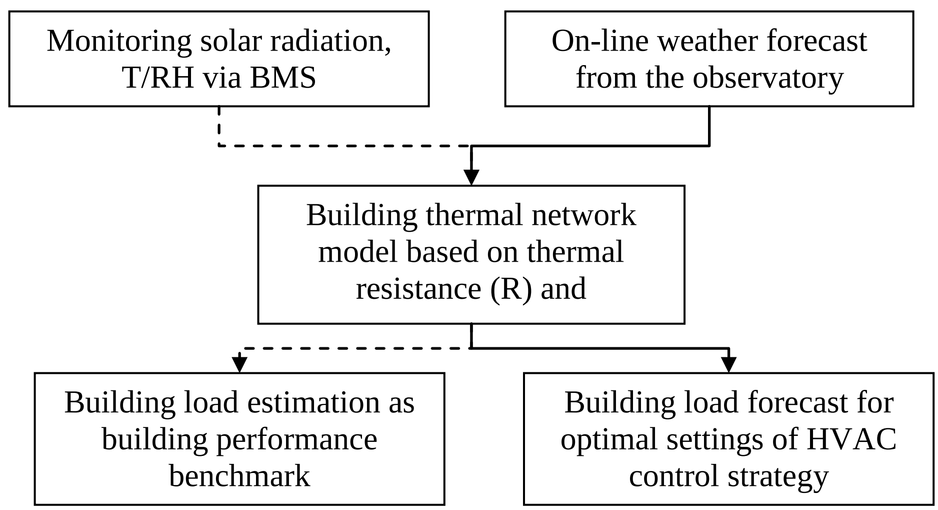

Figure 2.3 Overview of building load estimation/forecast scheme

2.3 System-level FDD

The system-level FDD scheme for HVAC systems mainly consists of two FDD function modules, i.e., a sensor FDD&E module and a system FDD module, as shown in Figure 2.4. The sensor FDD&E module is implemented to obtain the correct or reasonable sensor readings prior to the use of the system FDD module. It is a guarantee of the input of the system FDD module, as well as a guarantee of the system performance monitoring and control stability. The sensor FDD&E module takes advantage of principal component analysis (PCA) method of capturing the interrelationship of a group of sensor measurements. The sensor measurements correlate with each other based on the heat balance or mass balance. If the Q-statistic deduced from the PCA model violates the Q-threshold determined by the training data, the faulty sensor needs to be recovered. The recovered sensor measurement is used as the input of the system FDD module. In the system-level FDD scheme for HVAC systems, some typical HVAC sub-systems are considered, including cooling tower system, chiller system, secondary pump system before and after heat exchangers, and heat exchanger system. A number of performance indices (PIs) are proposed to indicate the health status of each sub-system. PI residual is defined as the difference between the actual PI and PI benchmark predicted by the regression model. If PI residual violates the on-line adaptive threshold, the corresponding sub-system is considered as abnormal. The details of the system-level FDD scheme are given in Chapter 5 and in Chapter 6.

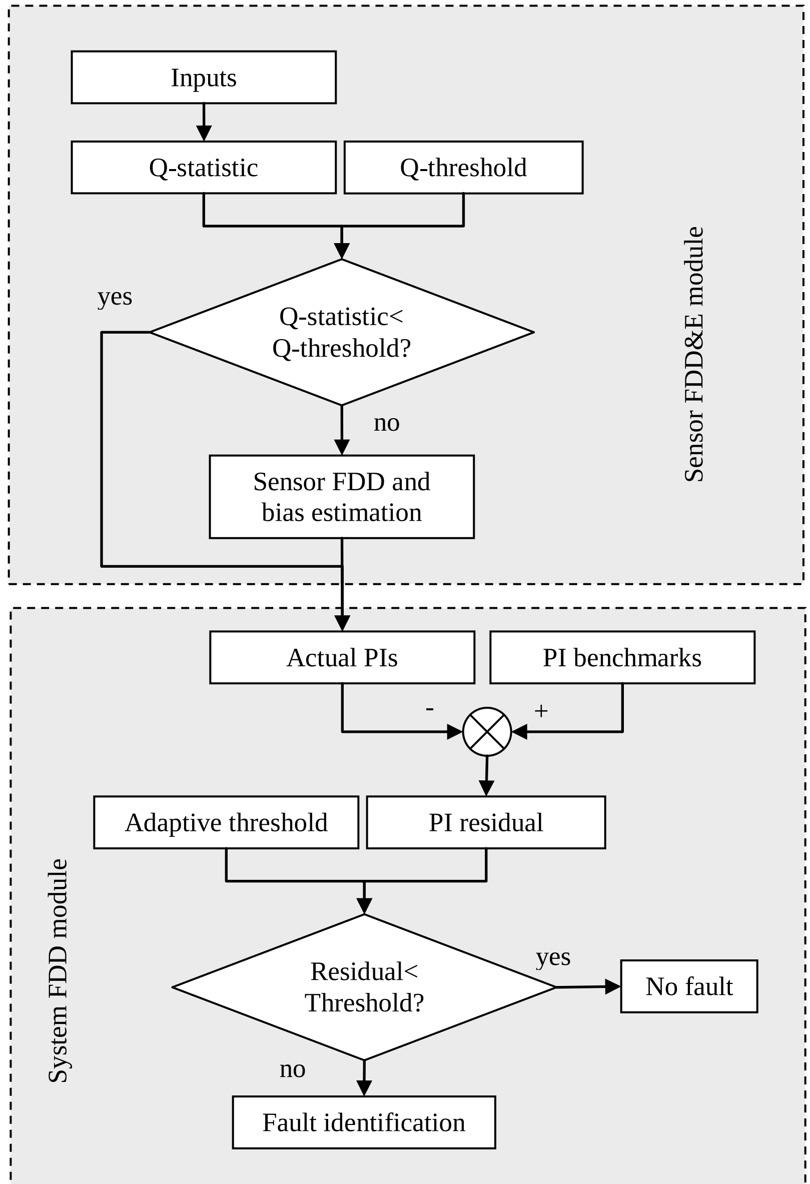

Figure 2.4 Overview of the system-level FDD scheme for HVAC systems

2.4 Component-level FDD

The component-level FDD scheme for the chiller consists of two parts as shown in Figure 2.5. One is the quantification of chiller PI residuals. The other is fault identification. Chiller PI residuals are defined as the difference between the PI model estimations using normal data and those using fault data. The traditional diagnostic classifier is composed of the trend pattern of the PI residuals corresponding to particular faults. However, it is ineffective or disabled to distinguish the faults when they have the same rule patterns. Based on the analysis, the quantitative impacts of different faults on the PIs are different. The traditional diagnostic classifier is quantified using the proposed fuzzy model. The new quantitative diagnostic classifier is composed of the standardized quantitative PI residuals (SQPs). The fault identification deploys artificial neural network (ANN) to match the SQPs with the particular faults. The ANN is the backpropagation networks with three layers. The detailed description of the component-level FDD scheme for the chiller can be found in Chapter 7, as well as Chapter 8 for the validation results.

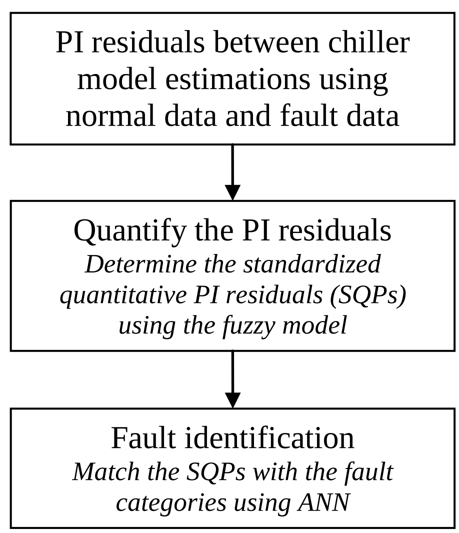

Figure 2.5 Overview of the component-level FDD scheme for the chiller

2.5 Summary

The chapter briefly introduces the structure of the whole strategy for building system performance evaluation and diagnosis. The strategy is implemented in three levels. The building load estimation/forecast scheme is developed based on a building network model. The system-level FDD scheme for HVAC systems consists of a sensor FDD&E module and a system FDD module. The sensor FDD&E module is used as the guarantee of measurement reliability and is implemented prior to the use of the system FDD module. The component-level FDD scheme focusing on the chiller employs fuzzy models to quantify the PI residuals and then employs ANN technique for identifying the fault based on the quantified PI residuals accordingly.

CHAPTER 3 BUILDING LOAD ESTIMATION/FORECAST SCHEME

The chapter presents a building load estimation/forecast scheme at the building level. As the basis of the scheme, a thermal network model is used to estimate and forecast the building cooling load. In the building thermal network model, the building envelops and internal mass are representative of thermal resistances (R) and capacitances (C). The weather-related inputs (e. g. solar radiation, outdoor air temperature/relative humidity) of the thermal network model can be chosen from building management system (BMS) monitoring or the forecast of the observatory. The building load estimation using the monitoring weather information via BMS is used as benchmark in the building-level diagnosis. The building load forecast using the weather forecast information as the inputs of the thermal network model is to decide the optimal settings of some HVAC system control strategies. In the building load forecast scheme, two weather prediction modules are integrated to the building thermal network model. One is the solar radiation prediction module based on the regression technique. The other is the outdoor air temperature/relative humidity (T/RH) prediction module based on the grey dynamic model (GM).

Section 3.1 depicts the whole structure of the building load estimation/forecast scheme and briefs the introduction of scheme applications. Section 3.2 presents the building thermal network model using thermal resistances (R) and capacitances (C) to represent the building envelopes and internal mass. The structure of the building thermal network model is analyzed in Section 3.3 based on the source of heat gain. Section 3.4 presents two weather prediction modules. One is the T/RH prediction module based on grey dynamic models. The other is the solar radiation prediction module based on the weather forecast information from the observatory. Section 3.5 is the summary.

3.1 Scheme Structure

Figure 3.1 illustrates the schematics of the building load estimation/forecast scheme and its applications. The building load estimation scheme is mainly based on the building thermal network model (Wang and Xu 2006). The weather inputs (e.g. solar radiation, outdoor air T/RH) are collected on line from the sensor measurements via BMS. The building load estimation as benchmark of building performance is applied in the building-level diagnosis. The on-line actual load measurements are compared with the benchmark to decide if the building performance is normal or not. The scheme of building load estimation is described in detail in Wang and Xu (2006). This chapter focuses on the building load forecast scheme. In the building load forecast scheme, two weather prediction modules are integrated with the building thermal network. One is the solar radiation prediction module. The other is the outdoor air T/RH prediction module. The weather forecast information used in the two prediction modules are collected on line from the website of the Hong Kong Observatory via an internet interface named DCOM. Distributed component object model (DCOM) is widely used for data communication among software components distributed across computers on the network. The weather forecast information includes cloud amount, sky conditions, outdoor air maximum and minimum temperature/ relative humidity. The forecast scheme is used to determine the optimal settings of HVAC system control strategies, such as peak demand reduction and optimal chiller start etc. In peak demand control methods, proper amount of cooling energy and zone temperature setpoint are used as the optimized parameters. In optimal chiller start control methods, the number of chillers put into operation and the starting time of chillers are usually the optimized parameters.

As the building-level diagnosis based on the building load estimation is discussed in Xu (2005), this chapter focuses on the building load forecast used for HVAC system optimal control strategy. The building load estimation/forecast scheme as a function module, together with the optimal control strategies for the HVAC systems is incorporated into the IBmanager (addressed in Chapter 9). The building load estimation scheme is to estimate the cooling load demand for building-level diagnosis, while the building load forecast is to forecast the building load demand for optimal settings of control strategies (e.g. peak demand reduction and optimal chiller start).

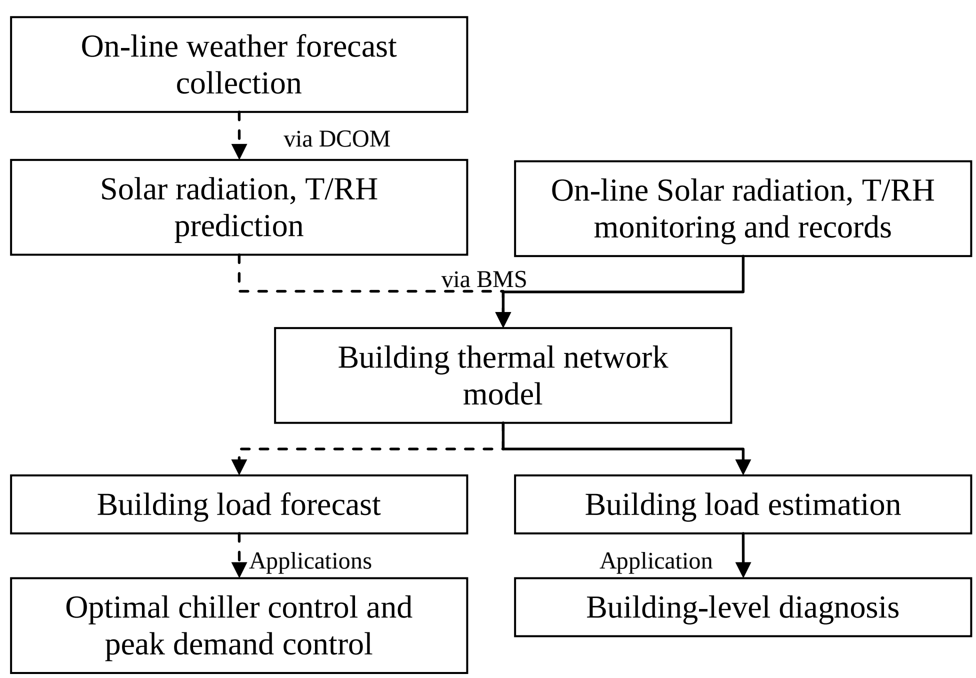

Figure 3.1 Schematics of the building load estimation/forecast scheme and its applications

3.2 Introduction of the Building Thermal Network Model

3.2.1 A Brief on Model Formulation

The schematics of the simplified building thermal network model (Wang and Xu, 2006) are shown in Figure 3.2. Usually, the indoor air temperature is assumed uniform since the building is considered as whole. This assumption is adopted by most simulation packages.

In this model, the heat transfer through walls, roofs and windows, heat charge and discharge through internal mass and internal air are all considered. Furthermore, the heat transfer by fresh air, infiltration, the convection of occupants, lights and equipments, and latent heat gain are also brought into the model. The exterior walls and roofs constitute the building envelopes. They are simplified by using 3R2C models. For exterior walls, the orientation is an important factor affecting the forcing functions determined by the sun position. In Figure 3.2, the thermal capacity of the window is neglected, and the window is represented using a pure resistance. The internal mass includes partitions, equipment, furniture etc. It is simplified by using 2R2C model. The internal mass absorbs the radiant heat from solar radiation, occupants, lighting and computers etc, while it releases the heat to the air space gradually.

The relationship and heat balance of heat transfer processes of building envelopes, internal mass and windows etc. are shown as follows.

$$C_{rf,2}\frac{dT_{rf,2}(t)}{dt}=\frac{T_{sol,rf}(t)-T_{rf,2}(t)}{R_{rf,1}}-\frac{T_{rf,2}(t)-T_{rf,4}(t)}{R_{rf,3}} \tag{3.1}$$

$$C_{rf,4}\frac{dT_{rf,4}(t)}{dt}=\frac{T_{rf,2}(t)-T_{rf,4}(t)}{R_{rf,3}}-\frac{T_{rf,4}(t)-T_{in}(t)}{R_{rf,5}} \tag{3.2}$$

$$C_{ei,2}\frac{dT_{ei,2}(t)}{dt}=\frac{T_{sol,ei}(t)-T_{ei,2}(t)}{R_{ei,1}}-\frac{T_{ei,2}(t)-T_{ei,4}(t)}{R_{ei,3}} \tag{3.3}$$

$$C_{ei,4}\frac{dT_{ei,4}(t)}{dt}=\frac{T_{ei,2}(t)-T_{ei,4}(t)}{R_{ei,3}}-\frac{T_{ei,4}(t)-T_{in}(t)}{R_{ei,5}} \tag{3.4}$$

$$C_{im,1}\frac{dT_{im,1}(t)}{dt}=Q_{r,1}-\frac{T_{im,1}(t)-T_{im,2}(t)}{R_{im,1}} \tag{3.5}$$

$$C_{im,2}\frac{dT_{im,2}(t)}{dt}=Q_{r,2}+\frac{T_{im,1}(t)-T_{im,2}(t)}{R_{im,1}}-\frac{T_{im,2}(t)-T_{in}(t)}{R_{im,2}} \tag{3.6}$$

$$\begin{aligned} Q_{r,1}+Q_{r,2} &= Q_{r,Total} \\ &= Q_{r,sol}+Q_{r,occup}+Q_{r,light}+Q_{r,equip} \end{aligned} \tag{3.7}$$

$$Q_{win}=\frac{T_{out}(t)-T_{in}(t)}{R_{win}} \tag{3.8}$$

$$Q_{conv}=Q_{conv,sol}+Q_{conv,occup}+Q_{conv,light}+Q_{conv,equip} \tag{3.9}$$

$$\begin{aligned} Q_{est} =& \sum_{i=1}^{n}\left(\frac{T_{ei,4}(t)-T_{in}(t)}{R_{ei,5}}\right)+\frac{T_{rf,4}(t)-T_{in}(t)}{R_{rf,5}}+\frac{T_{im,2}(t)-T_{in}(t)}{R_{im,2}}+Q_{win} \\ & -C_{in}\frac{dT_{in}(t)}{dt}+(Q_{conv}+Q_{fr}+Q_{la,occup}) \end{aligned} \tag{3.10}$$

$$Q_{est}\approx Q_{act} \tag{3.11}$$

Where, C and R are resistance and capacitance, T is temperature, subscript *rf*, *im*, *ei*, *in*, and *win*, indicate roof, internal mass, the *i*-th exterior wall and inside, and windows respectively. Subscript *r*, *Total*, *conv*, *sol*, *occup*, *light* and *equip*, indicate radiation heat, total radiation heat, convective heat, solar radiation, occupants, lighting and equipments respectively. $Q_{r,1}$ and $Q_{r,2}$ absorbed by the nodes $C_{im,1}$ and $C_{im,2}$ respectively are the radiation which includes the radiation from solar radiation through windows, from occupants, lighting and equipments. $Q_{conv,sol}$ and $Q_{r,sol}$ is the convective heat and radiation heat of solar radiation through windows respectively. Q_{fr} is the heat transfer because of fresh air induction and infiltration (exfiltration). $Q_{la,occup}$ is latent heat gain from occupants. Q_{est} and Q_{act} are the estimated cooling load with the model and the actual cooling load which can be measured in the chiller plant.

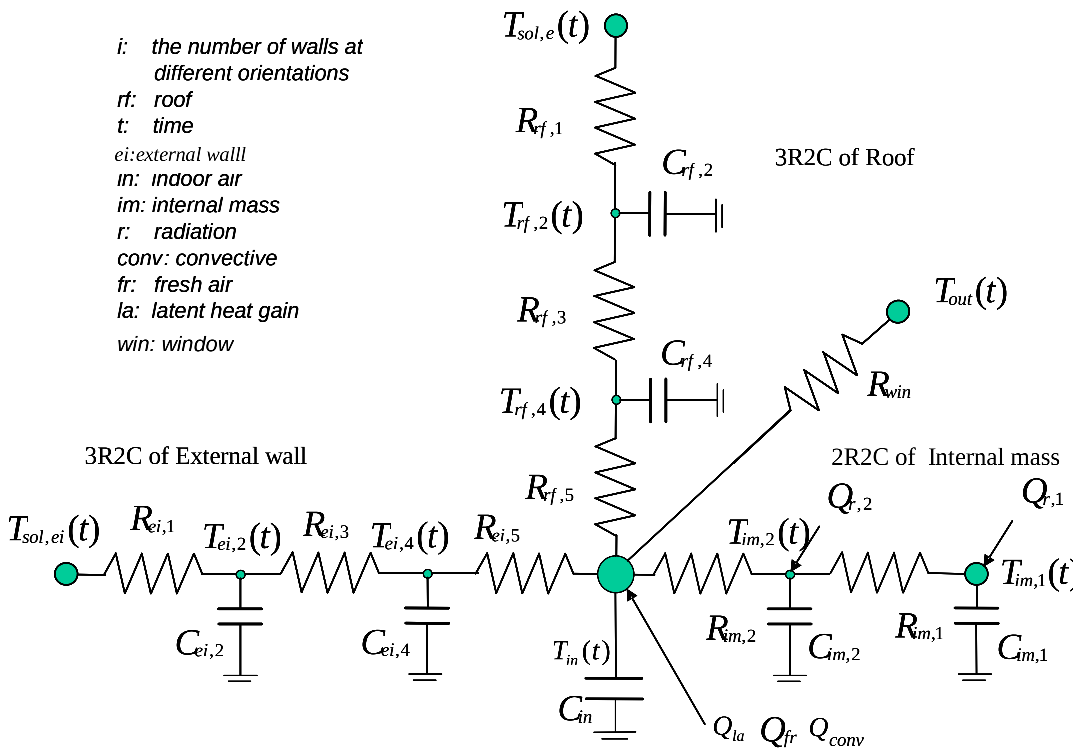

Figure 3.2 Schematic structure of the simplified building thermal network model

3.2.2 Parameter Determination of 3R2C Models of Building Envelopes

Three resistances and two capacities are the parameters of the 3R2C model for exterior walls and roofs. Determination of these parameters is realized by comparing the theoretical frequency response characteristics with the frequency response characteristics of the simplified model. Generic algorithm is used to minimize the difference.

Wall and roof can be seen as a one-dimensional homogeneous multilayer plane. The deduction of transmission matrix of heat transfer through the plane in Laplace domain is briefed as follows.

The transmission equation of temperatures and heat flows at the inner side and outer side using Laplace variable *s* is show in Equation (3.12).

$$\begin{bmatrix} T_{in}(s) \\ q_{in}(s) \end{bmatrix} = M(s) \begin{bmatrix} T_{out}(s) \\ q_{out}(s) \end{bmatrix} = \begin{bmatrix} A(s) & B(s) \\ C(s) & D(s) \end{bmatrix} \begin{bmatrix} T_{out}(s) \\ q_{out}(s) \end{bmatrix} \tag{3.12}$$

Where, $M(s)$ is the transmission matrix of the entire wall, q is the heat flow. $M(s)$ is the product of all individual layer transmission matrices. The elements of the transmission matrices are expressed using hyperbolic functions as follows.

$$A_i = D_i = \cosh(L_i \sqrt{\frac{s}{a_i}}) \tag{3.13}$$

$$B_i = -\frac{\sinh(L_i \sqrt{\frac{s}{a_i}})}{\lambda_i \sqrt{\frac{s}{a_i}}} \tag{3.14}$$

$$C_i = -\lambda_i \sqrt{\frac{s}{a_i}} \sinh(L_i \sqrt{\frac{s}{a_i}}) \tag{3.15}$$

Where, $a_i = \dfrac{\lambda_i}{\rho_i C_{Pi}}$, λ, ρ, C_P, are the thermal conductivity, density and specific heat respectively. *i* is the *i*-th layer of the wall.

The transmission equation can be further expressed in Equation (3.16).

$$\begin{bmatrix} q_{out}(s) \\ q_{in}(s) \end{bmatrix} = \begin{bmatrix} -G_X(s) & G_Y(s) \\ -G_Y(s) & G_Z(s) \end{bmatrix} \begin{bmatrix} T_{out}(s) \\ T_{in}(s) \end{bmatrix} \tag{3.16}$$

Where, $G_X(s)$, $G_Y(s)$ and $G_Z(s)$ are the transfer functions of external, cross and internal heat conduction of the construction respectively.

$$G_X(s) = \frac{A(s)}{B(s)} \tag{3.17}$$

$$G_Y(s) = \frac{1}{B(s)} \tag{3.18}$$

$$G_Z(s) = \frac{D(s)}{B(s)} \tag{3.19}$$

When substituting s wth $j \cdot \omega$, $G_X(j\omega)$, $G_Y(j\omega)$ and $G_Z(j\omega)$ are the theoretical frequency characteristics of the external, cross and internal heat conduction. These frequency characteristics can be expressed by using amplitude and phase lag. They are used as the baseline to identify the parameters of the 3R2C model.

Frequency characteristics of simplified models of building envelopes

According to Wang and Xu (2006), a one-dimensional homogeneous multilayer plane wall can be discretized using four nodes as shown in Figure 3.3. These four nodes are connected with three resistances and two capacitances. The transmission equation can be deduced as follows.

$$\begin{aligned}\begin{bmatrix} T_{in}(s) \\ q_{in}(s) \end{bmatrix} &= M'_{in}(s) M'_4(s) M'_2(s) \begin{bmatrix} T_{out}(s) \\ q_{out}(s) \end{bmatrix} \\ &= \begin{bmatrix} 1 & -R_5 \\ 0 & 1 \end{bmatrix} \begin{bmatrix} 1 & -R_3 \\ -C_4 s & C_4 R_3 s + 1 \end{bmatrix} \begin{bmatrix} 1 & -R_1 \\ -C_2 s & C_2 R_1 s + 1 \end{bmatrix} \begin{bmatrix} T_{out}(s) \\ q_{out}(s) \end{bmatrix} \\ &= \begin{bmatrix} A' & B' \\ C' & D' \end{bmatrix} \begin{bmatrix} T_{out}(s) \\ q_{out}(s) \end{bmatrix}\end{aligned} \tag{3.20}$$

Where,

$$A' = 1 + (C_4 R_3 + C_2 R_3 + C_2 R_5)s + C_4 C_2 R_5 R_3 s^2 \tag{3.21}$$

$$\begin{aligned}B' = &-(R_5 + R_3 + R_1) - (C_4 R_3 R_1 + C_2 R_3 R_1 + C_2 R_5 R_1 + C_4 R_5 R_3)s \\ &- C_4 C_2 R_5 R_3 R_1 s^2\end{aligned} \tag{3.22}$$

$$C' = -(C_4 + C_2)s - C_4 C_2 R_3 s^2 \tag{3.23}$$

$$D' = 1 + (C_4 R_1 + C_4 R_3 + C_2 R_1)s + C_4 C_2 R_3 R_1 s^2 \tag{3.24}$$

The transmission equation can be rearranged as follows.

$$\begin{bmatrix} q_{out}(s) \\ q_{in}(s) \end{bmatrix} = \begin{bmatrix} -G'_X(s) & G'_Y(s) \\ -G'_Y(s) & G'_Z(s) \end{bmatrix} \begin{bmatrix} T_{out}(s) \\ T_{in}(s) \end{bmatrix} \tag{3.25}$$

Where,

$$G'_X(s) = \frac{A'(s)}{B'(s)} \tag{3.26}$$

$$G'_Y(s) = \frac{1}{B'(s)} \tag{3.27}$$

$$G'_Z(s) = \frac{D'(s)}{B'(s)} \tag{3.28}$$

$G'_X(j\omega)$, $G'_Y(j\omega)$ and $G'_Z(j\omega)$ are the frequency characteristics of the external, cross and internal heat conduction of the simplified building envelope model. They are used to compare with the baseline (theoretical frequency characteristics) to identify the parameters of 3R2C models.

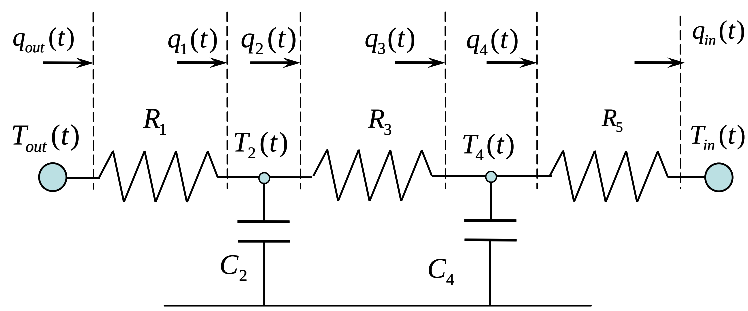

Figure 3.3 Schematics of 3R2C models of building envelopes

<u>Parameters identification of simplified models of building envelopes</u>

To obtain the optimal parameters of the 3R2C model, an objective function is defined as Equation (3.29) to minimize the difference between the theoretical frequency response characteristics and the frequency response characteristics of the simplified model.

$$\begin{aligned} J(R_1, R_5, C_4) = \sum_{n=1}^{N} \sum_{m=X,Y,Z} \quad & (w_m^{AM} \left\| G_m(j\omega_n) \right| - \left| G'_m(j\omega_n) \right\| + \\ & w_m^{PL} \left| PL(G_m(j\omega_n) - PL(G'_m(j\omega_n) \right|) \end{aligned} \tag{3.29}$$

Where, J is the objective function, PL is phase lag (denoted as $PL(G(j\omega))$), the superscripts AM and PL are amplitude and phase lag respectively, w are weighting factors associated with the amplitudes and phase lags of frequency characteristics of the external, cross and internal heat conductions respectively.

Generic algorithm is used to optimize the objective function. The flow chart of parameter identification of the 3R2C model is shown in Figure 3.4.

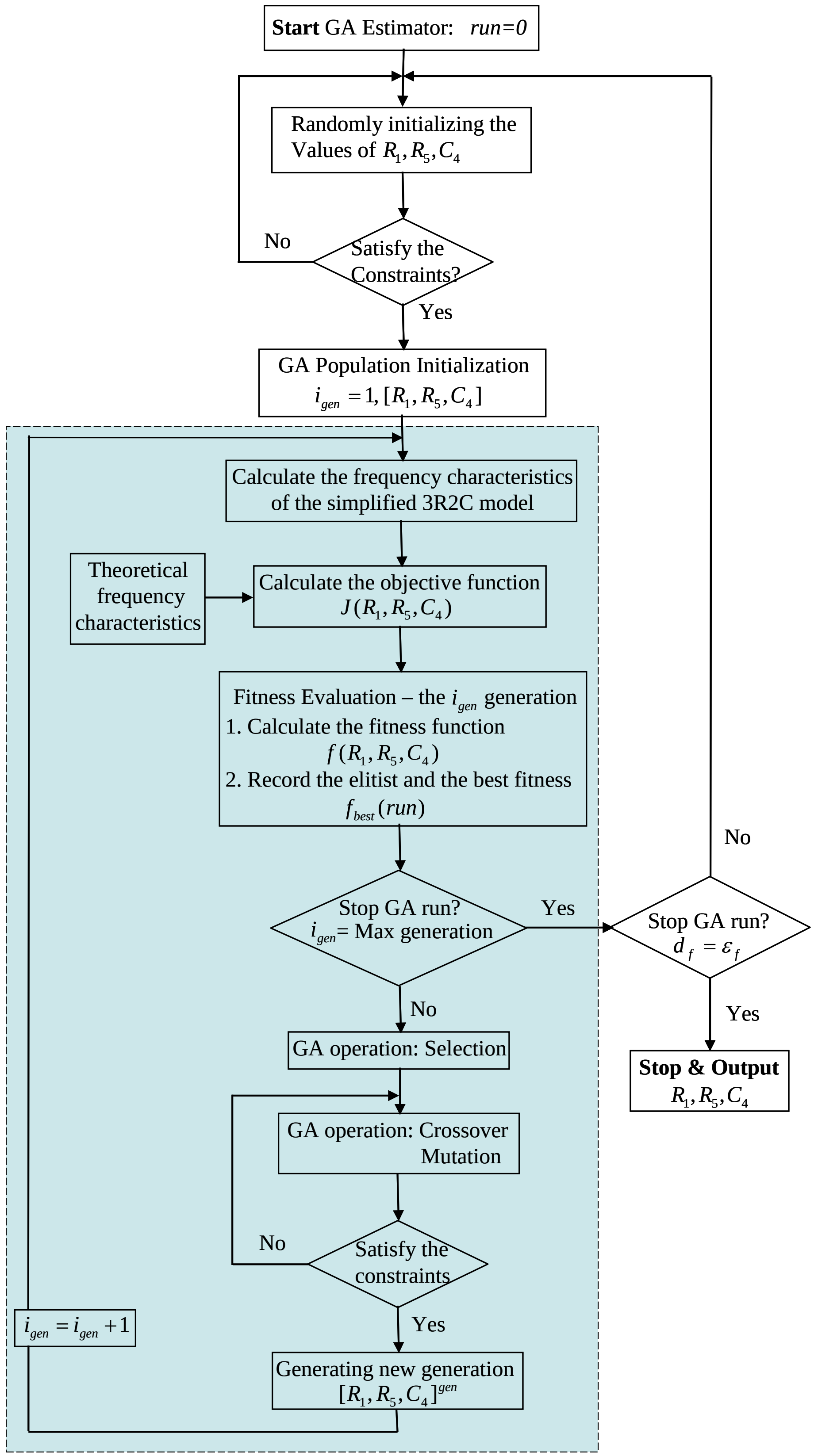

Figure 3.4 Parameters identification of the 3R2C model using generic algorithm

3.2.3 Parameter Identification of the 2R2C Model for Building Internal Mass

The mass of all staff in the buildings (excluding building envelope) can be viewed as the building internal mass, such as internal walls, floors, partitions, furniture etc. It absorbs the radiation and release the heat to the indoor air gradually resulting in a part of the building load.

The internal mass is simplified using two resistances and two capacitances. The heat transfer through the thermal network is shown in Figure 3.5.

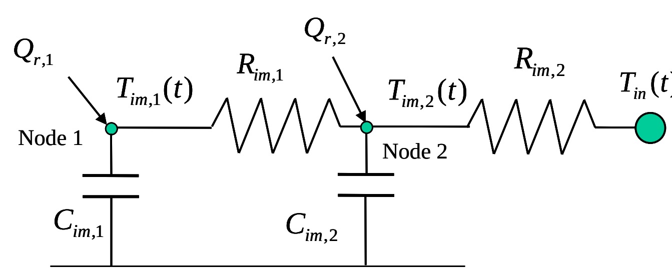

Figure 3.5 Schematic of the 2R2C model of building internal mass

To obtain the optimal parameters of the 2R2C model, an objective function is defined as Equation (3.30) in the form of the root-mean-square error.

$$J(C_{im,1}, R_{im,1}, C_{im,2}, R_{im,2}) = \sqrt{\frac{\sum_{k=1}^{N}(Q_{act,k} - Q_{est,k})^2}{N-1}} \tag{3.30}$$

Generic algorithm is used to optimize the objective function so that the difference between the actual cooling load measurement and estimated cooling load by using the simplified building model is minimized. The flowchart of parameter identification of the internal mass model is shown in Figure 3.6.

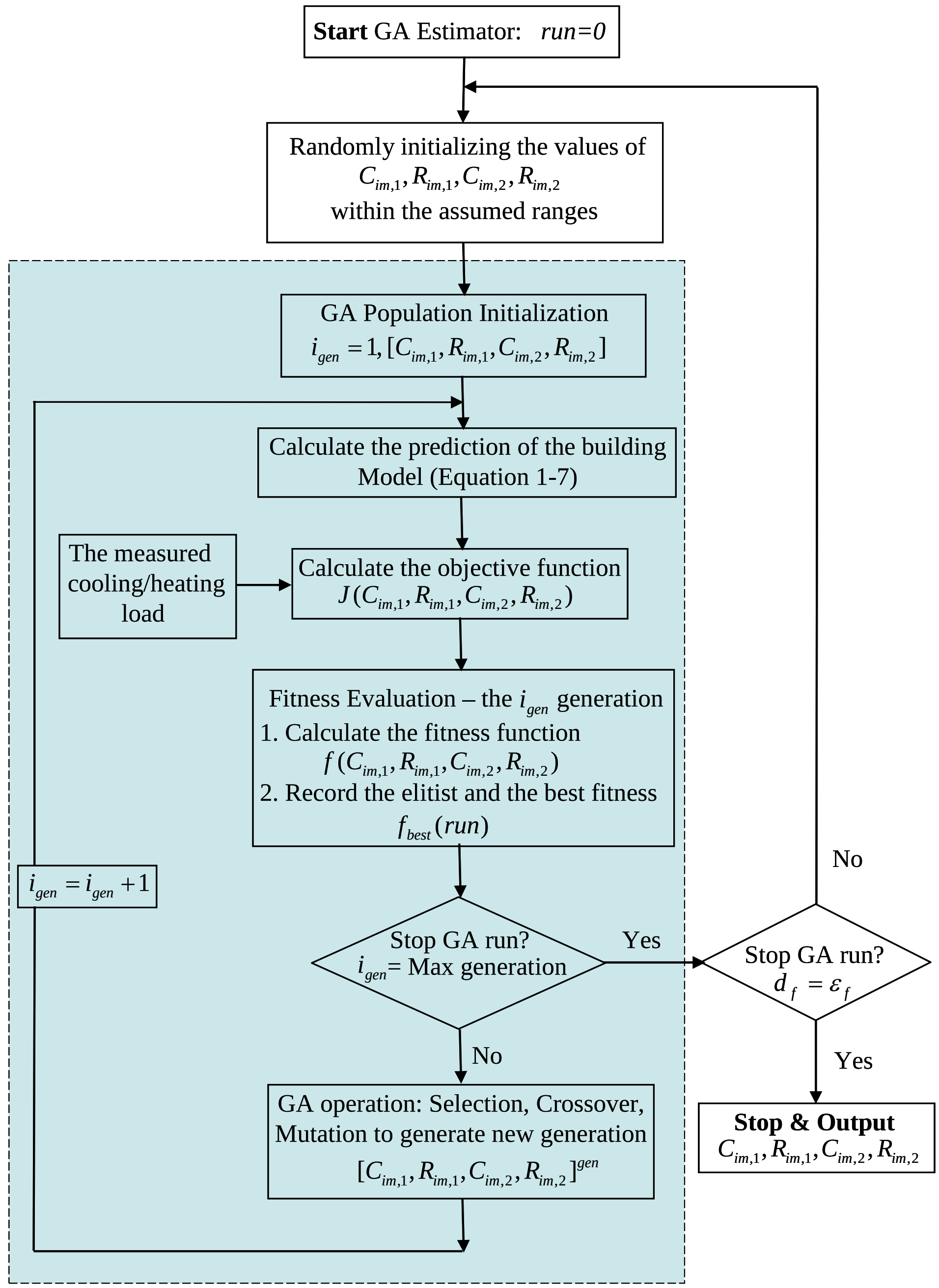

Figure 3.6 Parameter identification of the 2R2C model using generic algorithm

3.3 Modeling Approach for Forecast Purpose

Based on the introduction above, the simplified building load model consists of two major parts, the simplified model of building envelopes and the simplified model of building internal mass.

For the building envelope model, a transmission equation of heat transfer for one-dimensional homogeneous multilayer plane construction in Laplace domain is utilized to deduce the transfer functions of external, cross and internal heat conduction of the construction using physical constructional parameters such as thermal conductivity, density and specific heat. These three transfer functions are the physical frequency characteristics. The same three frequency characteristics are also calculated from the transmission equation in terms of three resistances and two capacitances representative of hypothetical building walls and roof. The five parameters, 3R2C, are then optimized by minimizing the difference between the physical frequency characteristics and the calculated ones with genetic algorithm. The parameters of 3R2C can be identified by matching frequency response characteristics of physical walls with those of simplified models using genetic algorithm.

For the model of building internal mass, a series of dynamic heat transfer function of the thermal network model is formulated to deduce the total estimated building thermal load (Q_{est}). The four parameters, 2R2C, are then optimized by minimizing the difference between the estimated and actual building load using genetic algorithm. Since the resistances and capacitances reflect the physical characteristics of the building envelope and internal mass, they are all assumed to be time invariant.

The simplified building load model involves five heat gain modules. These modules are also viewed as the five parts of the building heat gains source as listed in Table 3.1. In the table, the first column of inputs is acquired based on the operation schedule or some assumptions; the second column of inputs is related to the weather and geography information.

Table 3.1 Five heat gain modules of building thermal load prototype and their inputs analysis

Heat gain module description	Inputs	
	Schedule or assumptions	Weather or geography
heat gain by conduction through walls	None	solar radiation, indoor air temperature, solar incidence and latitude angels
heat gain from internal mass	heat gain by radiation from occupancy, lighting, appliances	Solar radiation, solar incidence and latitude angels
heat gain through windows	None, shading	Solar radiation, solar incidence and latitude angel, outdoor air and indoor air temperature
heat gain from fresh air and air infiltration	flow rate of fresh air supply and air infiltration	outdoor air temperature and outdoor relative humidity
heat gain from occupants, appliances, lightings	based on the operation schedule	none

If the inputs in the second column are the forecasted weather information, the building thermal network model can be used for forecast purpose. The profiles of hourly solar incidence and latitude angels with regard to the geography are fixed if the location is determined.

3.4 Weather Prediction Modules

For the weather prediction, an internet interface developed using DCOM technology is used as shown in Figure 3.1. IBmanager can collect and store the real-time weather forecasting information from the website of the Hong Kong Observatory. The forecasting information includes the maximum and minimum temperatures, the sky conditions and the cloud amount of the coming day. The collected information is further used for predicting the outdoor air temperature /relative humidity as well as solar radiation by using temperature/relative humidity prediction module and solar radiation prediction module.

3.4.1 Solar Radiation Prediction

The global solar radiation affects the heat gain through walls, windows and internal mass. It is one of the most important inputs of the building thermal network model. The method to predict the solar radiation is developed based on the forecasted weather information (sky condition, cloud amount, maximum and minimum temperature) of the coming day.

The global solar radiation is decided by many factors, such as sunshine duration, temperatures, cloud amount and relative humidity, etc. (Hargreaves et al. (1985), Barker (1992), Davies and McKay (1988), Supit and Van Kappel (1998), Bristow and Campbell (1984), Thornton and Running (1999), Ehnberg and Bollen (2005)). Hargreaves et al. (1985) developed a model for global solar radiation prediction with regression technique. In this model, the forecasted maximum and minimum temperatures were used as regressors. Supit and Van Kappel (1998) combined the information of extreme temperatures and cloud amount to predict the global solar radiation. Although the model is not accurate as Angstrom-Prescott (Prescott 1940) method, it was tested in many locations and proved valid, especially when the sunshine duration is not available.

For solar radiation prediction in practical applications, a study of correlation coefficient between solar radiation and the influencing factors in Hong Kong was conducted in advance. The daily meteorological data of two years 2005 and 2006 were utilized to show the correlation coefficients between solar radiation and influencing factors as shown in Table 3.2. The comparison shows that the daily global solar radiation is mainly related to the total bright sunshine

(sunshine duration), mean cloud amount and total evaporation. It is also related to the difference between maximum and minimum temperature as well.

Table 3.2 Correlation coefficients between daily solar radiation and influencing factors

Year	Maximum-Minimum Temp. (℃)	Mean Temp. (℃)	Mean Dew Point (℃)	Mean Relative Humidity (%)	Mean Amount of Cloud (%)	Total Rainfall (mm)	Total Bright Sunshine (hours)	Total Evaporation (mm)
2005	0.4640	0.4440	0.2533	-0.3481	-0.6913	-0.2797	0.9069	0.7847
2006	0.5064	0.4125	0.2221	-0.4776	-0.6969	-0.3265	0.9302	0.8394

Since the forecasted sunshine duration and total evaporation cannot be obtained from the Hong Kong Observatory, other alternative information is used in the solar radiation prediction module for the hourly solar radiation prediction.

The model used for solar radiation prediction is modified based on the study of Supit and Van Kappel (1998). The model developed by Supit and Van Kappel (1998) as Equation (3.31) is used for daily solar radiation estimation by using the cloud amount, maximum and minimum temperature difference as the regressors.

$$I_{global} = I_0 \cdot (a_1 + a_2\sqrt{T_{\max} - T_{\min}} + a_3\sqrt{1 - C/8}) \tag{3.31}$$

Where, a_1, a_2 and a_3 are coefficients. They are obtained by the recursive least square algorithm. I_{global} is the daily global solar radiation (W/m^2). T_{max} is the daily maximum temperature. T_{min} is the daily minimum temperature. C is the average daily cloud coverage. I_0 is daily extraterrestrial solar radiation, constant for a known region. $I_0 = I_{const}[1 + 0.033 \times \cos(2\pi \cdot \frac{Day}{365})]$. *Day* is the day number in a year. I_{sc} is the solar constant (1370W/m^2).

This model developed by Supit and Van Kappel (1998) aimed to estimate the daily global solar radiation. To apply the model in the hourly prediction, modifications using the hourly temperatures are needed as shown by Equation 3.32.

$$I_{global} = I_0 \cdot (a_1 + a_2 \sqrt{\frac{T - T_{\min}}{T_{\max} - T_{\min}}} + a_3 \sqrt{1 - \frac{C_m}{8}}) \tag{3.32}$$

Where, T is the hourly air temperature of the coming day, obtained from the temperature prediction. C_m is the average cloud coverage of the coming day

The cloud amount forecast of the coming day is handled as follows. The cloud amount forecast provided by the Hong Kong Airport includes forecast of five intervals as shown in Table 3.3. Zero Oktas indicates no cloud in the sky, while eight Oktas indicates that the sky is totally covered by cloud. The cloud amount forecast is so rough that it is difficult to pick up the accurate value from the forecast range. To make use of the forecast in a more reliable way, the sky condition is utilized to correct the cloud amount. The sky condition forecast is issued by the Hong Kong Observatory for the whole day at midnight. For each could amount interval forecast, the up-limit is utilized as the forecast value (except zero Oktas), and then is corrected by multiplying the weight factor corresponding to the sky condition. The final cloud amount is deduced as shown in Table 3.4 based on the cloud amount forecast interval and the sky condition. For the could amount forecast with zero Oktas, the final value of the cloud amount is taken as one Oktas, which is acceptable for the correction of sky condition and model application, and it is a rare occasion of zero Oktas in hourly cloud amount record. Since the period of the forecast of cloud amount spans the whole day, the hourly forecast can be seen as the daily average value which constrains the cloud amount variety in a day. In actual cases, the cloud amount does not change much in a day in normal weather. The same treatment is applied to the forecast of the sky conditions. Although it is usually updated once in every two hours, it does not change often like the forecast of the cloud amount. So it is reasonable to adopt the average daily amount and sky conditions as the approximate hourly values of them.

Table 3.3 Intervals of cloud amount forecast

Cloud amount forecast	Value
0	1
1-2	2
3-4	4
5-7	7
8	8

Table 3.4 Cloud amount forecast considering the sky condition

Sky condition	Original cloud amount(Oktas)	Weight	Final cloud amount (Oktas)
sunny	0	1	1
	1-2	0.9	1.8
	3-4	0.8	3.2
	5-7	0.7	4.9
fine	0	1	1
	1-2	0.8	1.6
	3-4	0.7	2.8
	5-7	0.6	4.2
sunny periods	0	1	1
	1-2	1.2	2.4
	3-4	1	4
	5-7	0.8	5.6
sunny intervals	1-2	1.4	2.8
	3-4	1.2	4.8
	5-7	0.9	6.3
cloudy	1-2	1.6	3.2
	3-4	1.4	5.6
	5-7	1	7
	8	0.9	7.2
over cloudy	3-4	1.5	6
	5-7	1	7
	8	1	8
overcast	5-7	1.1	7.7
	8	1	8

3.4.2 Temperature and Relative Humidity Prediction

For a grey system (e.g. prediction of outdoor air temperature/relative humidity) with incomplete information, a method can be used for the information prediction based on the grey dynamic model (GM). The Grey theory was proposed by Deng (1985). Grey prediction is a quantitative prediction method by considering each stochastic variable as a grey quantity changing in a certain range. The theory deals directly with the original data, and identifies the intrinsic regularity, instead of relying on a statistical method to deal with the grey quantity. Grey prediction based on the grey system theory has successfully been found in application in many fields (Morita et al. 1996, Hsu 2003). Many applications are also found in HVAC field. Wang et al. (1999) used GM (1, 1) model to predict the annual energy consumption in a hotel and the prediction accuracy is fairly high. Jiang et al. (2004) examined the application of GM (1, 1) to predict the change ratio of the coefficient of performance of an air cooled water chiller.

Weather forecast is a typical grey system. Although the variety range and some affecting factors are known, there is no definite equation or abundant information to calculate the future numeric value theoretically in an accurate way. So the prediction for outdoor air temperature and relative humidity can be conducted by grey dynamic models. Therefore, a temperature and relative humidity prediction module is developed using the grey dynamic model (GM) for temperature and relative humidity prediction.

3.4.2.1 A Brief on the Principle of the Grey Dynamic Model

The mechanism of a complex system usually can be reflected by the behavior characteristics of some performance data. Sometimes it is difficulty to find the regularity from the random data. Accumulated generating operation (AGO) is an important transformation to transfer the random original data sequence into a new regular and smooth data sequence. This operation can be described as follows.

For a given time series data, such as temperature or relative humidity,

$$X^{(0)}=\{x^{(0)}(t)\}, t=1, 2, \ldots, n$$

New data sequence is obtained by the first-order accumulated generating operation (1-AGO) as Equation (3.33). AGO is capable of transferring the random original data sequence into a new regular and smooth data sequence.

$$X^{(1)}=\{x^{(1)}(t)\},\ t=1,\ 2,\ \ldots,\ n, \tag{3.33}$$

where, $x^{(1)}(k)=x^{(0)}(1)+x^{(0)}(2)+\ldots+x^{(0)}(k)=\sum_{j=1}^{k}x^{(0)}(j)$

AGO transformation have the following features.

a. It alters the original data into the approximately exponential data;

b. It can reduce noise influence effectively;

c. The approximately exponential curve is easy to establish grey dynamic model.

The tendency of the new generating time sequence can be approximated by an exponential function. Therefore, the first order differential equation (denoted as GM(1,1)) can be established as follows.

$$\frac{dX^{(1)}}{dt}+aX^{(1)}=b \tag{3.34}$$

Where, $X^{(1)}$ is the generated data sequence with 1-AGO from the original data sequence, *a* and *b* are parameters of the model. The parameters of GM(1,1) model can be determined with the least square regression as follows.

$$A=(B^{T}B)^{-1}B^{T}Y \tag{3.35}$$

where,

$$A = \begin{bmatrix} a & b \end{bmatrix}^T \qquad (3.36)$$

$$B = \begin{bmatrix} -Z^{(1)}(2) & 1 \\ -Z^{(1)}(3) & 1 \\ \cdots & \cdots \\ -Z^{(1)}(N) & 1 \end{bmatrix} \qquad (3.37)$$

$$Y = \begin{bmatrix} X^{(0)}(2) & X^{(0)}(3) & \cdots & X^{(0)}(N) \end{bmatrix}^T \qquad (3.38)$$

Where, $Z^{(1)}(k)$ is the whiten background value of $X^{(1)}(k)$.

$$Z^{(1)}(k) = \frac{1}{2}(X^{(1)}(k) + X^{(1)}(k-1)) \qquad (2 \le k \le N) \qquad (3.39)$$

When the parameters are determined, the grey dynamic model can be solved easily, and the discrete solution is as follows.

$$\hat{X}^{(1)}(k+1) = [X^{(0)}(1) - \frac{b}{a}]e^{-ak} + \frac{b}{a} \qquad (3.40)$$

The empirical constants, *a* and *b*, can be determined by using the least square regression algorithm. The cap ^ indicates the predicted value. The predicted values for the original data can be obtained by inversed accumulated generating operation,

$$\hat{X}^{(0)}(k+1) = \hat{X}^{(1)}(k+1) - \hat{X}^{(1)}(k) \qquad (3.41)$$

3.4.2.2 Modification Using T/RH Forecast

To utilize the forecasted information sufficiently to make the predicted temperature or humidity profile more accurate, the forecasted maximum and minimum temperature or humidity are used to enhance the prediction model.

The scale factors are introduced to correct the GM(1,1) and defined as follows.

$$\delta_h = \frac{x_h - x_{avg}}{x_{p,\max} - x_{avg}} \tag{3.42}$$

$$\delta_l = \frac{x_{avg} - x_l}{x_{avg} - x_{p,\min}} \tag{3.43}$$

Where, $x_{p,max}$ and $x_{p,min}$ are the predicted maximum and minimum temperatures or relative humidity (RH). x_{avg} is defined as $\frac{x_h + x_l}{2}$. x_h and x_l are the forecasted maximum and minimum temperature or RH. With the scale factors, the predicted temperature profile is corrected as follows.

$$x_i = \begin{cases} x_{avg} + \delta_h (x_{P,i} - x_{avg}) & When\ x_{P,i} \geq x_{avg} \\ x_{avg} - \delta_l (x_{avg} - x_{P,i}) & When\ x_{P,i} < x_{avg} \end{cases} \qquad (1 \leq i \leq 24) \tag{3.44}$$

Where, x_i is the corrected predicted temperature at *i*-th hour of the next day with the forecasted information, $x_{P,i}$ is the unmodified predicted temperature at *i*-th hour of the next day.

The grey models which use the forecasted maximum and minimum temperature and relative humidity are called the modified grey models (modified GM (1, 1)) in the study.

3.5 Summary

The building load estimation/forecast scheme is presented based on a building thermal network model. The building load estimation is used as benchmark to evaluate the overall building performance, while the building load forecast is used to provide reference to the HVAC system optimal control. The forecast scheme mainly includes a simplified building thermal network model, and the solar radiation prediction module and the T/RH prediction module. Because Wang and Xu (2006) has elaborated on how to estimate the building load for performance evaluation, this chapter focuses on how to use the building thermal network model and weather prediction modules to forecast the building load. The basis of the building load estimation/forecast is the thermal network model using thermal resistance and capacitance to represent the building envelope and internal mass. The building exterior walls and the roof are representative of 3R2C, while the internal mass such as internal walls and furniture is representative of 2R2C. The heat transfer through the building envelopes and internal mass is simplified into the heat transfer through the RC-based thermal network. For other routes of heat gain, i.e. gain through windows, gain by fresh air and infiltration, the convection of occupants, lights and equipments, and latent heat gain are also considered into the model.

In the building load forecast scheme, two weather prediction modules are incorporated into the basic thermal network model to make it applicable in the load forecast. One is T/RH prediction module developed based on grey dynamic model (GM(1,1)). The module is improved by using the forecasted maximum and minimum outdoor air T/RH. The other is the solar radiation prediction module developed by using the outdoor air temperature prediction and the forecast of cloud amount from the observatory. The weighting factors corresponding to the specific sky condition are adopted to improve the cloud amount prediction.

The building load estimation/forecast scheme is validated in the next chapter.

CHAPTER 4 VALIDATION OF THE BUILDING LOAD ESTIMATION/FORECAST SCHEME

The validation of the outdoor T/RH prediction module and solar radiation prediction module using weather information records and the on-line forecast from the observatory is presented following by the validation of the building load estimation/forecast scheme.

Section 4.1 presents the validation results of the outdoor temperature and relative humidity prediction modules. Temperature and RH predictions of both conventional grey models and modified grey models are compared with the actual measurements. Section 4.2 presents the validation results of the solar radiation module using the data in March and September from the Hong Kong Observatory. Considering the temperature, RH and solar radiation prediction modules into the building thermal network model, the validation for the building load estimation/forecast scheme is conducted in section 4.3. Section 4.4 gives a summary of the chapter and some discussions about the results.

4.1 Validation of the Outdoor Air T/RH Prediction Module

Hourly temperature records of consecutive five days were used to train 24 grey models. Each model is used to predict the temperature for each hour of one day. These 24 grey models predict the temperatures at 24 hours resulting in the temperature profile of the coming day. The prediction results of conventional grey models (GM (1, 1)) (i.e., the model without modification) and modified grey models (GM (1, 1)) are shown in Figure 4.1 and 4.3 for March 3-4 and September

12-15, 18-22 of 2007 respectively. The modified grey models make use of forecasted minimum and maximum temperatures to enhance the grey models. It can be observed that the prediction of modified grey models was much closer to the actual temperature profiles when compared with that of conventional grey models. As the trend of the temperature within the five days before March 4 was increasing, temperature prediction by the conventional grey models for March 4 was expected to rise further. But the actual recorded temperature profile was near the same as the day before probably due to the weather change. However, the modified grey models improved the prediction with the increase of R^2 from 0.7334 to 0.8624 for the test days in March and from 0.6613 to 0.7153 for the test days in September as shown in Table 4.1. The prediction results of September 18 and 20 are not very good although they are better than that of the conventional grey models since the weather of these two days changed significantly without following the trend of the weather of the previous five training days. Figure 4.2 and 4.4 present the scatter of points comparing hourly predicted (modified GM(1,1)) and observed outdoor air temperatures with 1:1 line for reference.

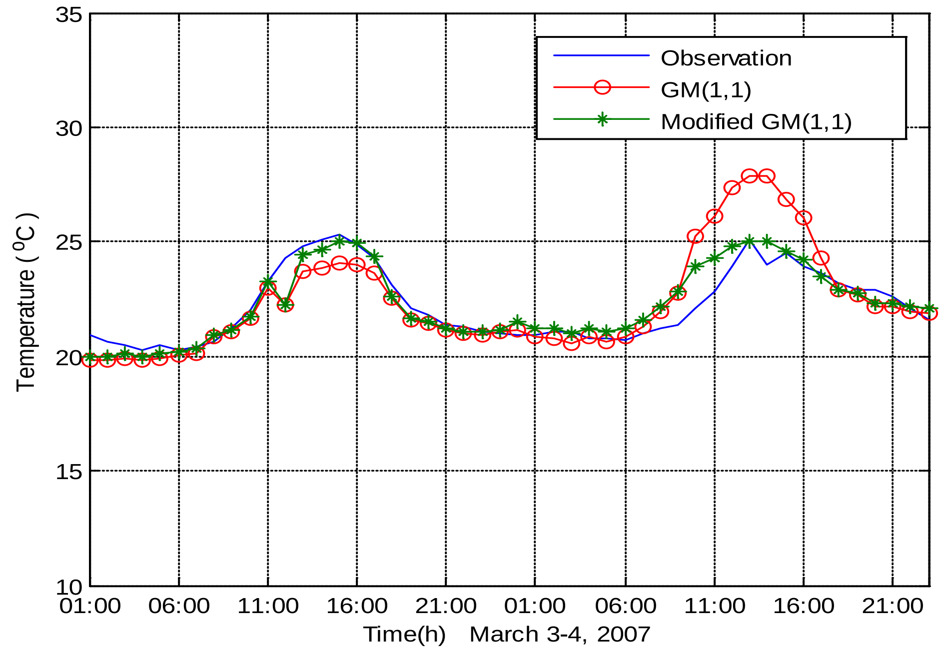

Figure 4.1 Comparison between observed and predicted ambient temperatures using different models (March 3-4, 2007)

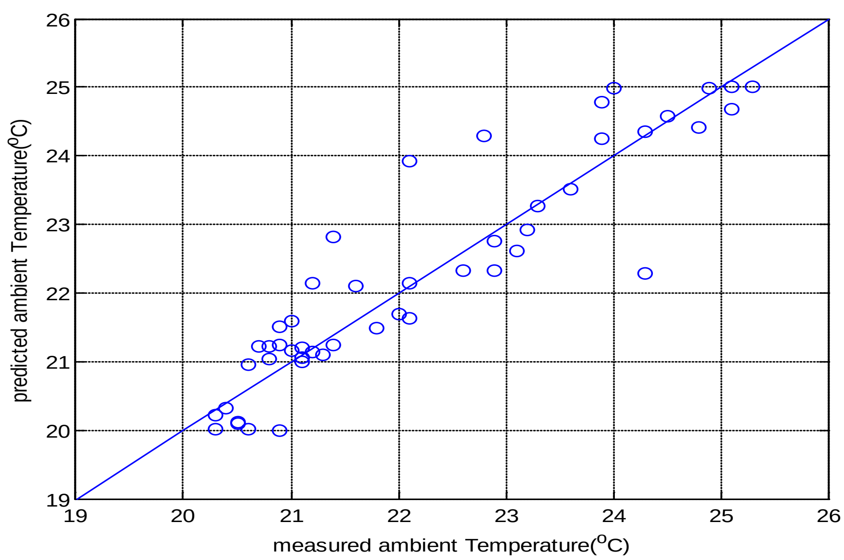

Figure 4.2 Observed ambient temperature vs prediction using modified GM (1,1) (March 3-4, 2007)

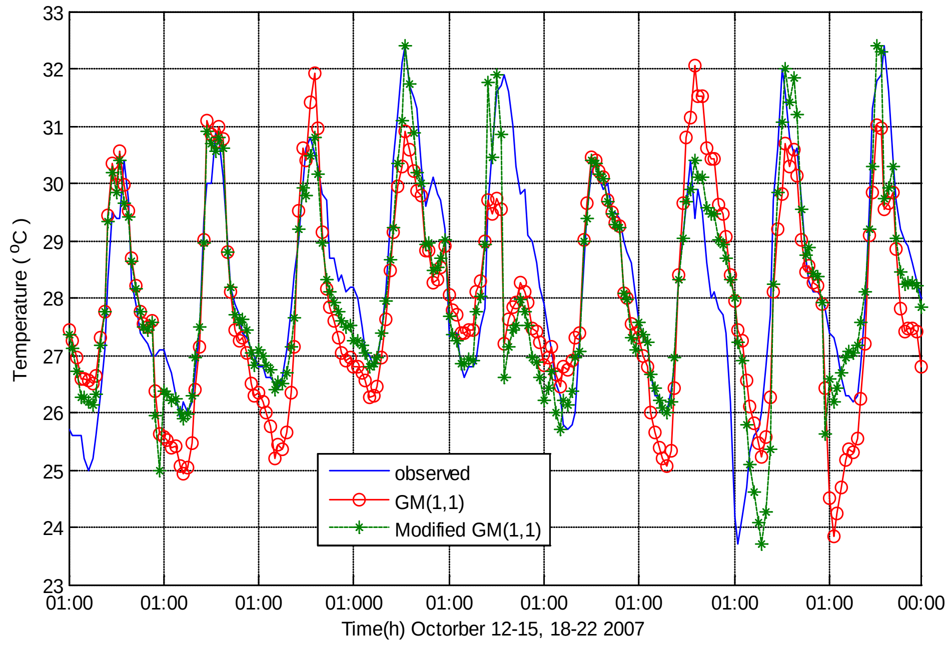

Figure 4.3 Comparison between observed ambient temperature and prediction (September 12-15& 18-22, 2007)

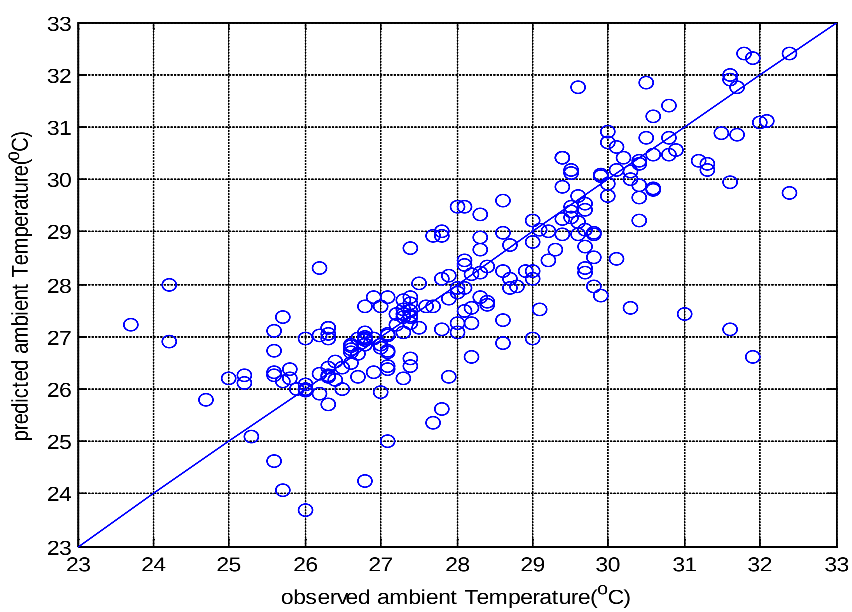

Figure 4.4 Observed ambient temperature vs prediction using modified GM(1,1) (September 12-15& 18-22, 2007)

Table 4.1 Performance of outdoor air temperature prediction models

Model		RMSE	MBE	R^2
GM(1,1)	Mar.	1.1710	-0.1690	0.7334
	Sept.	1.2852	0.3214	0.6613
Modified GM(1,1)	Mar.	0.3593	-0.0519	0.8624
	Sept.	1.1826	0.1789	0.7153

Remarks: RMSE is root mean square error, MBE is mean bias error, R^2 is coefficient of determination

Validations on RH predictions were also conducted by using the same nine-day data in September as presented in Figure 4.5. The RMSE, MBE and R^2 were 13.2580, -0.6386 and 0.4508 respectively. It could be seen that the variance between the observation and prediction in most of the nine days was less than 10%. It is reliable enough for the engineering application. However, the discrepancy between the observation and prediction was large on the 18th day, at the night of the 20th day and in the morning of 21st day in September. During these periods, RH varied irregularly probably due to temporary weather changes.

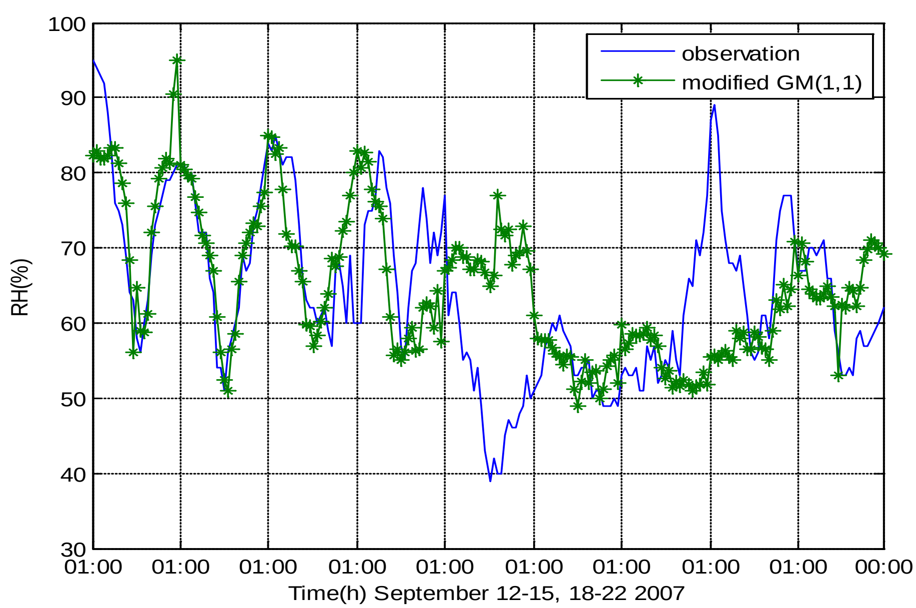

Figure 4.5 Comparison between observed RH and prediction (September 12-15 & 8-22, 2007)

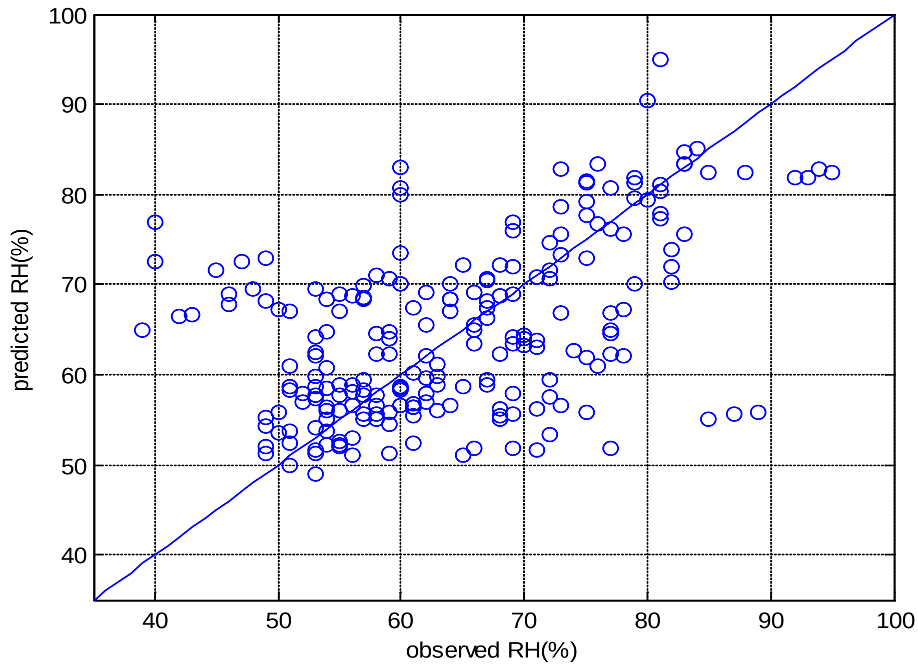

Figure 4.6 Observed RH vs predicted RH (September 12-15& 18-22 2007)

4.2 Validation of the Solar Radiation Prediction Module

Figure 4.7 and 4.9 show the predicted solar radiation compared with the observation on March 3-4 and September 12-15 & 18-22, 2007 respectively. The sky condition forecasts of the nine days are sunny period, sunny period, fine, fine, sunny period, sunny interval, sunny interval, cloudy and cloudy respectively. Prediction 1 is the prediction of the solar radiation module trained using the observed ambient temperatures. Prediction 2 is the prediction of the solar radiation module trained using the temperatures predicted by the above temperature prediction module (i.e., modified GM(1,1)). It was observed that both predicted solar radiation profiles were very close to the observed profile, and the solar prediction using the predicted ambient temperatures by the modified GM (1, 1) (Prediction 2) was very close to that using the same model trained using actual observed ambient temperatures (Prediction 1).

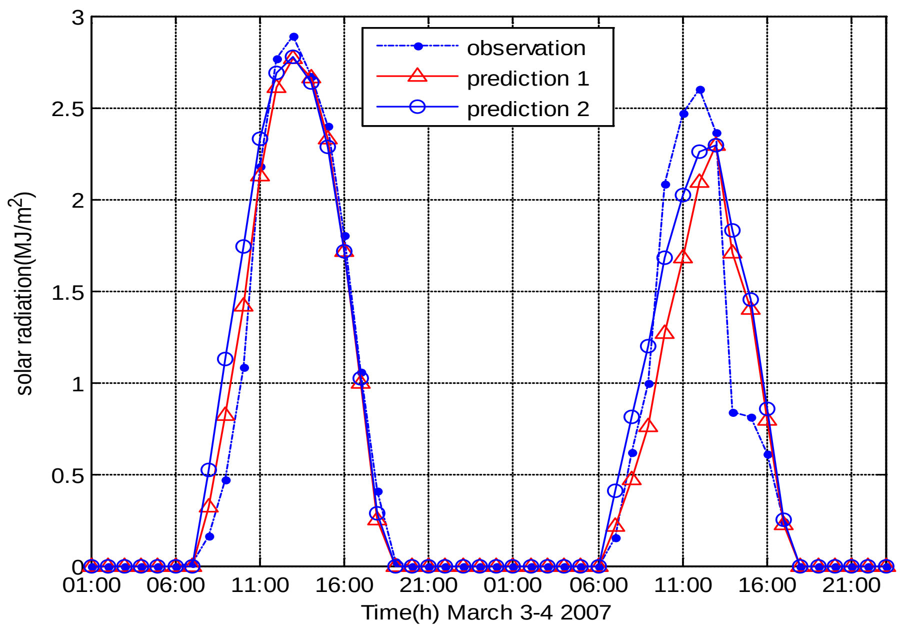

Figure 4.7 Comparison between observed and predicted solar radiations (March 3-4, 2007)

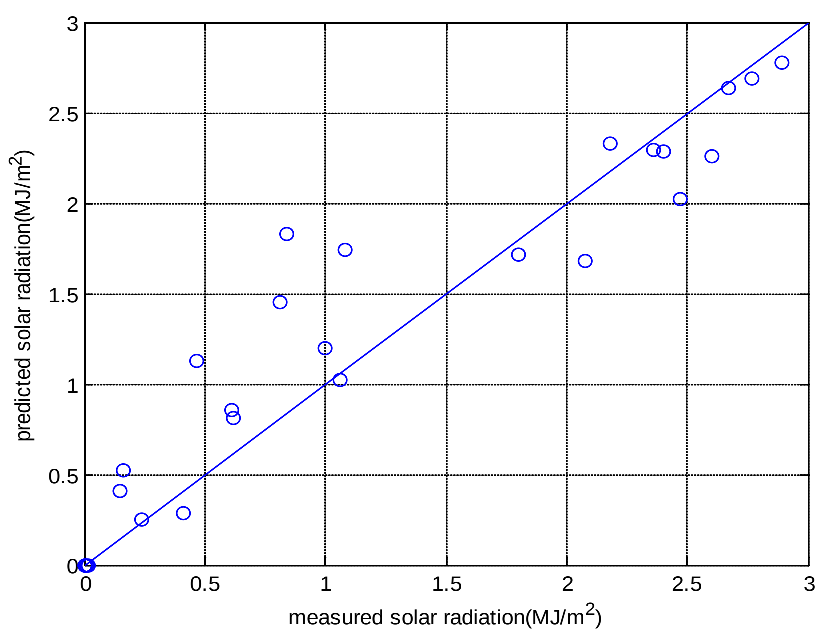

Figure 4.8 Observed solar radiation vs prediction using Prediction 2 (March 3-4, 2007)

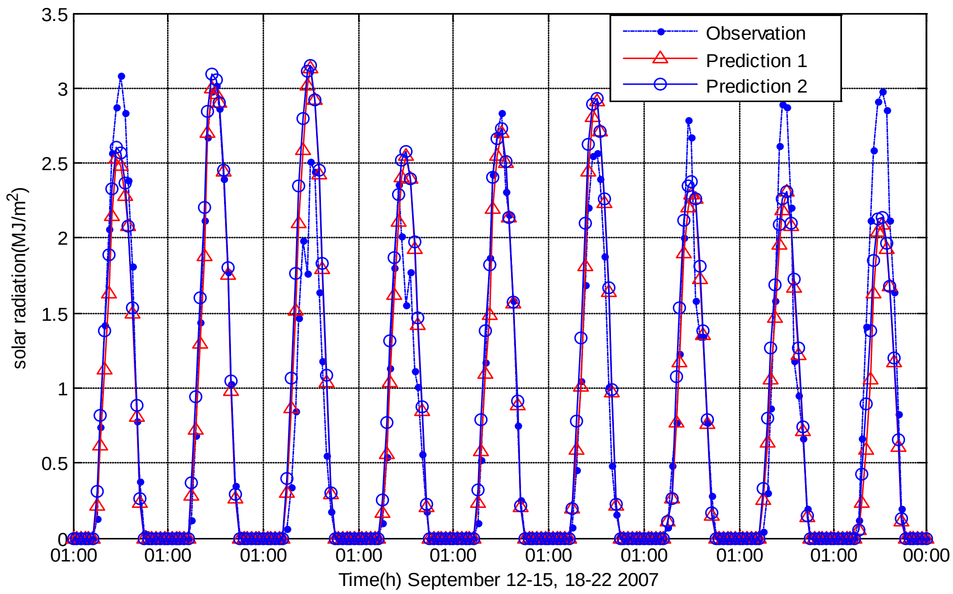

Figure 4.9 Comparison between observed and predicted solar radiations (September 12-15 & 18-22, 2007)

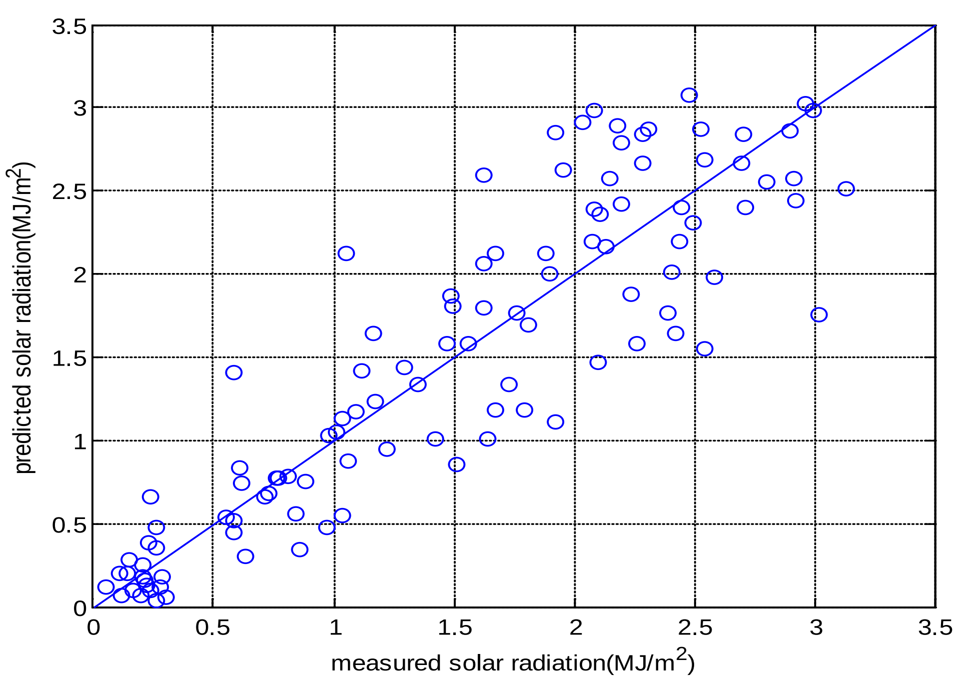

Figure 4.10 Observed solar radiation vs prediction using Prediction 2 (September 12-15 & 18-22, 2007)

For March 3-4, the prediction profiles followed nearly the actual profile except few abrupt points which might be due to some temporary weather changes. When the weather in the daytime is stable, the solar radiation profile conforms to a sine curve in which the highest radiation appears at 13:00. But sometimes a short term of weather changes over the recorded period, such as isolated shower and occasional shower etc., may affect the profile. It is obvious that the observation of solar radiation on March 3rd was relatively stable, and the prediction was therefore highly accurate with the coefficient of determination over 0.95 as shown in Table 4.2 (predicted using the predicted temperatures). On March 4th, there was a sharp ascend between 10:00 and 11:00 and descend between 14:00 and 15:00 in the observation curve. The model gave a prediction of low accuracy with the coefficient of determination below 0.89. Similar situation happened on September 14th and 15th. The solar radiation was under- predicted on September 21st and 22nd. It might be due to the inadequate training data or weather changes. Figure 4.8 and 4.10 present the scatter of points by comparing the hourly predicted global solar radiation (i.e., Prediction 2) and the observed global solar radiation. The solar radiation prediction for the "whole day" includes the prediction of nighttime. Since the solar radiation is zero at nighttime, it is the "daytime" prediction which reflects the prediction performance.

Table 4.3 presents a summary of prediction performance of the solar radiation prediction module in these two test days in March and nine test days in September. The R^2 of Prediction 1 was a little higher than that of Prediction 2 when using the data at the daytime, while it was contrary when using the data of Whole days. Although the accuracy of the solar radiation prediction was affected by the accuracy of the ambient temperature prediction, it is not sufficient to conclude that Prediction 1 using the observed temperatures was better than Prediction 2 using temperatures predicted by the modified GM (1, 1). The R^2 of Prediction 1 was much higher than that of Prediction 2 on March 3rd, while it was contrary in March 4 as shown in Table 4.2. The observed temperature used in the Prediction 1 might cause the solar radiation to be underestimated, but it might be offset by the overestimated temperature of Prediction 2 as the case on March 4th.

Table 4.2 Comparison of Prediction 1 and Prediction 2 by R^2

	Prediction 1		Prediction 2	
	Daytime	Whole day	Daytime	Whole day
Mar. 3	0.9613	0.9859	0.8803	0.9601
Mar. 4	0.6582	0.8301	0.7136	0.8874

Daytime: solar radiation in the daytime after sunrise.

Whole day: 24-hour solar radiation.

Table 4.3 Prediction performance of solar radiation prediction models

		RMSE		MBE		R^2	
		Daytime	Whole days	Daytime	Whole days	Daytime	Whole days
Prediction 1	Mar.	0.1636	0.1151	-0.0063	0.0132	0.8308	0.9257
	Sept.	0.0654	0.0462	0.0268	-0.0031	0.8161	0.9131
Prediction 2	Mar.	0.5363	0.3588	-0.1129	0.1287	0.8147	0.9312
	Sept.	1.1732	0.8296	0.2877	-0.0564	0.8126	0.9178

4.3 Validation of the Building Load Estimation/Forecast Model

4.3.1 Building Description

The building in consideration is located in Hong Kong. It is composed of a main building of 50 floors, an attached building of 7 floors, and a basement of 3 floors. Each floor of the main building has an area of 2262 m^2. And the area of each attached building floor is 1738m^2. The main building is 180 meters high, including four floors for shopping centers and restaurants, one floor for the chiller plant, one floor for banquet hall, and the others for commercial offices. The building envelope is constructed with heavy weight steel concrete and consists of five layers of homogeneous materials. The properties of the external wall are listed in Table 4.4. The area ratio of window to wall is about 25%. The overall heat transfer coefficient of the windows is about 6.42 *W/(m²K)*. The heat transfer of the glass curtain is about 5.60 *W/(m²K)*.

Table 4.4 Properties of the external wall construction

Description	Thickness and thermal properties				
	$L(mm)$	$\lambda(Wm^{-1}K^{-1})$	$\rho(kgm^{-3})$	$C_p(Jkg^{-1}K^{-1})$	$R(m^2KW^{-1})$
Outside surface film	-	-	-	-	0.059
Face brick	13	1.333	2002	920	0.00975
High density concrete	300	1.731	2243	840	0.17331
Plaster or gypsum	13	0.727	1602	840	0.01788
Inside surface film	-	-	-	-	0.121

4.3.2 Validation of the Building Load Estimation/Forecast Model

There are some assumptions clarifying here. The roof of the 49th floor is considered as adiabatic as the 50th floor is air conditioned separately; The roof of the 7th floor of the attached building is considered as adiabatic as it is covered with a swimming pool; The ground floor is merged into building internal mass.

The simplified building thermal network model was validated using site data as shown in Figure 4.11. The results show that the reliability of the model prediction as indicated by the mean absolute percentage error (MAPE) is quite acceptable for applications The MAPE is less than 10% when using operation data of the real building in the summer season of 2004 and coincident weather records from the Hong Kong Observatory. The heat gain from lighting, occupants, appliances was estimated according to the HK-BEAM (2003). The detailed building system description and validation results of the building load estimation model can be referred to Wang and Xu (2006) and Xu (2005).

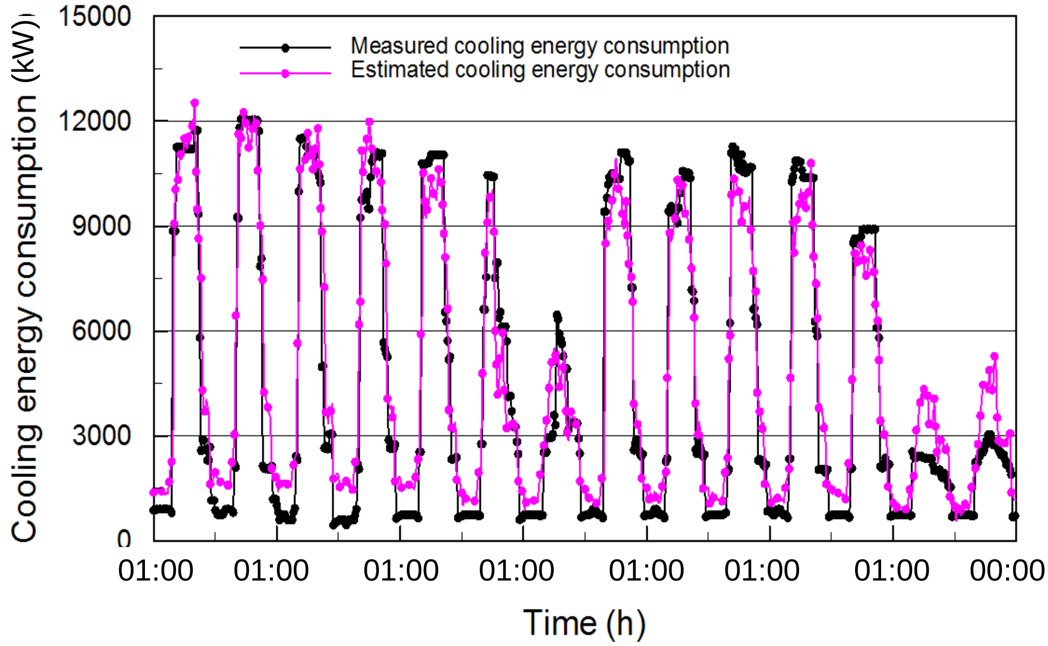

Figure 4.11 Actual measured cooling load vs model predicted cooling load

Because the weather forecast information such as cloud amount, sky conditions were collected after 2007, it did not match the original validation data. However, since the building load model was validated with good performance using the data of 2004, the building cooling load estimated with the same building parameters and the observed weather data of September 12-15 & 18-22 of 2007 could be used as the reference for the validation of the building model developed in this study. As shown in Figure 4.12, the building loads in the nine days were used for validation study by comparing the predicted building load (i.e., prediction load) with the reference building load. The reference load was calculated by the building load model using the observed weather. Two prediction loads are used (i.e., Prediction Load 1 and Prediction Load 2). Prediction Load 1 was predicted using the building load model with the predicted weather using the modified GM(1,1) as inputs. Prediction Load 2 was predicted using the building load model with the predicted weather using the conventional GM(1,1). The MAPE was improved from 8.81% by Prediction Load 2 to 7.34% by Prediction Load 1. It also can be seen that the over-predicted building load in the daytime of the 14th and in a few hours in the afternoon of the 15th and the under-predicted load in the daytime of the 21st and 22nd were due to the over-predicted and under-predicted solar radiations. The over-predicted load in the 18th and under-predicted load in a few hours in the afternoon of the 15th were due to the over-predicted and under-predicted RH

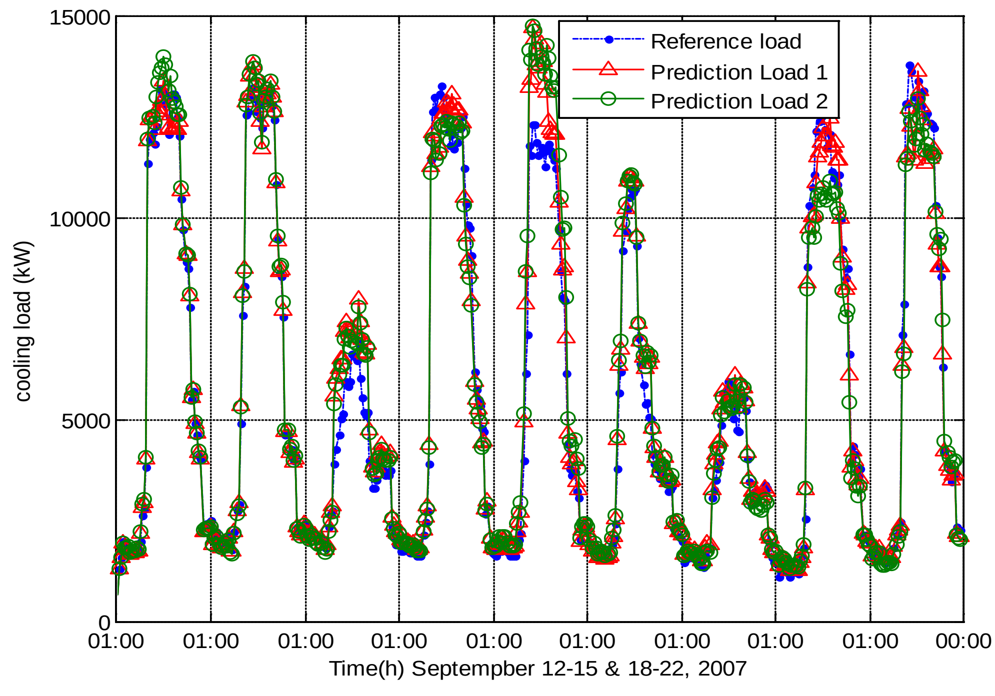

Figure 4.12 Comparison between building reference load and predicted loads

The impact of the weather information on the building model prediction performance was also studied. The building load forecast model was used to forecast the building load by choosing different types of weather inputs. For the situation using the predicted solar radiation and the observed T/RH, the MAPE is 7.07% between the reference load and the prediction load. The MAPE is 3.68% with the predicted temperature and observed solar radiation and RH. The MAPE is 3.32% with the predicted RH and the observed solar radiation and RH. Based on the comparison, the solar radiation affected the building load model most with the largest MAPE. That is because the solar radiation decides the heat gain through walls, internal mass, windows (see Table 3.1), and these heat gains account for the most of the building thermal load in the daytime. The ambient temperature and relative humidity affects very less with a smaller MAPE.

4.4 Summary

The developed building load estimation/forecast scheme in Chapter 3 is useful as benchmark for evaluating the building performance and as reference for HVAC system optimal control. The building load scheme is validated using the site field data. The T/RH prediction module and the solar radiation prediction module are also validated using the data retrieved from the observatory.

The overall performance of building load estimation/forecast scheme given by the proposed model is satisfactory (with MAPE below 8%). The performance of building load forecast model is improved when the model is trained using weather data (i.e., ambient temperature & RH) predicted by modified GM (1,1) compared with the model trained using weather data predicted by conventional GM (1,1). The weather prediction modules are occasionally affected by the temporary weather changes especially for the relative humidity prediction during some test days.

Results and experience show that the building load forecast model is particularly suitable for the on-line forecast of building load in the coming day and the coming hours.

In the building thermal network model, the properties of building envelop is assumed to be known. In the case that the building descriptions cannot obtained, the black-box models can be deployed, such as the regression models using the historical building load data and weather data as regressors. The building load estimation scheme is effective to benchmark the normal performance of the overall building system, while the building load forecast scheme is important for the parameter optimization of some HVAC optimal control strategies, such as peak demand control and optimal control for chillers start etc.

CHAPTER 5 FAULT DETECTION AND DIAGNOSIS SCHEME FOR HVAC SYSTEM: SYSTEM-LEVEL FDD

The chapter presents a fault detection and diagnosis (FDD) scheme for HVAC systems at the system level (i.e., system FDD). This scheme includes a system FDD module and a sensor FDD&E module. The HVAC systems considered in this study are cooling tower system, chiller system, secondary chilled water pump (SCHWP) system before heat exchangers (HX), heat exchanger system and SCHWP system after HX. In the system FDD module, some performance indices (PIs) are proposed to indicate the performance status (normal or faulty) of the systems of concern. Regression models are used to estimate the PIs as benchmarks for comparison with the actually calculated PIs. The reliability of the system FDD is dependant on the health of sensor measurements. They may affect the reliability of the system FDD by affecting the PI benchmarks and the calculated PI. The sensor FDD&E module is developed based on principal component analysis (PCA) to detect and diagnose the sensor fault, and to correct the sensor bias if the bias exists for the subsequent system FDD. Normal tests and fault tests of different HVAC systems are simulated in a dynamic simulation platform based on TRNSYS.

Section 5.1 illustrates the basic scheme structure of the sensor FDD&E module and the system FDD module, and how to combine the two modules together for enhancing the system FDD performance. Section 5.2 describes the central chilling systems in a real building and the dynamic simulation platform of the HVAC systems as well as the system of concern in this study. Section 5.3 presents the HVAC system FDD module in details. The data are preprocessed using an outlier removing method and date filter. The faults are introduced into the system by tuning the parameters of the dynamic models on the simulation platform. How to model the performance indices and how to determine the on-line thresholds are also elaborated in section 5.3. Section 5.4 presents the sensor FDD&E module. The sensors at the HVAC system level are selected based on the heat energy balance and sensitivity to the system FDD. A PCA-based method is used to apply in the sensor fault detection and diagnosis. An iteration approach is used to estimate the bias of the faulty sensors and recover it. A summary is presented in Section 5.5.

5.1 Scheme Structure

The FDD scheme for HVAC systems includes two modules as described in Figure 5.1. One is the sensor FDD&E module based on PCA method for validating the health of sensor measurements and correcting the faulty sensor readings. The other is the system FDD module for system fault detection and diagnosis to validate system efficiency and health of the HVAC systems.

In the first step, all the data used for sensor FDD&E are preprocessed by filtering and removing outliers. Q-statistic is a performance indicator to evaluate the sensor health status. The deviation between the Q-statistic and predetermined threshold is used to detect the sensor fault. How to obtain Q-statistic is introduced in Section 5.4.3.1. Contribution of individual sensor measurement to the Q-statistic is defined as Q-contribution. It is used to identify the faulty sensor by finding the largest contribution. The faulty sensor is corrected to provide the proper measurements for the subsequent system FDD module. The system FDD module is implemented by using the normal or corrected sensor measurements. The normal sensor measurements are used to train benchmark models of PIs. In FDD process, the difference between the predicted PIs by models and actually calculated PIs are compared with their on-line adaptive thresholds to detect which sub-system is abnormal. The on-line adaptive threshold determined by training data and monitoring data needs considering both model-fitting errors and measurement errors simultaneously. A number of PIs are selected to characterize health status (normal or faulty) of each HVAC sub-system of concern. The faulty sub-system can be isolated by the corresponding abnormal PI residuals with the highest detection ratios.

The system-level FDD scheme used in this study is not supposed to identify the specific faults of a HVAC sub-system (such as tube fouling and refrigerant leakage in a chiller) nor the fault of a specific component (a chiller or a pump), but to isolate the sub-system in unhealthy conditions among the whole sub-systems of concern. It means that the system-level FDD scheme is implemented at the system level, not at the component level.

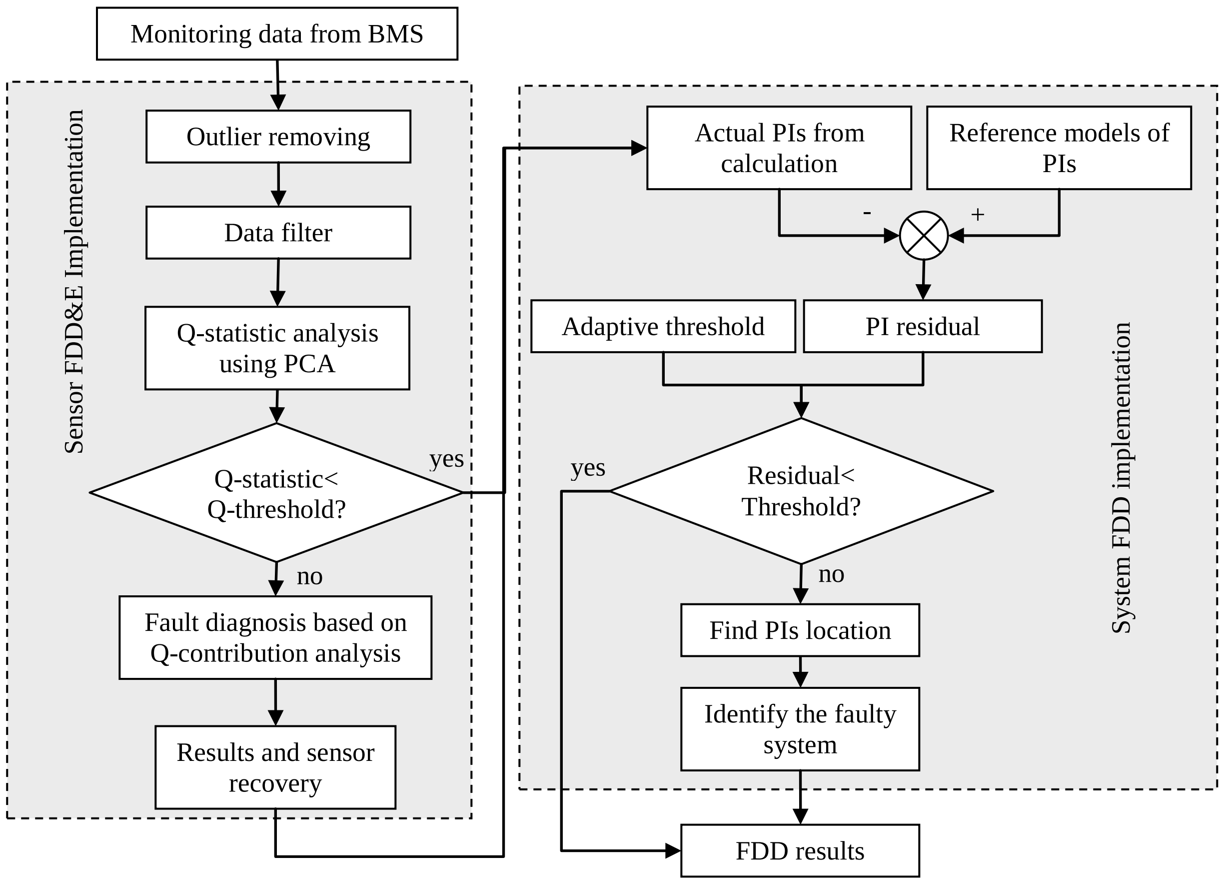

Figure 5.1 Schematics of the FDD scheme at system level

5.2 Introduction of the Complex Dynamic Simulation Platform

The system-level FDD scheme is developed for practical implementation in a new commercial building system. This building is being constructed in Hong Kong. To study the control and diagnosis strategy for energy efficiency improvement, a dynamic simulation platform for the central chilling system based on TRNSYS was developed by Ma (2008) and Ma and Wang (2008). The whole platform simulates the central chilling system with five zones in the building of concern. The building system and simulation platform are briefed as follows.

5.2.1 Building and System Description

The building consists of a basement of four floors, a block building of six floors and a tower building of 98 floors. The total height is about 490 meters and the total floor area is about 321,000 m^2. The building is divided into five zones with separate water systems for satisfying the pressure duration requirements of these equipments. The 6th, 42nd, 78th and 99th floors are mechanical floors for accommodating HVAC equipments such as chillers, cooling towers, heat exchangers, pumps, PAUs, etc. The schematics of the whole central chilling system are shown in Figure 5.2.

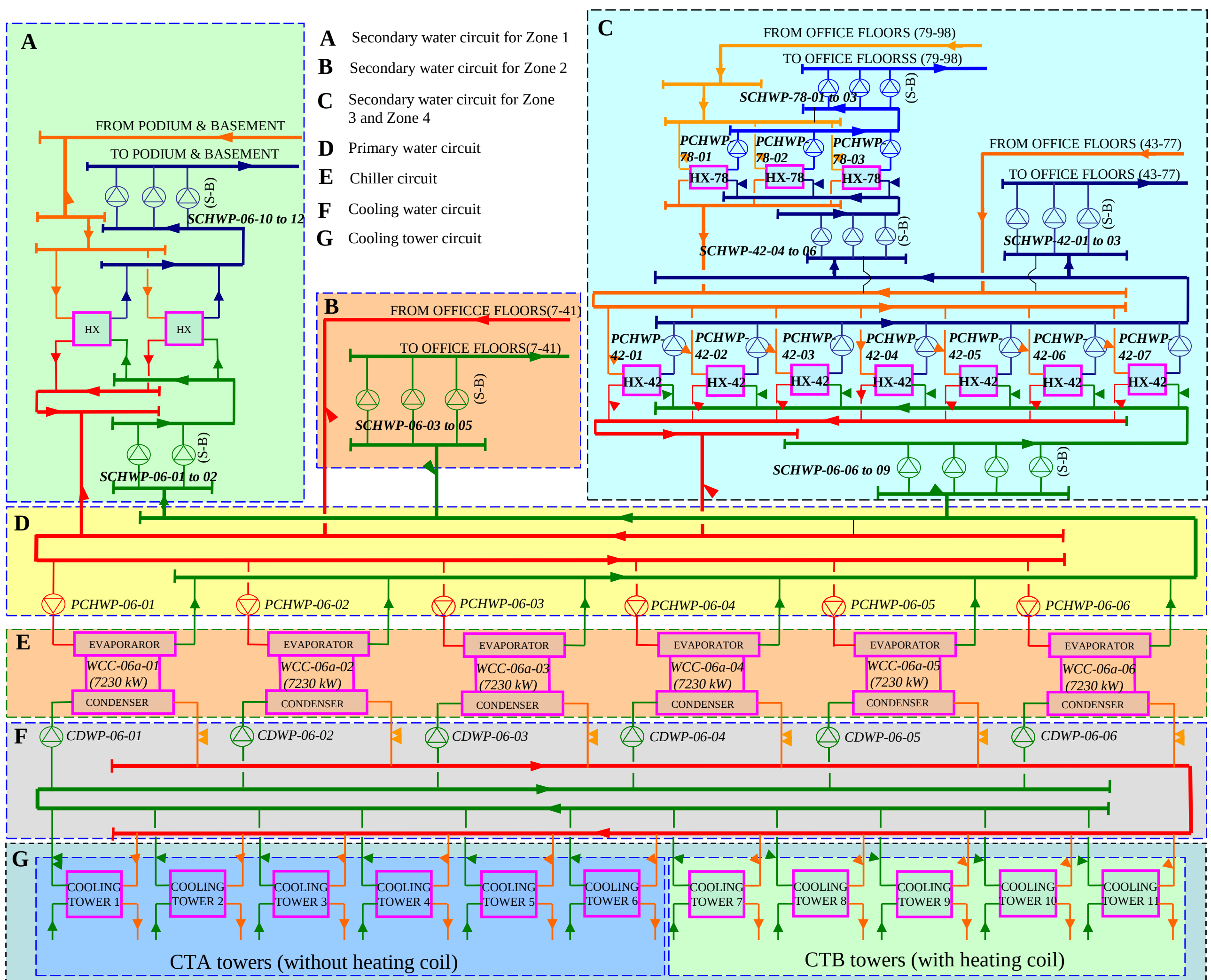

Figure 5.2 Schematics of the central chilling system

The HVAC system serving *Zone* 1 (four floors for basement and six floors of the block building) is considered in this study. There are eleven cooling towers with heat rejection capacity of 5234kW (six towers) and 4016kW (five towers) respectively, six chillers with capacity of 7230kW, two heat exchangers with heat transfer capacity of 3245kW, six constant-speed condenser pumps with design flow rate of 410L/s, six constant-speed primary pumps with design flow rate of 345L/s, two secondary variable-speed pumps with design flow rate of 345L/s before heat exchangers and three secondary variable-speed pumps with design flow rate of 345L/s after heat exchangers. The specification description of the main equipments used in the HVAC system can be referred to Table 5.1 (Ma 2008).

Table 5.1 Specifications of the main equipment in the central chilling system

Chillers		N	$M_{w,ev}$ (L/s)	$M_{w,cd}$ (L/s)	CAP (kW)	W (kW)	W_{tot} (kW)
WCC-06-01 to 06		6	345.0	410.1	7,230	1,346	8,076
Cooling Towers		N	M_w (L/s)	M_a (m^3/s)	Q_{rej} (kW)	W (kW)	W_{tot} (kW)
CTA-06-01 to 06		6	250.0	157.2	5,234	152	912
CTB-06-01 to 05		5	194.0	127.0	4,061	120	600
Pumps		N	M_w (L/s)	$Head$ (m)	η (%)	W (kW)	W_{tot} (kW)
CDWP-06-01 to 06		6	410.1	41.60	83.6	202	1,212
PCHWP-06-01 to 06		6	345.0	31.60	84.5	126	756
SCHWP-06-01 to 02		1	345.0	24.60	82.2	101	101
SCHWP-06-03 to 05		2	345.0	41.40	85.7	163	326
SCHWP-06-06 to 09		3	345.0	30.30	84.2	122	366
SCHWP-06-10 to 12		2	155.0	39.90	78.8	76.9	153.8
PCHWP-42-01 to 07		7	149.0	26.00	84.9	44.7	312.9
SCHWP-42-01 to 03		2	294.0	36.50	87.8	120	240
SCHWP-42-04 to 06		2	227.0	26.20	84.3	69.1	138.2
PCHWP-78-01 to 03		3	151.0	20.60	84.3	36.1	108.3
SCHWP-78-01 to 03		2	227.0	39.20	85.8	102	204
Air-side	PAU fan	29	/	/	/	/	513
	AHU fan	152	/	/	/	/	4,600

Design total power load			
	Chillers	**8,076** kW	**43.38%**
	Cooling towers	**1,512** kW	**8.12%**
	Pumps	**3,918.2** kW	**21.04%**
	AHU and PAU fans	**5,113** kW	**27.46%**
	Total	**18,619.2** kW	---

Where, N is the number of components, M is the flow rate, CAP is the chiller capacity, Q is the heat transfer rate, η is the efficiency, W is the power consumption, and subscripts w, a, ev, cd, rej and tot indicate water, air, evaporator, condenser, rejection and total, respectively.

5.2.2 Outline of the Simulation Platform

A dynamic simulation platform based on TRNSYS is developed to evaluate control strategies and diagnosis strategies for the central chilling system. TRNSYS is a transient simulation program with a library including many components in thermal and electrical energy systems (Klein et al. 1990). Figure 5.3 shows the interrelationship of the different component models in a DECK file. The platform involves chiller models, cooling tower models, pump models, heat exchangers models, AHU models, pipe models, PID controllers, etc.

The basic control strategy in the platform is listed as follows.

a. The minimum ratio of the fresh air to supply air is assumed as 20%

b. The indoor air temperature is 23℃ in summer and autumn and 21℃ in winter and spring with humidity ratio of 50%.

c. The AHU supply air temperature is controlled at the set-point which varies with the season.

The detailed models of water networks and HVAC components can refer to Wang et al. (2000) and Ma (2008).

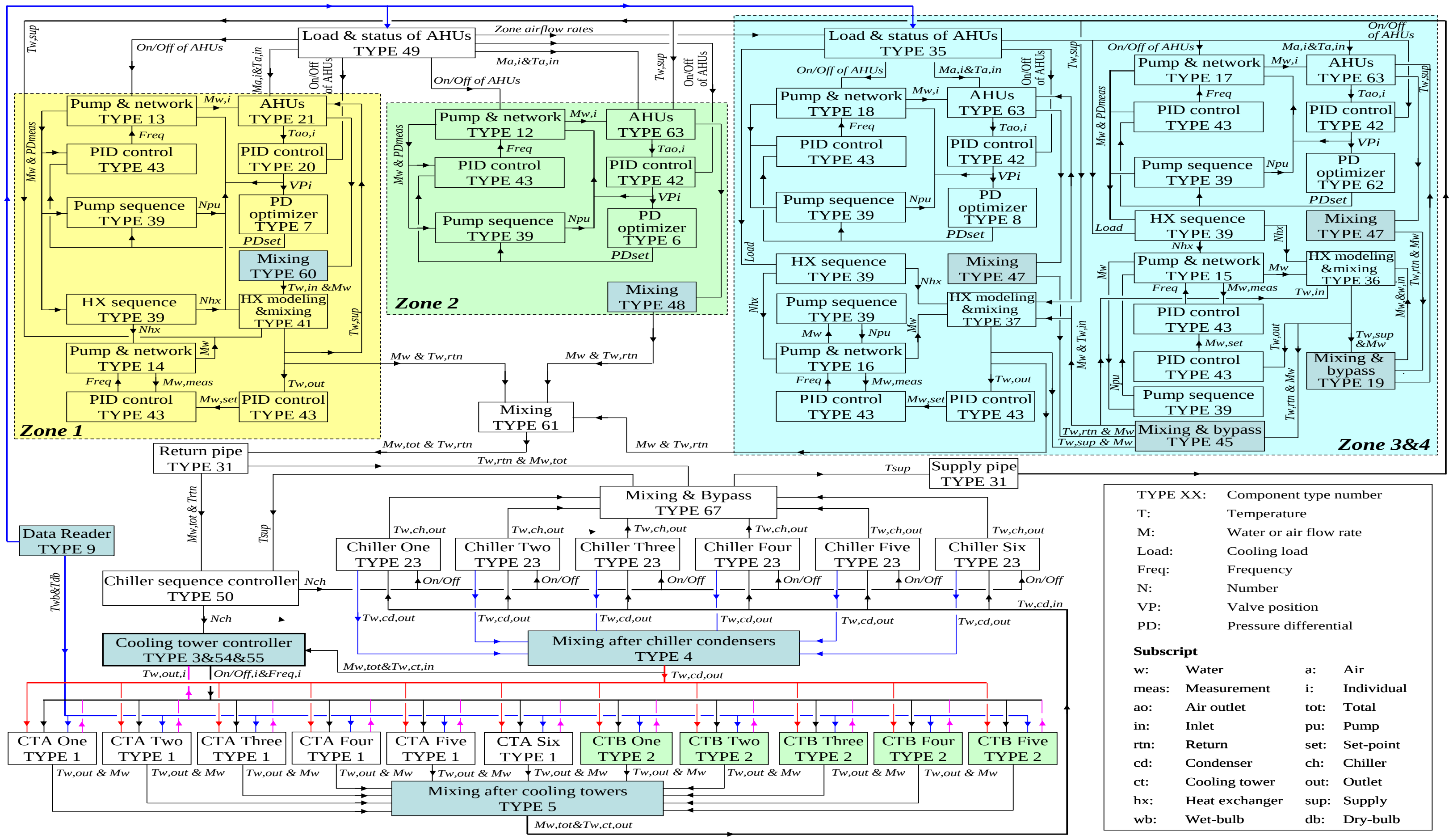

Figure 5.3 Schematics of TRNSYS simulation DECK

5.3 Formulation of the System FDD Module

5.3.1 Introduction of the System FDD Module

Figure 5.4 depicts the aggregate HVAC sub-systems and sensors serving Zone 1. This zone has four-floor basement and six-floor block buildings. The central chilling water system serving *Zone* 1 includes a chiller system, a cooling tower system, a heat exchanger system, and two secondary water pump systems. These aggregate sub-systems which may consist of two or more components are the research objects of the system-level FDD scheme. The health of sensors including temperature sensors and flow meters in the return/supply headers affects the results of the system-level FDD scheme. They are the study object of sensor FDD&E introduced in Section 5.4. The scheme of FDD for HVAC system is divided into two parts as described in Figure 5.5. In these two parts, the data used for training and implementation (validation) are all needed to be preprocessed by removing outliers and filtering. In the model training process, the preprocessed data are used to calculate the proposed PIs which determine the regression parameters of different sub-system models. These parameters are used to estimate the PIs compared with the PI calculation in the validation process. The residual between the estimation and calculation is compared with the on-line adaptive threshold to determine which PI is abnormal. The on-line adaptive threshold determined on-line by training data and monitoring data considers both model-fitting errors and measurement errors. A number of PIs are selected to characterize each HVAC sub-system's status (normal or faulty). The faulty sub-system is isolated by the corresponding abnormal PI residuals with the highest detection ratios.

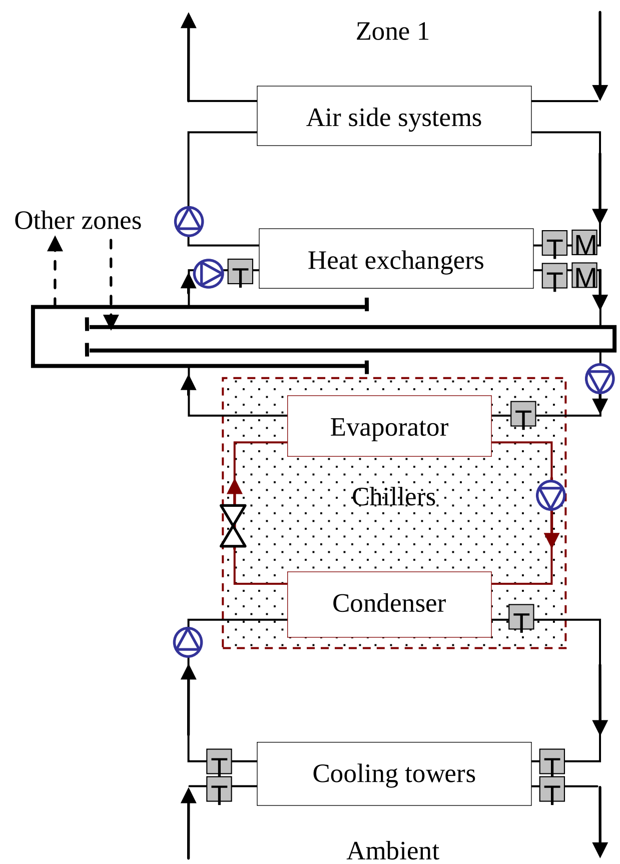

Figure 5.4 Aggregate HVAC sub-systems and sensors serving *Zone* 1

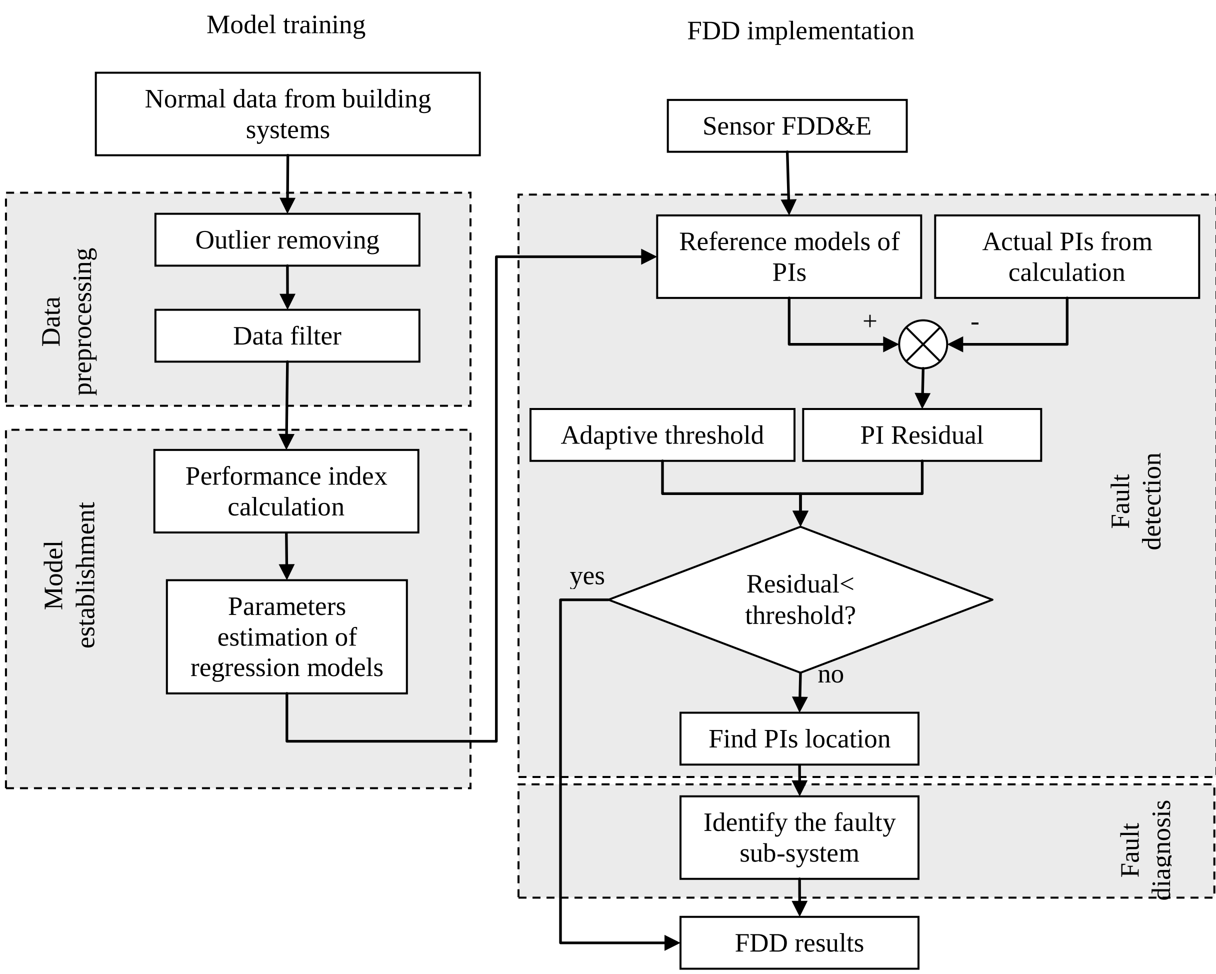

Figure 5.5 Schematics of the system FDD module

5.3.2 Data Preprocessing

Data collected from the site are usually containing outliers, noise and even errors. Detecting and diagnosing the errors are one of tasks as delivered in Section 5.4. As for the noise and outliers, they are the main concern in this section in terms of preprocessing. Data preprocessing is used to transform the raw data into a format which is useful and effective for some purposes. Two functions of data preprocessing named outlier removing and data filtering are helpful to make the FDD scheme more reliable and convincible. Although the data preprocessing does not include a steady-state detector, the data processed by data filter and outlier removal can satisfy the use of the FDD strategy. One can also use a steady-state filter which may be defined diversely to achieve the data preprocessing purpose.

a. outlier removing

In a data set, some points may dramatically differ from the rest and do not appear to be consistent with most the data. These points can be considered as the outliers. In this study, if a data value is more than three standard deviations away from the mean, it will be removed from the data set as an outlier.

There is a risk in the data outlier removing. Removing an outlier leads to a smaller standard deviation of the remaining data. This is risky to the remaining data as some points may be falsely detected.

b. data filtering

A data filter is used to eliminate the noise such as high-frequency fluctuations. A general tapped delay-line filter as follows is used in this study.

$$a_1 \cdot y_n = \sum_{i=1}^{N_a} b_i \cdot x_{n-N_a+1} - \sum_{j=2}^{N_b} a_j \cdot y_{m-N_b+1} \tag{5.1}$$

Where, n is the index of the data, N_a is the order of the polynomial described by vector a, and N_b is the order of the polynomial described by vector b. The output y_n is a filtered data decided by the current and previous inputs, x_n, x_{n-1}..., and previous outputs, y_{n-1},y_{n-2}….

Specifically, a moving-average filter with a four-interval window is used to smooth the data. *a* and *b* are equal to 1 and 1/4 respectively.

$$y_n = \frac{1}{4}x_n + \frac{1}{4}x_{n-1} + \frac{1}{4}x_{n-2} + \frac{1}{4}x_{n-3} \tag{5.2}$$

5.3.3 Performance Indices (PIs) and Fault Modeling

Table 5.2 shows various typical faults usually happening in HVAC sub-systems. How to model the system faults and PIs proposed to indicate the operating status (normal or faulty) of these sub-systems is also presented in this table. These faults are introduced into sub-systems on the simulation platform one by one. It is realized by tuning the parameters of the related dynamic model in the platform. There are many kinds of faults possibly occurring in HVAC systems. To validate the effectiveness of the system FDD system at the system level, one or two faults are considered in each HVAC sub-system. A detailed description on how to model the faults and how to determine the PIs is discussed as follows.

Table 5.2 Typical faults and their modeling methods of HVAC sub-systems and corresponding mathematical PI formulations

System	Fault	Fault modeling	PI Formulation
Cooling tower system	motor degradation	air flow rate reduction	$\varepsilon_{T\_CT} = \frac{T_{win\_CT} - T_{wout\_CT}}{T_{win\_CT} - T_{wetin}}$ $T_{approach\_CT} = T_{wout\_CT} - T_{wetin}$ $W_{CT} = \sum W_{i\_CT}$
Chiller system	motor degradation or condenser and evaporator fouling,	increase electromechanical power loss, decrease heat transfer coefficient of chillers	$COP = \frac{\sum COP_i}{n}$ $W_{chiller} = \sum W_{i\_chiller}$
Secondary (variable-speed pump) pump system	partially clog in the pipe	increase the pipe resistance	$W_{pump} = \sum W_{i\_pump}$
Heat exchanger system	tube fouling	decrease the heat transfer coefficient	$UA_{HX} = \frac{Q_{HX}}{LMTD_{HX}}$ $\varepsilon_{T\_HX} = \frac{T_{wout\_bfHX} - T_{win\_bfHX}}{T_{win\_afHX} - T_{win\_bfHX}}$ T_{wout_bfHX}, measurement

a. cooling tower system

For the cooling tower system, the unhealthy performance may be caused by typical faults such as motor degradation and heat transfer degradation. To simulate the motor fault of cooling towers, the mass air flow rate is decreased by two levels through reducing the coefficients of dynamic models of cooling towers. These coefficients are not the inputs to the other units of

TRNSYS, so the modification of these coefficients only affects the operating performance of the cooling tower system. The operating performance of other sub-systems may be affected indirectly by the deterioration of cooling tower system performance. The temperature effectiveness, approach temperature and power consumption are chosen to model PIs based on Ahn et al. (2001). These three PIs were proved to be valid in diagnosing the fan fault due to blockage and motor degradation in their study. The discharge water temperature should have been chosen as a PI because the residual of discharge water temperature between the prediction by the model and the monitored value can indicate if it is out of control and how much it affects the operating performance of the chiller system. However, it is not included for evaluating the cooling tower system performance since it has the same PI residuals with the approach temperature.

b. chiller system

For the chiller system, the unhealthy performance may be caused by some typical faults such as motor degradation and condenser fouling etc. The faults of motor degradation and chiller fouling are introduced into the chiller system by increasing electromechanical power loss and decreasing heat transfer coefficient of condensers and evaporators. These two parameters are constant input of the dynamic models on the simulation platform. Some researchers discussed how to use the COP to indicate its operating performance in different faulty conditions such as Cui and Wang (2005), Comstock et al. (2001) and McIntosh and Mitchell (2000) etc. It is sensitive to almost all kinds of chiller faults. Power consumption is a noticeable PI to evaluate economic impact of the fault on the electricity consumption. Chilled water supply temperature is usually maintained at the fixed set point. Its large bias may cause an alarm in the building management system (BMS), so it is not considered in the chiller system diagnosis. However, it is still a basic and important performance indicator to monitor the chiller system status.

c. heat exchanger system

For the heat exchanger system, the performance degradation may be caused by typical faults such as tube fouling and blockage etc. In the dynamic simulation, classical ε-*NTU* method is used to model the performance of heat exchangers (Wang 1998). The overall conductance-area product (UA_{design}) at the design condition is a parameter of the heat exchanger model. Reducing this parameter simulates the tube fouling or performance degradation of heat transfer efficiency. The conductance-area product and temperature effectiveness are typically used to evaluate the heat transfer efficiency of the heat exchanger. Like the chilled water supply temperature, the outlet water temperatures after HX is controlled at its set-point and useful to indicate if it is out of control and how much it affects the operating performance of the AHU system, but it is not included in the PIs.

d. Secondary variable-speed pump (SCHWP) system

For the SCHWP system both before HX and after HX, the unhealthy performance may be caused by typical faults such as pipe leakage, partial clog and motor degradation. The pipe resistance as a constant input of the dynamic variable-speed pump model is increased to simulate the fault of the partial pump or pipe clog in the secondary pump system both before HX and after HX. It causes more power consumption of pump system using a fixed differential pressure control strategy. The fault is introduced into the secondary pump system by increasing the pipe resistance.

Power consumption corresponding to water flow rate is a sensitive PI. to indicate the performance and to evaluate economic impact of the fault.

Because one chiller is dedicated to one constant-speed condenser water pump and one constant-speed primary chilled water pump, the operating performance can be evaluated by simply monitoring the water flow rate and pump power in practical applications. Therefore, performance monitoring and FDD for the condenser pump system and primary pump system are not considered in this study.

5.3.4 Reference Models for HVAC Systems

Reference models of PIs are used to characterize the fault-free operating status of different HVAC sub-systems. They are established in a regression pattern by choosing the driving variables as the regressors. Chilled water supply temperature (T_{wout_EV}), entering condenser water temperature (T_{win_CD}) and cooling load are commonly used as driving variables in the regression model of the chiller system as discussed in Braun (1988), Cui and Wang (2005). Similarly, the reference models of PIs for the cooling tower and heat exchange are established by choosing related driving variables in this study. The driving variables in the reference models of cooling tower PIs are total heat rejection, inlet water temperature and inlet air wet-bulb temperature. The driving variables in the reference models of HX PIs are two inlet water temperatures and two water mass flow rates before and after HX. The reference model for the variable-speed pump is established using a fourth-order polynomial function of mass flow rate. Although all these regression models are developed for single components, they can be used in a system which is composed of a number of these components of the same type and capacity. For example, chillers used in this building are the same in terms of type, capacity and working conditions. For the system which has a combination of components with different types and capacities (e.g. cooling towers in this building have two capacities, six in one group, the other five in another group), the regression model can also be used to estimate the PIs of a system due to its mechanism of parameters recognition. For the other sub-systems, the components of the same type and capacity are installed in parallel connection for a system. The models of PIs for different HVAC sub-systems are summarized as follows.

a. PI models of aggregate cooling towers

$$PI_{CT} = \sum_{i=0}^{2}\sum_{j=0}^{2}\sum_{k=0}^{2} a_{ijk} \cdot Q_{tot\_CT}^{i} \cdot T_{win\_CT}^{j} \cdot T_{airin\_wb}^{k} \tag{5.3}$$

b. PI models of aggregate chillers

$$PI_{chiller} = \sum_{i=0}^{2}\sum_{j=0}^{2}\sum_{k=0}^{2} b_{ijk} \cdot Q_{tot\_chiller}^{i} \cdot T_{chws}^{j} \cdot T_{ecw}^{k} \tag{5.4}$$

c. PI models of aggregate heat exchangers

$$PI_{HX} = \sum_{i=0}^{1}\sum_{j=0}^{1}\sum_{k=0}^{1}\sum_{l=0}^{1} c_{ijkl} \cdot T_{in\_bfHX}^{i} \cdot T_{in\_afHX}^{j} \cdot M_{bfHX}^{k} \cdot M_{afHX}^{l} \tag{5.5}$$

d. PI models of aggregate variable-speed pumps

$$PI_{pump} = \sum_{i=0}^{3} d_i \cdot M_{pump}^{i} \tag{5.6}$$

5.3.5 On-line Estimation of FDD Threshold

The FDD thresholds of these PI residuals are the standard to evaluate if the residuals of PIs are in normal range or not. The on-line estimation of the FDD threshold is derived from uncertainty of the fitting errors of the reference models and the propagation of the current measurement errors. The two uncertainties are both affected by the operation conditions.

Given a certain confidence level, the FDD threshold of PI residuals is determined by,

$$\begin{aligned} Th_{0,i} &= U(\tilde{r}_i) \\ &= t_{\alpha/2, n-p}\,\tilde{\sigma}_{\tilde{r}_i - r_i} \end{aligned} \tag{5.7}$$

Where, $Th_{0,i}$ is the threshold of the ith PI residual, $\tilde{r}_i$ is the estimator of the residual of the ith performance index. The residual (r_i) is the difference between the measurement and model predicted value of the ith performance index. $U(\tilde{r}_i)$ is the uncertainty of the residual at a certain confidence level. $\tilde{\sigma}^2_{\tilde{r}_i - r}$ is determined by Equation 5.8 and $t_{\alpha/2, n-p}$ is the value of the t distribution with n-p degrees of freedom at a confidence level of (1-α). n is the number of training data points used in the model regression and p is the number of coefficients estimated from the training data.

$$\tilde{\sigma}^2_{\tilde{r}_i - r_i} = \underbrace{\sum_j \left[\left(\frac{\partial g_i}{\partial z_j}\right)\sigma_{z_j}\right]^2}_{\textit{Uncertainty 1}} + \underbrace{\tilde{\sigma}^2_{Y_i}[1 + \mathbf{X}_0^T(\mathbf{X}^T_{reg}\mathbf{X}_{reg})\mathbf{X}_0]}_{\textit{Uncertainty 2}} \tag{5.8}$$

Where, g_i is the formula for calculating the ith performance index as shown in Table 5.2. z_j is the jth element in the vector of measured variables ($\mathbf{z}$), which is used to calculate the ith performance index (Y_i). σ_{z_j} is the standard deviations of z_j and $\tilde{\sigma}^2_{Y_i}$ is the estimated variance of the regression error of *i*th performance index. $\mathbf{X}_0$ is the vector of regressors for the current prediction and $\mathbf{X}_0^T$ is the transpose of $\mathbf{X}_0$. $\mathbf{X}_{reg}$ is the matrix of regressors associated with the training data and $\mathbf{X}_{reg}^T$ is the transpose of $\mathbf{X}_{reg}$. *Uncertainty 1* is measurement uncertainty and *Uncertainty 2* is modeling uncertainty.

5.4 Formulation of the Sensor FDD&E Module

5.4.1 Sensor Fault Modeling

Usually the sensor faults can be categorized into two types, hard failure and soft failure (such as bias error). The hard failure is very harmful to the stability of the system especially when the sensor is a feedback point in the control strategy. However, it can be easily found using value limitation widely adopted by BMS as an alarm trigger. Bias error is difficult to be detected and has potentially negative impacts on the data analysis and performance evaluation. In the proposed HVAC system-level FDD scheme, PI calculation and PI models are affected by the health of sensor measurements.

In the HVAC system of concern, totally eight sensors are considered in FDD&E. They are the inlet air dry-bulb temperature of cooling towers (T_{dryin}), inlet water temperature of cooling towers (T_{win_CT}) related to ε_{T_CT} and $T_{approach\_CT}$, inlet water temperature of evaporators (T_{win_EV}) related to *COP*, inlet water temperatures before HX and after HX (T_{win_bfHX} and T_{win_afHX}), outlet water temperature before HX (T_{wout_bfHX}) related to these three proposed PIs of the heat exchanger system, and water flow rates before HX and after HX (M_{bfHX} and M_{afHX}) related to power consumption of the corresponding SCHWP system. The faults are introduced into these sensors by adding a fixed bias to model the sensor soft fault. Only one sensor bias was considered in each test in this study.

5.4.2 Introduction of PCA

As a multi-variate statistical process control (SPC) method, PCA can be used to transform a number of correlated variables to a lower dimension of uncorrelated variables without much loss of information. An observation space of variables can be divided into two sub-spaces by PCA, principal component subspace (score space) and residual subspace. The component subspace captures the relationship between the variables, while the residual subspace accounts for the random noise in the variables. The detailed introduction on PCA method can be referred to Jolliffe (2002).

Assume a group of data with n samples and m variables, $\mathbf{Z}$ ($\mathbf{Z} \in \Re^{n \times m}$). To avoid the influence of different units of variables, normalization is needed firstly by using the operations of mean and standard deviation. A new matrix is formed with x as elements.

$$M_i = \frac{1}{n}\sum_{j=1}^{n} z_{j,i} \tag{5.9}$$

$$\sigma_i = \sqrt{\frac{1}{n-1}\sum_{j=1}^{n}(z_{j,i} - M_i)^2} \tag{5.10}$$

$$x_{j,i} = \frac{z_{j,i} - M_i}{\sigma_i} \tag{5.11}$$

Where, M_i is the mean of the ith variable, σ_i is standard deviation of the ith variable.

The covariance matrix of the new variable observations **X** ($\mathbf{X} \in \Re^{n\times m}$) is

$$\mathbf{S} = \frac{\mathbf{X}^T \mathbf{X}}{n-1} \tag{5.12}$$

To obtain the loading matrix (**U**), the eigenvalue decomposition of **S** is needed,

$$\mathbf{S = U\Lambda U}^T \tag{5.13}$$

$\mathbf{\Lambda}$ ($\mathbf{\Lambda} \in \Re^{m\times m}$) is the diagonal matrix with non-negative real elements in decreasing magnitude order. These elements are the eigenvalues of **S**, and **U** ($\mathbf{U} \in \Re^{m\times m}$) contains the corresponding eigenvectors. Where, $\mathbf{UU}^T$=**I.**

$$\mathbf{\Lambda} = \begin{bmatrix} \lambda_1 & & & \\ & \lambda_2 & & \\ & & \cdots & \\ & & & \lambda_m \end{bmatrix} \tag{5.14}$$

Usually in PCA method, a minimal number of eigenvectors in **U** are retained to capture the original interrelationship among different variables. This number is decided by how many eigenvalues are kept to satisfy the predetermined *CPV* (cumulative percent variance).

$$CPV(a) = \frac{\sum_{j=1}^{a} \lambda_j}{\sum_{j=1}^{m} \lambda_j} \times 100\% = \frac{\sum_{j=1}^{a} \lambda_j}{tr(\mathbf{S})} \times 100\% \geq CPV_\alpha \tag{5.15}$$

Where, a is number of eigenvalues, $tr(\mathbf{S})$ is the trace of the covariance matrix (**S**). CPV_α, is the predetermined benchmark, e.g., 95%

The first a (a is a number) largest eigenvalues are the principal components (PCs). The retained eigenvectors which has the same dimension of eigenvalues are the loading matrix, **P** ($\mathbf{P} \in \Re^{m \times a}$). There are some other methods to determine the number a such as the proportion of trace explained method and the screen test (Jolliffe 2002).

Using the loading matrix **P** to determine the same dimensional loading vectors in **U**, one can obtain the projections of the observations. The lower dimensional space is **Y** ($\mathbf{Y} \in \Re^{m \times a}$).

$$\mathbf{Y} = \mathbf{XP} \tag{5.16}$$

A new term called the score subspace is deduced from **Y** and **P**. It is representative of the largest portion of correlated relationship of the normalized process variables.

$$\hat{\mathbf{X}} = \mathbf{YP}^T = \mathbf{XPP}^T \tag{5.17}$$

The difference between **X** and $\hat{\mathbf{X}}$ is defined as the residual subspace, **E. E** reflects the remaining interrelationship which the score subspace cannot explain.

$$\mathbf{E} = \mathbf{X} - \hat{\mathbf{X}} = \mathbf{X} - \mathbf{XPP}^T = \mathbf{X}(\mathbf{I} - \mathbf{PP}^T) \tag{5.18}$$

The relationship between the **X,** $\hat{\mathbf{X}}$ and **E** are shown in Figure 5.6. From Figure 5.6, the PCA method decomposes a vector into two orthogonal subspaces. One is the score subspace which accounts for the main variation; the other is the residual subspace which reflects the minor variation or noise.

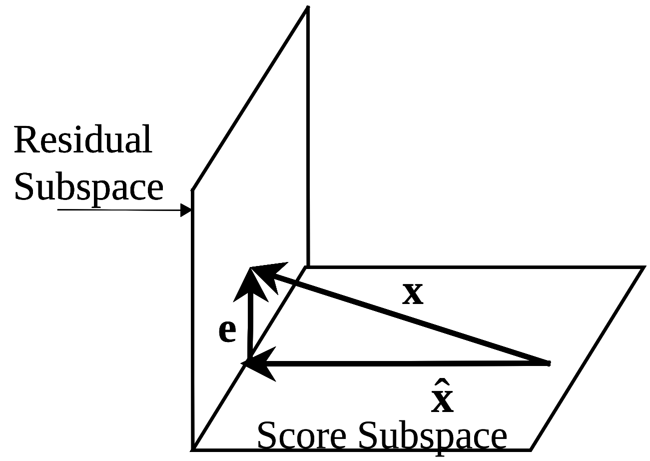

Figure 5.6 Decomposition of a normalized vector

5.4.3 PCA Models for Sensor FDD&E

5.4.3.1 Application of PCA Method in FDD

One can follow the procedure described in Figure 5.7 to understand how to implement the PCA method both in training process and FDD process. In the training process, the training data in normal conditions are processed by outlier removing and data filter to eliminate the noise and outliers. The processed data are then normalized with zero and unit variance to eliminate the influence of different units of variables. The normalized data are used to determine the eigenvalues and eigenvectors of the covariance matrix. By determining the number of eigenvalues using *CPV*, the same dimensional eigenvectors are decomposed into score space and residual space. In the FDD process, the score subspace is used to calculate the estimate of the new data. The Q-statistic determined by the new data and their estimates is compared with the threshold to judge whether the data are in healthy conditions or not. How to determine the Q-statistic and its threshold is stated in this section.

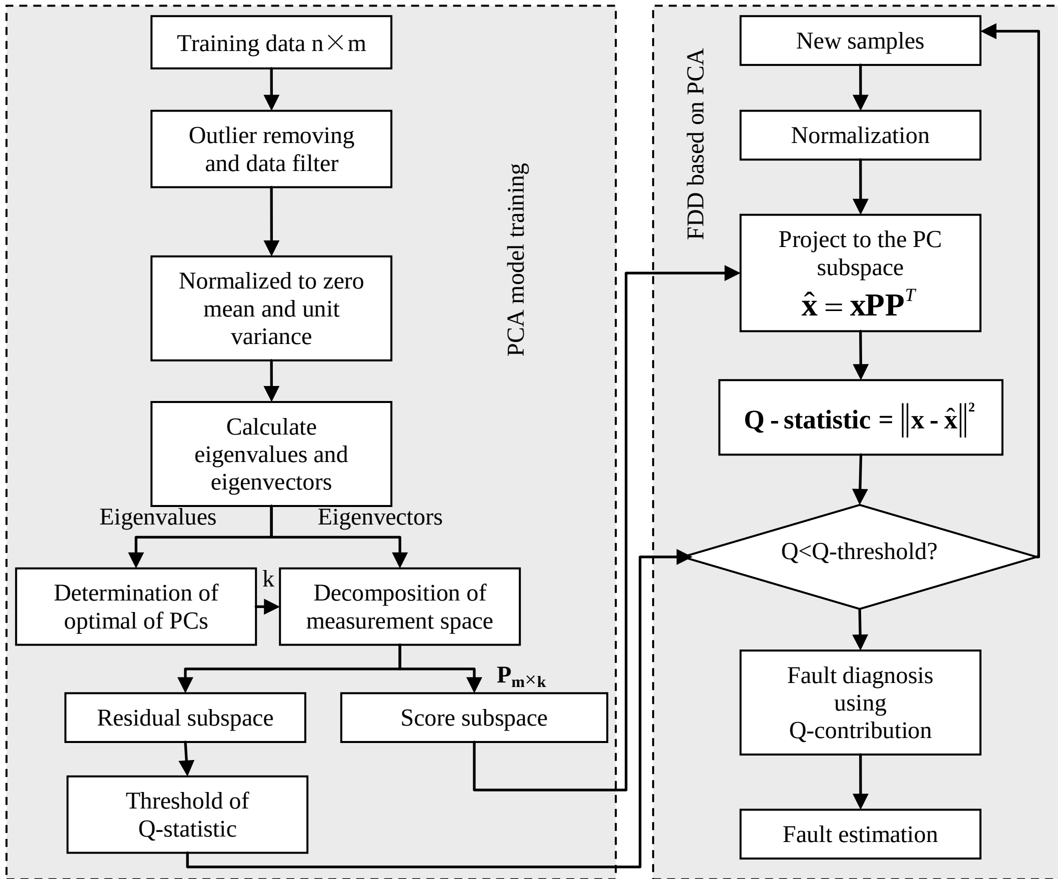

Figure 5.7 Flow chart of the application of PCA method in FDD

The PCA method can use T^2-statistic (Kresta et al. 1991) and Q-statistic (Jackson and Mudholkar 1979) to indicate the sensor measurement health status.

The Q-statistic is also known as the squared prediction errors (SPE). It is defined as the squared sum of residuals between sensor measurements ($\mathbf{x}$) and their estimates ($\hat{\mathbf{x}}$).

$$Q - statistic = SPE = \mathbf{e}^T\mathbf{e} = \|\mathbf{x} - \hat{\mathbf{x}}\|^2 = \left\|\mathbf{x}\left(\mathbf{I} - \mathbf{P}\mathbf{P}^T\right)\right\|^2 \tag{5.19}$$

A threshold of the Q-statistic, proposed by Jackson (1991), is adopted as the benchmark to determine the normal range.

$$Q_\alpha = \theta_1 \left[\frac{c_\alpha \sqrt{2\theta_2 h_0^2}}{\theta_1} + 1 + \frac{\theta_2 h_0 (h_0 - 1)}{\theta_1^2} \right]^{\frac{1}{h_0}} \tag{5.20}$$

Where, $\theta_i = \sum_{j=a+1}^{m} \lambda_j^i \quad (i = 1,\ 2,\ 3)$, $h_0 = 1 - \frac{2\theta_1\theta_3}{3\theta_2^2}$, c_α is the confidence limit for the $1-\alpha$ percentage in a normal distribution; *a* is the number of principal components; *m* is the number of variables and λ_j are the eigenvalues of the covariance matrix.

T^2-statistic is very effective to detect the change of the data variation, but a little too sensitive to reflect the true violation due to sensor faults especially when the sampling interval is short. In this study, Q-statistic is chosen as the indicator to evaluate the sensor performance.

The sensor FDD&E is accomplished in main three steps, fault detection, fault diagnosis and fault estimation.

a. Fault detection

The training data in normal conditions are used to determine the score subspace and residual subspace. The former captures the most variation of the sensor measurements, while the latter involving some noises are still in the acceptable range. The noises are considered into the threshold of the Q-statistic. The new samples of the sensor measurements are used to deduce the estimates by the PCA model using the score subspace of the training data. If the new samples do not contain sensor faults, the interrelationship of the sensor measurements is remained almost the same as the training data. The Q-statistic should be below threshold as shown in Equation 5.21. But if one or more sensor faults occur, the interrelationship of new sensor measurements will be broken. It results in the violation of Q-statistic from the threshold.

$$Q - statistic \leq Q_\alpha \tag{5.21}$$

b. Fault diagnosis

The sensor fault detection using the Q-statistic is the first step. The following step is to isolate the faulty sensors among a group of sensor measurements. It can be realized by calculating the contribution of each sensor measurement to the Q-statistic.

$$\eta_i = \frac{\|e_i\|^2}{Q - statistic} \tag{5.22}$$

Where, e_i presents the *i*th element of the residual vector **e** and η_i is the contribution of the *i*th variable to the squared sum of the residual vector.

The larger contribution of a sensor measurement leads to the more confidence of fault diagnosis. Therefore, the sensor fault is diagnosed by choosing the largest contribution which corresponds to a sensor measurement.

c. Fault estimation

In the real system, the performance evaluation is significantly affected by the sensor health. Although the unhealthy sensors can be detected using Q-statistic and diagnosed using Q-contribution, the true sensor readings are still unknown in real time. Before the commissioning of the faulty sensors or replacement with new ones, the control strategy, performance evaluation and FDD methods are still not reliable. Sensor fault estimation is a method to correct the fault in terms of reading. The recovery of the biased measurement is expected to be as close to the normal reading as possible. An iteration approach is used to fulfill this task as the following equation.

$$\hat{x}_i^{new} = \mathbf{x}\begin{bmatrix}\mathbf{c}_{-i} & 0 & \mathbf{c}_{+i}\end{bmatrix}^T + \hat{x}_i^{old} c_{ii} \tag{5.23}$$

Where, $\hat{x}_i^{new}$ is the new reconstruction by the PCA model; $\hat{x}_i^{new}$ is the estimation before the new estimation; **c** is obtained from the following deduction.

$$\begin{aligned}\hat{x}_i &= \mathbf{x}\,\mathrm{p}_i\mathrm{p}_i^{\mathrm{T}} \\ &= \mathbf{x}\,\mathbf{c}_{\mathrm{i}} \\ &= \begin{bmatrix}x_1 & x_2 & \cdots & x_i & \cdots & x_m\end{bmatrix}\begin{bmatrix}c_{1i} & c_{2i} & \cdots & c_{ii} & \cdots & c_{mi}\end{bmatrix}^T \\ &= \mathbf{x}\begin{bmatrix}\mathbf{c}_{-i} & 0 & \mathbf{c}_{+i}\end{bmatrix}^T + x_i c_{ii}\end{aligned} \tag{5.24}$$

The iteration for calculating the reconstruction of faulty sensor measurement proceeds until the new sensor reconstruction converges to a value (x_i^*).

$$x_i^* = \frac{\mathbf{x}\begin{bmatrix}\mathbf{c}_{-i} & 0 & \mathbf{c}_{+i}\end{bmatrix}^T}{1 - c_{ii}} \quad \text{when} \quad c_{ii} < 1, \tag{5.25}$$

For the case of $c_{ii} = 1$, $x_i^* = x_i$, It implies that the sensor measurement is not correlated to the other sensor measurements. The sensor fault estimation method will fail in such occasion. However, it can be avoided because the sensor measurements selected in the construction of sensor matrix are correlated with each other based on the heat balance.

There are some other approaches to accomplish the sensor fault recovery work, such as the missing data replacement method (Martens and Naes 1989) and the optimization method (Wise and Ricker 1991).

The sensor bias estimation and comprehensive description of application of PCA in AHU sensor FDD and chiller sensor FDD can be referred to Wang and Xiao (2004) and Wang and Cui (2005) respectively.

5.4.3.2 Construction of PCA Matrix for Sensor FDD&E

The PCA model is established based on two considerations. One is the energy balance in which the sensor measurements are correlated with each other. The other is if the sensor measurement is useful for system performance evaluation. The energy balance exists in HVAC sub-systems including the cooling tower system, chiller system, heat exchanger system and water pipes as shown in the following equations.

a. Heat balance in the cooling tower system

$$M_{air} \cdot (h_{airout} - h_{airin}) = C_{pw} \cdot M_{w\_CT} \cdot (T_{win\_CT} - T_{wout\_CT}) \tag{5.26}$$

b. Heat balance in the chiller system

$$C_{pw} \cdot M_{w\_CT} \cdot (T_{wout\_CD} - T_{win\_CD}) \approx C_{pw} \cdot M_{w\_EV} \cdot (T_{win\_EV} - T_{wout\_EV}) + W_{chiller} \tag{5.27}$$

c. Heat balance in the heat exchanger system

$$C_{pw} \cdot M_{bfHX} \cdot (T_{wout\_bfHX} - T_{win\_bfHX}) = C_{pw} \cdot M_{afHX} \cdot (T_{win\_afHX} - T_{wout\_afHX}) \tag{5.28}$$

The enthalpy can be expressed using the web-bulb temperature and dry-bulb temperature. Among the sensor measurements involved, T_{wout_CT}, and T_{win_CD} are measured using the same sensor in this study. They together with T_{wout_EV} and T_{out_afHX} are controlled at their fixed set-point.

M_{w_CT} and M_{w_EV} are constant due as constant speed pumps are used in the condenser water system and primary chilled water system. All the sensors with their measured variables controlled at fixed set-points are not included in PCA models for sensor FDD&E. Power meter faults of chillers, cooling towers and pumps are not considered because these sensors have less potential to be biased. A few tests were conducted to find a most suitable PCA matrix which is sensitive to the biases of all the eight sensors. A PCA matrix is finally constructed using the correlated sensor measurements for sensor FDD&E as described in Equation 5.29. Although the sensor measurements of T_{wetin}, T_{dryout}, T_{wout_CT} and W_{pump_afHX} are not considered in the sensor FDD&E, they are included in the construction of PCA models as they can improve the performance of the PCA model.

$$\begin{aligned} A = [&T_{wetin} \;\; T_{dryin} \;\; T_{dryout} \;\; T_{wout\_CT} \;\; T_{win\_CT} \;\; T_{win\_ev} \;\; T_{out\_bfHX} \;\ldots\ldots \\ &T_{in\_bfHX} \;\; T_{in\_afHX} \;\; M_{afHX} \;\; M_{bfHX} \;\; W_{pump\_afHX}] \end{aligned} \tag{5.29}$$

5.5 Summary

A fault detection and diagnosis scheme is developed for HVAC systems involving sensor faults. The HVAC sub-systems include cooling tower system, chiller system, SCHWP system before heat exchangers, heat exchanger system and SCHWP system after heat exchangers. One or more performance indices are proposed to indicate the performance status of each sub-system. The reference model of PIs of each HVAC sub-system is also proposed in regression patterns. The on-line adaptive thresholds determined by training data and monitored data are used as the normal ranges of PI residuals. The sub-system which has highest detection ratios (usually not less than 50%) of PI residuals is considered as faulty. The system faults are introduced by tuning the parameters of dynamic models on the simulation platform.

The sensor FDD&E module of the system-level FDD scheme is developed based on PCA method to detect and diagnose the sensor fault and correct the sensor bias. PCA is capable of capturing the interrelationship between different sensor measurements. If the variance of a new measurement samples is close to the training data (under the Q-threshold), the sensor measurements are considered as normal. If violated variance of the samples (out of the Q-threshold) is detected by the PCA method, these sensors will be diagnosed using the Q-statistic method. An iteration approach is developed to estimate the sensor bias and recover it for enhancing the performance of the system-level FDD scheme. The sensor recovery is a guarantee of data health before implementing the system FDD. Sensor faults are introduced by adding the fixed biases.

Not much research work can be found on the system-level FDD for a complex HVAC system. Although the PCA method for sensor FDD&E can be found in other system such as AHU, not much study can be found in the HVAC system-level FDD application. And the interaction between the sensor FDD and system FDD is also analyzed and discussed in the next chapter.

CHAPTER 6 VALIDATION OF THE FDD SCHEME FOR HVAC SYSTEMS

The FDD scheme for the HVAC systems at the system level is proposed in the Chapter 5. One function of the scheme is to isolate the system in the faulty condition using one or more performance indices. The other function is to detect and diagnose the sensor fault, and to correct the sensor bias for the use of the system FDD module. The validations of the system-level FDD scheme are presented in this chapter. These validations were conducted by using simulation data of normal tests and faulty tests of HVAC sub-systems of concern in a dynamic simulation platform.

Section 6.1 presents the validation results of the reference models of the defined performance indices of HVAC sub-systems of concern. The validations of both system FDD module and sensor FDD&E module of the FDD system are presented in Section 6.2 and 6.3 by artificially introduced system faults and sensor faults respectively. In Section 6.4, sensitivity analysis of sensor FDD&E to system faults is conducted. Subsequently, the validation of the system-level FDD scheme involving sensor faults and system faults existing simultaneously is presented in Section 6.5. Section 6.6 is the summary.

6.1 Validation of PI Benchmark Models

One-week (five working days) operation data of normal tests in the summer weather condition and one-week operation data of normal tests in winter weather condition are used for model training and model validation. The regression models of PIs of various HVAC sub-systems of concern were trained using the operation data of normal tests in three days in summer and the data in three days in winter respectively. The operation data of normal tests in the other two days in summer and two days in winter were used to validate these regression models. The validation results are shown in Figure 6.1 in terms of coefficient of determination (R^2). It can be seen that these PIs predicted by models fit well with those by calculation based on the measurements, as all the R^2 of identified reference models were larger than 90% except COP of the chiller system. The validation result of the COP model is acceptable with the largest relative error of only 0.61%.

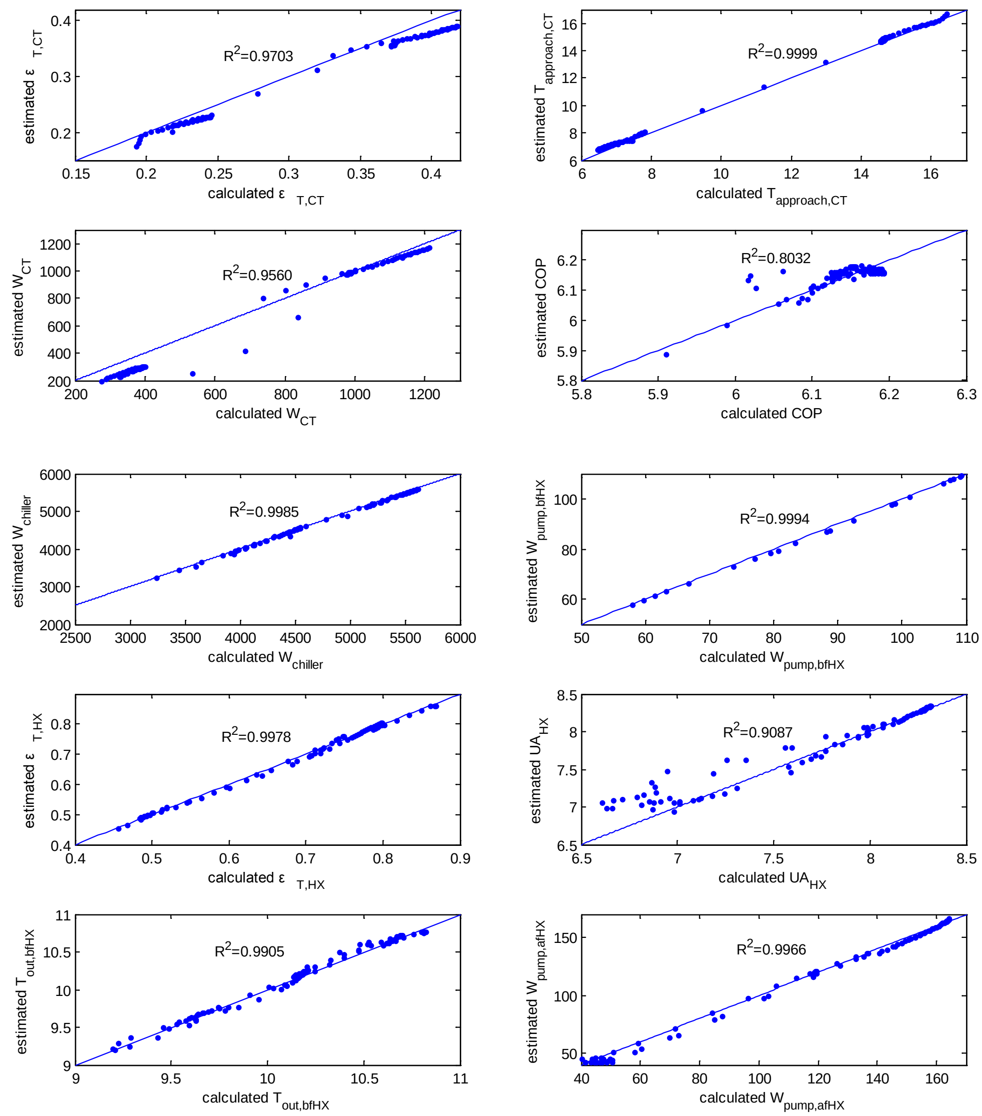

Figure 6.1 Estimated PIs vs calculated PIs of different HVAC sub-systems

6.2 Validation of the System FDD Module for HVAC Systems not Involving Sensor Faults

Tests were conducted in consecutive five days in summer season to generate normal operation data and fault operation data for the validation of the system FDD module. The normal operation data in the first consecutive three days were used to train the reference models of PIs. In the tests of the other two days, faults at two severity levels were introduced one by one to generate faulty data for validation. The introduction of various HVAC sub-system faults can be found as follows from section *a* to section *e*. To isolate the faulty one of the five sub-systems and consider the performance interaction between various sub-systems, all the PIs of the five sub-systems should be verified for each fault test. But due to the space limitation, only the validation results of PI residuals of the five sub-systems are shown in Figure 6.2 and 6.3 for only the fault test of cooling tower system at fault severity level 1. For other sub-system faulty tests, only their related PI residuals are shown in the following figures. All the quantitative validation results can be found in Table 6.1, where, the detection ratio is a percentage of the point number beyond the threshold among the total point number. In Table 6.1, all PI residuals of the five sub-systems were evaluated for each kind of faults in terms of detection ratios. The sub-system corresponding to the largest detection ratios (not less than 50%) of PI residuals is most likely to be faulty.

Table 6.1 Detection ratios of PI residuals for the fault tests of five HVAC systems

HVAC system	Faulty severity level	ε_{T_CT}	$T_{approach\_CT}$	W_{CT}	COP	$W_{chiller}$	ε_{HX}	UA_{HX}	T_{wout_bfHX}	W_{pump_bfHX}	W_{pump_afHX}
Cooling tower system	Level 1	30	32	100	0	61.3	0	4	0	0	0
	Level 2	100	100	100	40	84	0	5.3	0	8	0
Chiller system (power loss)	Level 1	8	8	14	16.7	78.7	0	4	0	8.7	0
	Level 2	20.7	18.7	18	100	100	0	2.7	0	7.3	0
Chiller system (heat transfer deterioration)	Level 1	12.7	11.3	12.7	36	80.7	0	0.7	0	8.7	0
	Level 2	20.7	17.3	17.3	70.7	89.3	0	3.3	0	8.7	0
SCHWP system before HX	Level 1	18.7	16	17.3	0	12	0	0.7	0	100	0
	Level 2	18.8	16.1	16.8	0	12.1	0	3.4	0	100	0
Heat exchanger system	Level 1	12.7	10	20.7	0	30	0	100	0.7	2.7	0
	Level 2	12.7	9.3	20.7	0	31.3	100	100	100	0	0
SCHWP system after HX	Level 1	18.7	14	16.7	0	19.3	0	9.3	0	17.3	35.3
	Level 2	12.7	8.7	16.7	0	32	0	23.3	8.1	18	99.3

a. Cooling tower system

PI residuals of the cooling tower system and chiller system deviated from the thresholds are shown in Figure 6.2 when the air flow rate of cooling towers was decreased by 10% (level 1). It can be seen that reduction of air flow rate by 10% resulted in the detection ratios of 100%, 30% and 32% for residuals of W_{CT}, ε_{T_CT} and $T_{approach\_CT}$ respectively. When the air flow rate reduced from 10% to 20% (level 2), all the detection ratios of the three PI residuals became 100% as shown in Figure 6.4. One may conclude that the most possible fault in HVAC systems may happen in the cooling tower system. The negative impact of the cooling tower system fault on the chiller system operating performance was enhanced with increased (false) detection ratios of COP and $W_{chiller}$ residuals by reducing the air flow rate from 10% to 20%. The air flow rate reduction at two levels almost had no effect on the other sub-systems as shown in Figure 6.3 and Table 6.1.

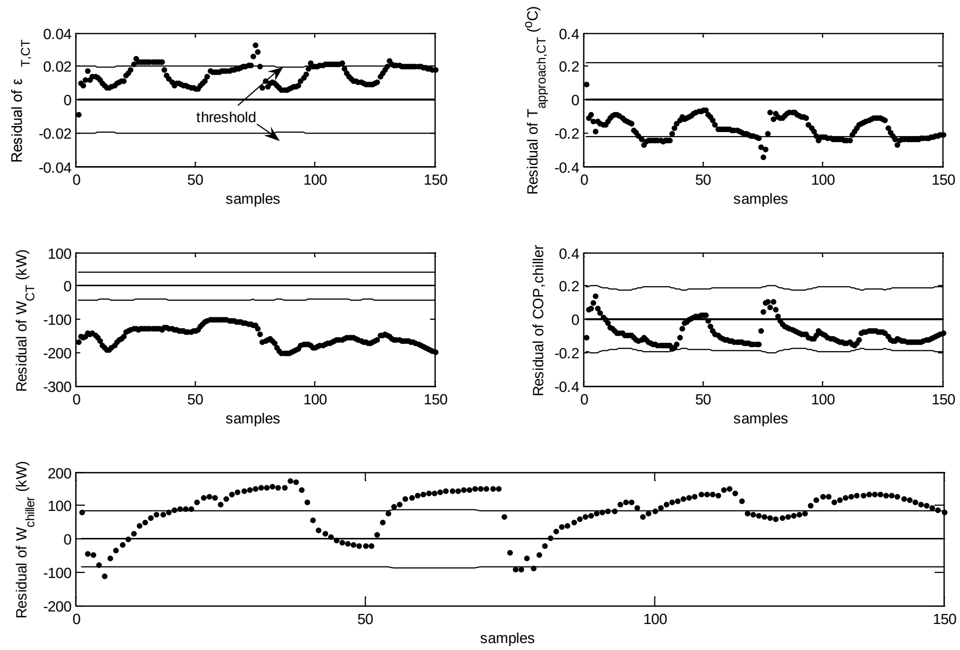

Figure 6.2 PI residuals of the cooling tower system and the chiller system with cooling tower air flow rate reduced by 10% (level 1)

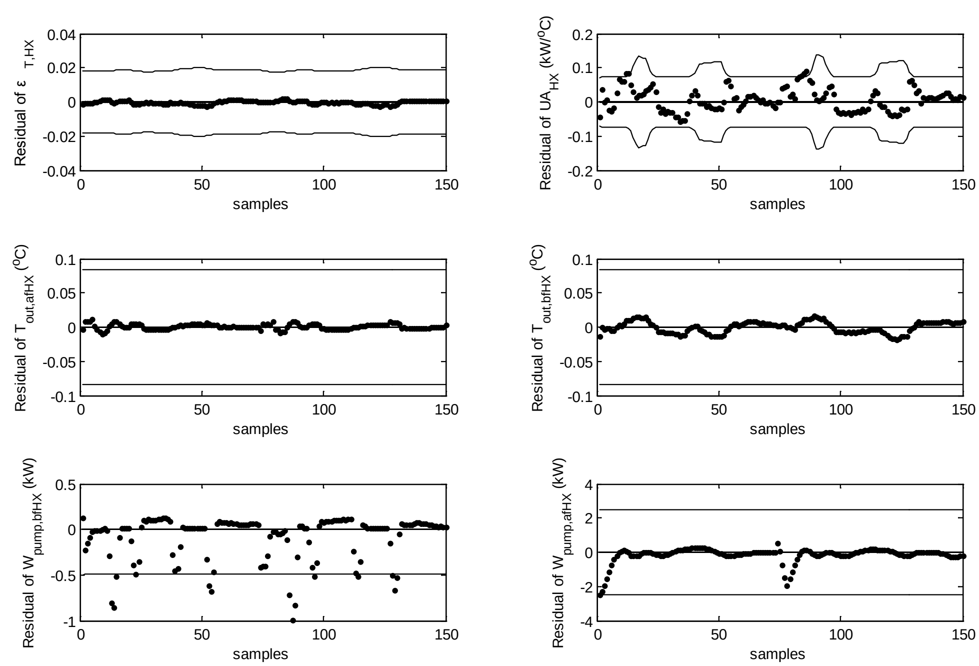

Figure 6.3 PI residuals of the heat exchanger system, secondary pump systems before and after the heat exchangers with cooling tower air flow rate reduced by 10% (level 1)

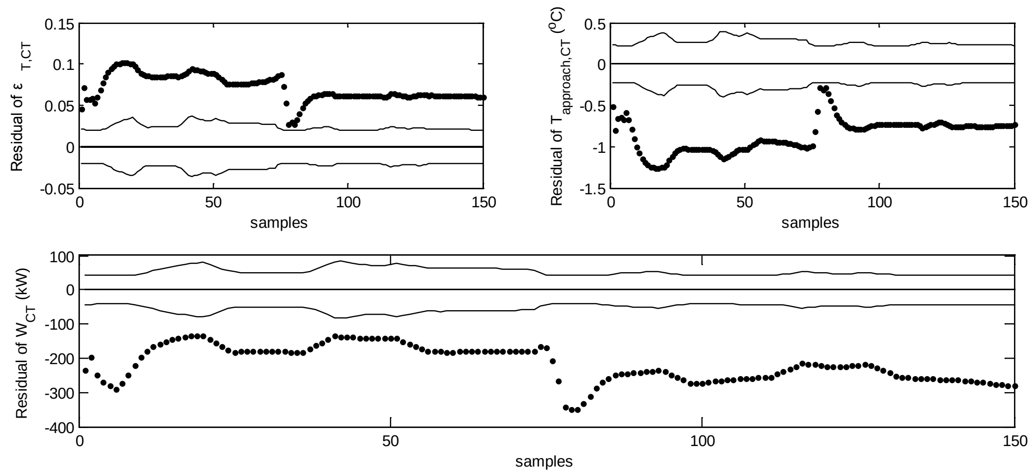

Figure 6.4 PI residuals of the cooling tower system and the chiller system with cooling tower air flow rate reduced by 20% (level 2)

b. Chiller system

Figure 6.5 shows the PI residuals and their thresholds of the chiller system when electromechanical power loss factor was increased by 5% (level 1) and 10% (level 2). Residual of $W_{chiller}$ was a sensitive PI to the electromechanical power loss at two severity levels with detection ratios of 78.7% and 100% respectively. Although residual of *COP* was not sensitive to the fault at level 1 with a detection ratio of 16.7%, it became sensitive to the fault at level 2 with a detection ratio of 100%.

Figure 6.6 shows the PI residuals of the chiller system when heat transfer coefficient of chillers (evaporator and condenser) was decreased by 20% (level 1) and 30% (level 2). Similar to the power loss in the chiller system, $W_{chiller}$ residual was sensitive to this fault both at level 1 and level 2 with detection ratios of more than 80%, while *COP* began to be sensitive when fault deteriorated from level 1 to level 2 with detection ratios of 36% and 70.7% respectively.

Although the impact of the chiller system faults (power loss and heat transfer deterioration) on the operating performance of other sub-systems became more noticeable by increasing the fault severity, the quantitative evaluation was not remarkable with regard to the (false) detection ratios of the PI residuals as they are all less than 21%. By identifying the fault using the highest detection ratios (not less than 50%) of PI residuals, one can also conclude that the most possible fault at two severity levels is the chiller fault.

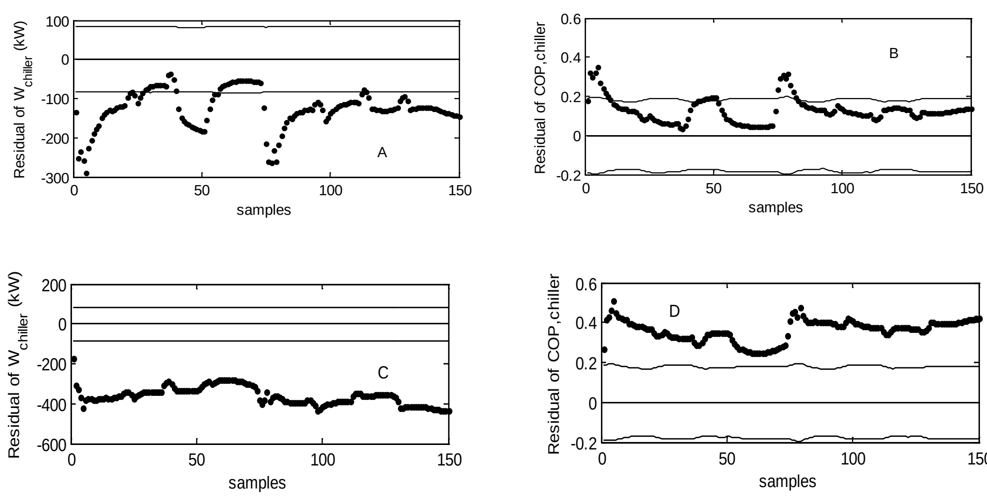

Figure 6.5 PI residuals of the chiller system with chillers electromechanical power loss increased by 5% (A-B) and 10% (C-D).

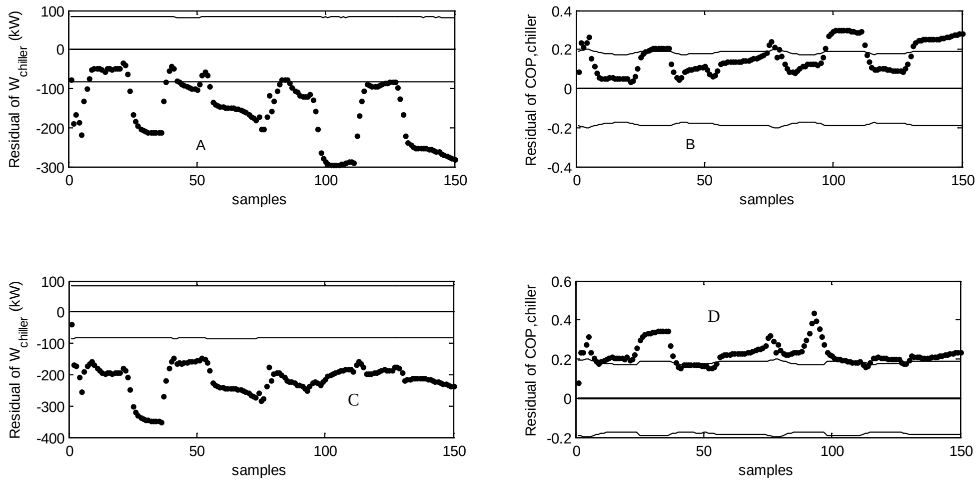

Figure 6.6 PI residuals of the chiller system with chillers heat transfer coefficient decreased by 20% (A-B) and 30% (C-D).

c. Heat exchanger system

Figure 6.7 shows the PI residuals and their thresholds of the heat exchanger system when the heat transfer efficiency was decreased by 10% (level 1) and 20% (level 2). Due to the degraded heat transfer efficiency, the temperature effectiveness, UA_{HX} and T_{wout_bfHX} were overestimated by the regression models compared with the monitored PIs. UA_{HX} was the most sensitive PI to this fault with detection ratios of 100% both at level 1 and 2. The other two PIs became sensitive when the heat transfer efficiency deteriorated from level 1 to level 2. The negative impact on operating performance of other sub-systems was not very significant with (false) detection ratios of less than 32%. Based on Table 6.1, the fault of heat exchanger system with degraded heat transfer efficiency can be identified by considering the largest detection ratios of PI residuals.

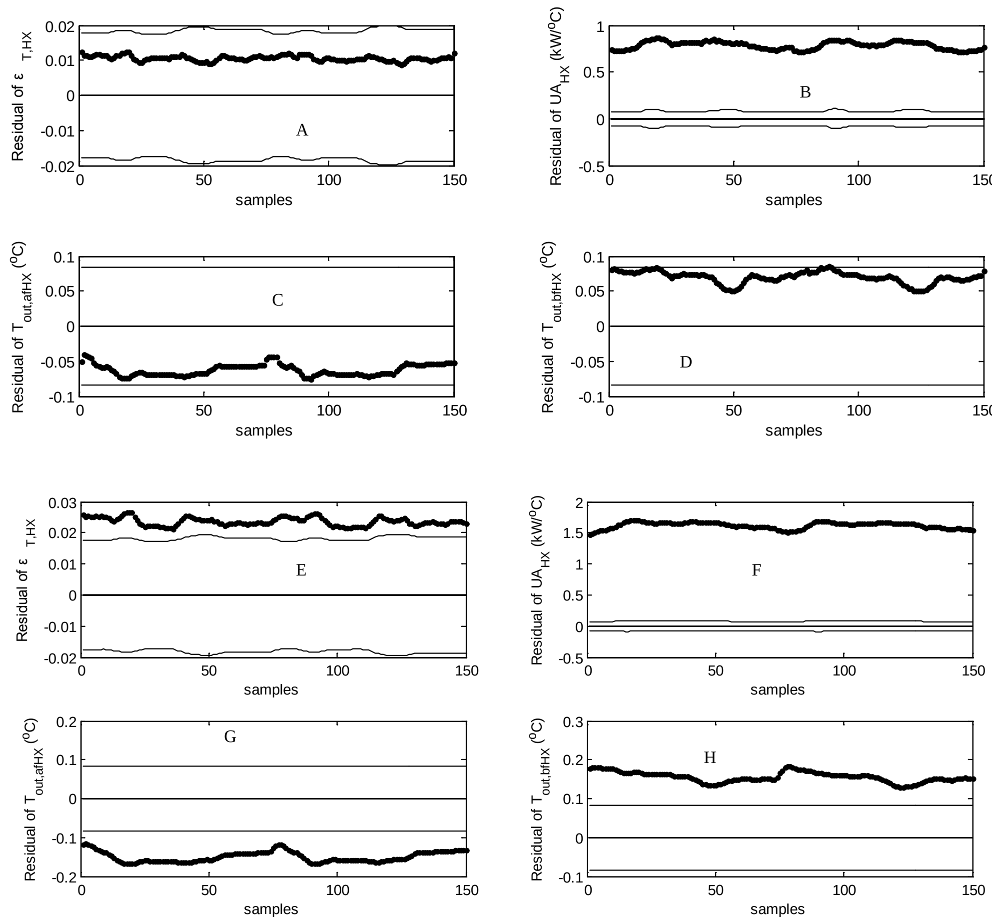

Figure 6.7 PI residuals of the heat exchanger system with heat transfer coefficient of heat exchangers reduced by 10% (A-D) and 20% (E-H)

d. Secondary pump system before heat exchangers

The validation results of FDD for SCHWP system before HX are shown in Figure 6.8 when the pipe resistance was increased by 5% (level 1) and 10% (level 2). Power consumption was a very sensitive PI to detect the clogged pump or clogged pipe line of the secondary pump system before HX with detection ratios of 100% both at level 1 and 2. Based on Table 6.1, it was easy to isolate this sub-system fault, because the (false) detection ratios of other PI residuals were all less than 20%.

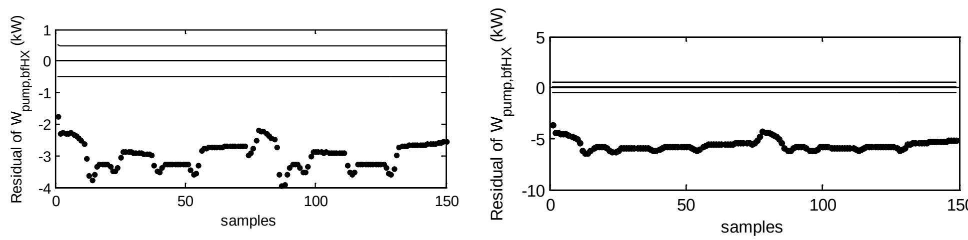

Figure 6.8 PI residuals of the secondary pump system before the heat exchangers with the pipe resistance increased by 5% (A) and 10% (B)

e. Secondary pump system after heat exchangers

Similarly to the SCHWP system before HX, the clogged pumps or clogged water pipe line of the SCHWP system after HX was introduced by increasing the pipe resistance by 10% (level 1) and 20% (level 2). The results are shown in Figure 6.9. The power as a PI was not very sensitive to the fault at level 1, but could detect the fault at level 2 with 100% of detection ratios. The other PI residuals with (false) detection ratios of less than 35% in this fault test were not sufficient to conclude other faults existing in the HVAC systems. When this sub-system fault happened at level 1, the diagnosis result was not reliable due to the low detection ratios (less than 50%) of all PI residuals. But when the fault deteriorated from level 1 to level 2, the diagnosis result was much more reliable with regard to the detection ratios of PI residuals as shown in Table 6.1.

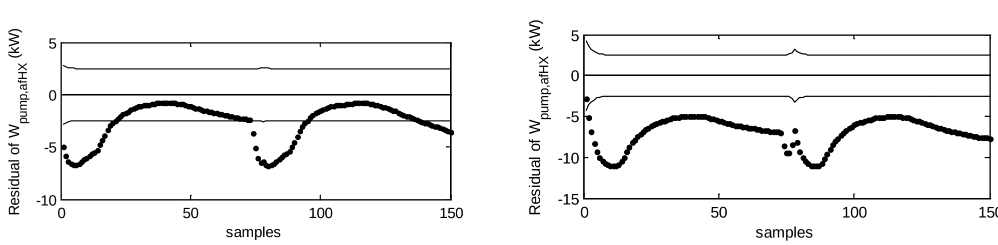

Figure 6.9 PI residuals of the secondary pump system after the heat exchangers with the pipe resistance increased by 10% (A) and 20% (B)

6.3 Validation of the Sensor FDD&E Module

To validate the sensor FDD&E module, no HVAC system faults were introduced into the HVAC sub-systems in the three-day tests in summer season. These normal data were used to train the PCA model to decide the principal component subspace (score space) and threshold of the Q-statistic. The training result is shown in Figure 6.10 with a threshold of 0.6934 and 7.24% of points beyond the threshold. In the same three days, sensor faults were introduced by adding the fixed bias to each sensor measurement contained in the PCA matrix. The validation results of sensor FDD&E module are shown in Figure 6.11 and Table 6.2. The thresholds in Figure 6.11 are 0.6934 for all the Q-statistics which were determined by the training data. In Table 6.2, the detection ratio is the ratio of number of points which violate the threshold to the total points. Diagnosis ratio is the ratio of number of points which is successfully diagnosed to the total violation points. Based on the results in Table 6.2, the PCA method was very effective to detect and diagnose the fixed-bias sensor faults with all detection ratios of more than 80% and diagnosis ratio more than 75%. The bias estimation method was also effective with all relative error less than 4.5%. Sensor FDD&E is reliable to identify the sensor fault with fixed biases and correct the sensor bias to enhance the reliability of the system-level FDD scheme.

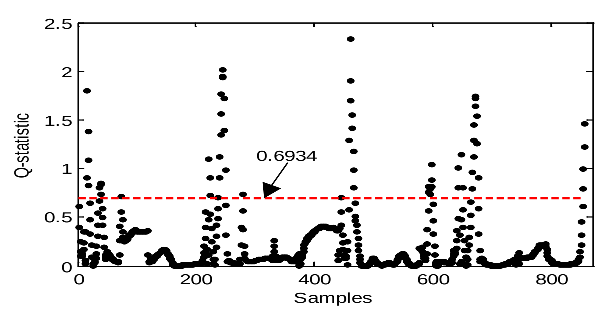

Figure 6.10 Q-statistic plot using the normal data

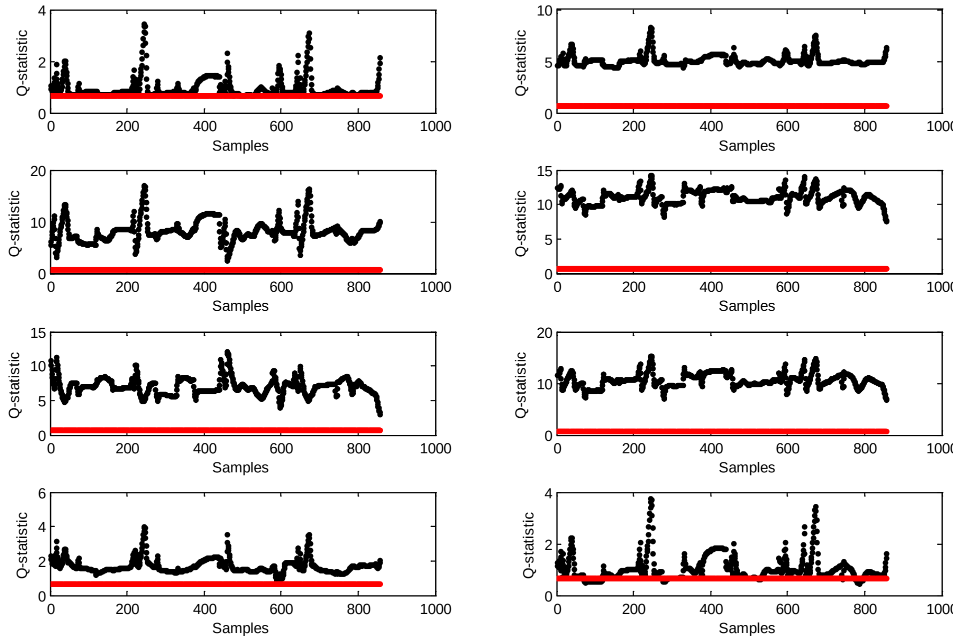

Figure 6.11 Q-statistic plot using the faulty sensor data by adding fixed biases

Table 6.2 Results of sensor FDD&E using fixed-bias sensor data

	T_{wetin} (℃)	T_{win_CT} (℃)	T_{win_EV} (℃)	T_{wout_bfHX} (℃)	T_{win_bfHX} (℃)	T_{wn_afHX} (℃)	M_{afHX} (L/s)	M_{bfHX} (L/s)
Added bias	2	1	1	1	1	1	-20	-30
Estimated bias	2.075	0.987	1	1	1	0.955	-2098	-32.253
Detection ratio (%)	96.4	100	100	100	100	100	100	82
Diagnosis ratio (%)	76.2	80	100	100	100	100	95.5	94.7

6.4 Sensitivity Analysis of Sensor FDD&E to System Faults

When system faults and sensor faults coexist in HVAC sub-systems, the quantitative impact of system faults on the FDD&E was described in Table 6.3. The tests were obtained by introducing one sensor bias and one HVAC sub-system fault simultaneously in the same three days described in Section 6.3. The added biases are the same with those in Table 6.2. For the cooling tower system and heat exchanger system at fault level 1, the chiller system, SCHWP system before HX and SCHWP system after HX at fault level 1 and level 2, the sensor faults can be detected with high detection ratios more than 74% and identified with high diagnosis ratios more than 77%. Most of sensor biases can be corrected with reasonable estimated biases by the estimation method. For the cooling tower system at fault severity level 2, the sensors of T_{dryin}, T_{win_CT} and M_{bfHX} cannot be estimated correctly. The same situation happened on the FDD&E for some sensors in heat exchanger system at fault severity level 2 with a large deviation of estimated biases from real biases and low diagnosis ratios. The malfunction of FDD&E for some sensors in these two sub-systems at fault level 2 may be due to the reason that the relationship among the correlated sensor measurements in fault tests of these two sub-systems is broken. The new systematic variations of measurements are so different from the variations of training data that the PCA cannot capture the new relationship using the normal training data.

Table 6.3 Estimated biases, detection ratios and diagnosis ratios of sensor FDD&E in fault tests of HVAC systems

system	Fault severity level	Validation results	Sensor measurement							
			T_{wetin} (℃)	T_{win_CT} (℃)	T_{win_EV} (℃)	T_{wout_bfHX} (℃)	T_{win_bfHX} (℃)	T_{win_afHX} (℃)	M_{afHX} (L/s)	M_{bfHX} (L/s)
Cooling tower system	Level 1	Estimated bias	1.95	0.91	1.00	1.00	1.00	0.95	-20.04	-31.28
		Detection ratio (%)	100	100	100	100	100	100	100	75.3
		Diagnosis ratio (%)	80	100	100	100	100	100	100	100
	Level 2	Estimated bias	*-2.56*	*-0.44*	*0.81*	*0.96*	*1.09*	*0.91*	*-19.74*	*0.00*
		Detection ratio (%)	*100*	*100*	*100*	*100*	*100*	*100*	*100*	*100*
		Diagnosis ratio (%)	-	-	*100*	*100*	*100*	*100*	*58.7*	-
Chiller system (power loss)	Level 1	Estimated bias	2.06	1.01	1.01	1.00	0.99	0.95	-20.15	-32.28
		Detection ratio (%)	100	100	100	100	100	100	100	74.7
		Diagnosis ratio (%)	98.7	100	100	100	100	100	100	98.2
	Level 2	Estimated bias	2.11	1.04	1.06	1.02	0.98	0.97	-20.34	-35.68
		Detection ratio (%)	100	100	100	100	100	100	100	83.3
		Diagnosis ratio (%)	99.3	100	100	100	100	100	100	100
Chiller system (heat transfer deterioration)	Level 1	Estimated bias	2.04	1.03	1.00	1.00	0.99	0.95	-20.15	-33.62
		Detection ratio (%)	100	100	100	100	100	100	100	75.3
		Diagnosis ratio (%)	91.3	100	100	100	100	100	99.3	98.2
	Level 2	Estimated bias	2.10	1.03	1.05	1.01	0.97	0.96	-20.38	-34.44
		Detection ratio (%)	100	100	100	100	100	100	100	83.3
		Diagnosis ratio (%)	99.3	100	100	100	100	100	100	100
SCHWP system before HX	Level 1	Estimated bias	2.07	1.03	1.04	1.01	0.99	0.96	-20.23	-35.47
		Detection ratio (%)	100	100	100	100	100	100	100	79.3
		Diagnosis ratio (%)	98.0	98.7	100	100	100	100	100	99.2
	Level 2	Estimated bias	2.13	1.02	1.08	1.03	0.99	0.98	-20.29	-37.23
		Detection ratio (%)	100	100	100	100	100	100	100	83.9
		Diagnosis ratio (%)	99.3	100	100	100	100	100	100	100
Heat exchanger system	Level 1	Estimated bias	1.96	1.00	0.97	0.88	0.91	0.83	-19.89	-31.00
		Detection ratio (%)	100	100	100	100	100	100	100	100
		Diagnosis ratio (%)	90.7	100	100	100	100	100	98.0	77.3
	Level 2	Estimated bias	*1.91*	*0.97*	*0.94*	*0.74*	*0.78*	*0.69*	*-20.21*	*-0.40*
		Detection ratio (%)	*100*	*100*	*100*	*100*	*100*	*100*	*100*	*100*
		Diagnosis ratio (%)	*69.3*	*98.7*	*100*	*99.3*	*100*	*100*	*66.0*	-
SCHWP system after HX	Level 1	Estimated bias	1.00	1.12	0.99	0.92	0.94	-24.62	-35.14	1.00
		Detection ratio (%)	100	100	100	100	100	100	100	83.9
		Diagnosis ratio (%)	99.3	100	100	100	100	100	100	100
	Level 2	Estimated bias	0.99	1.12	0.96	0.90	0.91	-28.39	-36.08	0.99
		Detection ratio (%)	100	100	100	100	100	100	100	100
		Diagnosis ratio (%)	98.0	97.3	100	100	100	100	100	91.3

6.5 Validation of HVAC System-level FDD Scheme Involving Sensor Biases

Since most of sensor biases can be diagnosed and recovered by the proposed sensor FDD&E, it is necessary to discuss how much the corrected measurements can affect the results of the system FDD. The main results of HVAC system FDD using the corrected measurements are summarized in Table 6.4. The tests were implemented by introducing one sensor bias and one HVAC sub-system fault simultaneously in the same three days described in Section 6.4. For relative errors between the added biases and estimated biases less than 5%, the system FDD results were not included due to minor impact of sensor FDD&E on system FDD. For the PIs not related to biased sensors, the detection results were not included, because the results for these PIs should be the same with those in Table 6.1. For the cooling tower system and heat exchanger system at fault severity level 2, the FDD results were not included due to the unreliable sensor bias correction. In Table 6.4, it can be seen that most of the system FDD results were still valid if the biased sensor measurements were corrected by sensor FDD&E. For the biased M_{afHX} and M_{bfHX} in some HVAC sub-systems in faulty conditions, although the sensor FDD&E can give reasonable estimations as shown in Table 6.3, the remaining bias still made SCHWP systems misdiagnosed with (false) detection ratios of 100%. For the SCHWP system before HX at fault level 2, the T_{win_EV} correction from bias of 1℃ to bias of 0.08℃ made the detection ratio of chiller PIs (COP and $W_{chiller}$) increase from the 0% and 12.1% to 53.7% and 73.2% respectively. The detection ratios of more than 50% of COP and $W_{chiller}$ can cause the false diagnosis in the chiller system. For the heat exchanger system at fault level 1, the T_{win_afHX} correction from bias of 1℃ to bias of 0.17℃ made the HX system PIs (UA_{HX} and T_{wout_bfHX}) vary from 100% and 0.7% to 57.3% and 14.7%. This also lowered the reliability of HX system FDD. For the SCHWP system after HX at fault level 1 and level 2, some sensor corrections by sensor FDD&E still caused false alarms of the system FDD due to the remaining sensor biases. To improve the reliability of the system FDD using the correct sensor, a wide range of training data for sensor FDD&E is recommended.

Table 6.4 Detection ratios of PI residuals for the five HVAC systems in faulty conditions using the corrected sensor measurements by sensor FDD&E

HVAC system	Fault severity level	Sensor correction	ε_{T_CT}	$T_{approach\_CT}$	W_{CT}	COP	$W_{chiller}$	ε_{HX}	UA_{HX}	T_{wout_bfHX}	W_{pump_bfHX}	W_{pump_afHX}
Cooling tower system	Level 1	T_{wetin}	38	40	100							
		T_{win_CT}	54	52.7	100							
Chiller system (power loss)	Level 1	T_{win_EV}				12	72					
		M_{bfHX}									100	
	Level 2	T_{win_EV}				89.3	100					
		T_{wetin}	25.3	22.6								
		M_{bfHX}									100	
Chiller system (heat transfer deterioration)	Level 1	M_{bfHX}									100	
	Level 2	T_{win_EV}				15.3	88					
		M_{bfHX}									100	
SCHWP system before HX	Level 1	M_{bfHX}									100	
	Level 2	T_{wetin}	24.2	22.2	6.7							
		T_{win_EV}				53.7	73.2					
		M_{bfHX}									100	
Heat exchanger system	Level 1	T_{out_bfHX}						100	100	100		
		T_{in_bfHX}						0	100	0		
		T_{in_afHX}						0	57.3	14.7		
		M_{bfHX}									100	
SCHWP system after HX	Level 1	T_{wetin}	26	24.7	21.3							
		T_{win_EV}				56.7	94.7					
		T_{in_bfHX}						0	100	0		
		T_{in_afHX}						0	100	0		
		M_{afHX}										100
		M_{bfHX}									100	
	Level 2	T_{wetin}	14	13.3	43.3							
		T_{win_EV}				55.3	93.3					
		T_{in_bfHX}						0	100	0		
		T_{in_afHX}						0	98.7	12		
		M_{afHX}										98.7
		M_{bfHX}									100	

6.6 Summary

The FDD scheme proposed in Chapter 5 for the HVAC systems involving sensor faults is validated in this chapter.

In this chapter, the PI models of various HVAC sub-systems of concern are validated in summer and winter weather conditions. In the validation of system FDD module, when the fault severity goes further, detection ratios of the PI residuals become higher (not less than 50%) and the FDD outputs become sensitive and reliable, such as the fault at level 2 of secondary pump system after HX. Due to the serial connection of all sub-systems and supervisory control strategy, one sub-system operating performance may be affected by the fault of the other sub-systems. The affection can be reflected by the offset of PI residuals such as the fault of the cooling tower system can result in violation of PI residuals of the chiller system from its adaptive thresholds. However, one can still isolate the actual faulty sub-system using the most sensitive PI residuals with the highest detection ratio(s).

In the validation of sensor FDD&E module, the sensor FDD&E are effective in identifying the biased sensor and recovering the bias based on the results. Although some system faults at the high fault severity level break the relationship of sensor measurements in the PCA matrix and the sensor bias correction may fail using the violated matrix, the sensor FDD&E method is still valid in detection and diagnosis. It is helpful to suggest BMS operators to do the commissioning on the potential biased sensors.

The system-level FDD scheme for HVAC systems is validated using the system-level sensor measurements of some introduced faults. Furthermore, it is supposed to be effective in identifying the system with other faults. To find the cause of the system performance degradation, a component-level FDD method is recommended.

CHAPTER 7 CHILLER FDD SCHEME: COMPONENT-LEVEL FDD

The chapter presents a FDD scheme for centrifugal chillers (i.e., Chiller FDD scheme) in HVAC systems. This scheme is developed based fuzzy modeling and artificial neural network (ANN) technique. Based on the sensitivity analysis of the performance indices (PIs) for chiller faults, these PI residuals between the PIs predicted by using the regression models in normal tests and the corresponding PIs predicted by using the regression models in faults are used to form a conventional qualitative diagnostic classifier. These PI residuals are normalized and then quantified by fuzzy models to deduce a quantitative diagnostic classifier which is composed of standardized quantitative PIs (SQPs). Fault identification is realized by using ANN technique by matching the SQPs in the quantitative diagnostic classifier with the known chiller faults. Use of this classifier in the scheme may overcome problems faced by conventional qualitative fault classifiers when different type faults have the same linguistic rule pattern. The implementation of this scheme needs operation data at normal operating conditions and faulty operating conditions at a range of load levels and fault severity levels.

Section 7.1 depicts an overview of the structure of the chiller FDD scheme. The techniques of fuzzy logic and artificial neural networks (ANNs) used in the FDD scheme are described in section 7.2. Section 7.3 presents how fuzzy logic and ANN technique are used for fault detection and diagnosis. Section 7.4 describes the test facility for the evaluation of the chiller FDD scheme. Section 7.5 presents the modeling approach based on fuzzy logic and ANN technique for the chiller FDD scheme. Section 7.6 is the summary.

7.1 Scheme Structure

The structure of the chiller FDD scheme is illustrated in Figure 7.1. This scheme includes three steps. The first step is the data preprocessing which includes outlier removing, performance indices formulation and normalization of PI residuals of concern. Outlier removing can be referred to Section 5.3.2. The chiller model was trained off-line with operation data from normal tests and fault tests. Chiller performance variables of concern are the control variables and performance indices introduced in Section 7.5.1.. The outcome of the first step is a qualitative (conventional) diagnostic classifier composed of the PI residual percentages with regard to fault category and fault severity levels.

The second step is to deduce a quantitative diagnostic classifier from the conventional qualitative classifier by using fuzzy models. In qualitative classifiers, conventional linguistic '*IF-THEN*' rules, such as '*IF A increase and B decrease THEN C is abnormal'*, are usually used. The quantitative diagnostic classifier is deduced from conventional qualitative classifiers by using fuzzification operations. The quantitative diagnostic classifier is composed of standardized quantitative PIs (SQPs). Determination of SQP is delivered in Section 7.5.3.

The third step is fault identification by mapping the quantitative diagnostic classifier with fault categories based on ANN, which is a very effective tool in pattern recognition for fault identification. In Figure 7.1, most processes in the model training and FDD scheme are the same, except three occasions. One is that data used in the chiller model establishment of training process and FDD process are different. The second is that the ANN model in the training process is used to determine the network connecting weights and biases for utilization of FDD process while it is applied in FDD process for fault identification. The third is that analysis on sensitivity of PI residual percentages to the faults is needed in the training process to determine the parameters (centers and widths) of the membership function (MF), and the parameters are used in FDD process for reconstruction of new quantitative diagnostic classifier. It is worth noticing that the fault detection and fault diagnosis are performed by the component-level FDD scheme simultaneously. Therefore, there is no separation between fault detection and diagnosis processes in Figure 7.1.

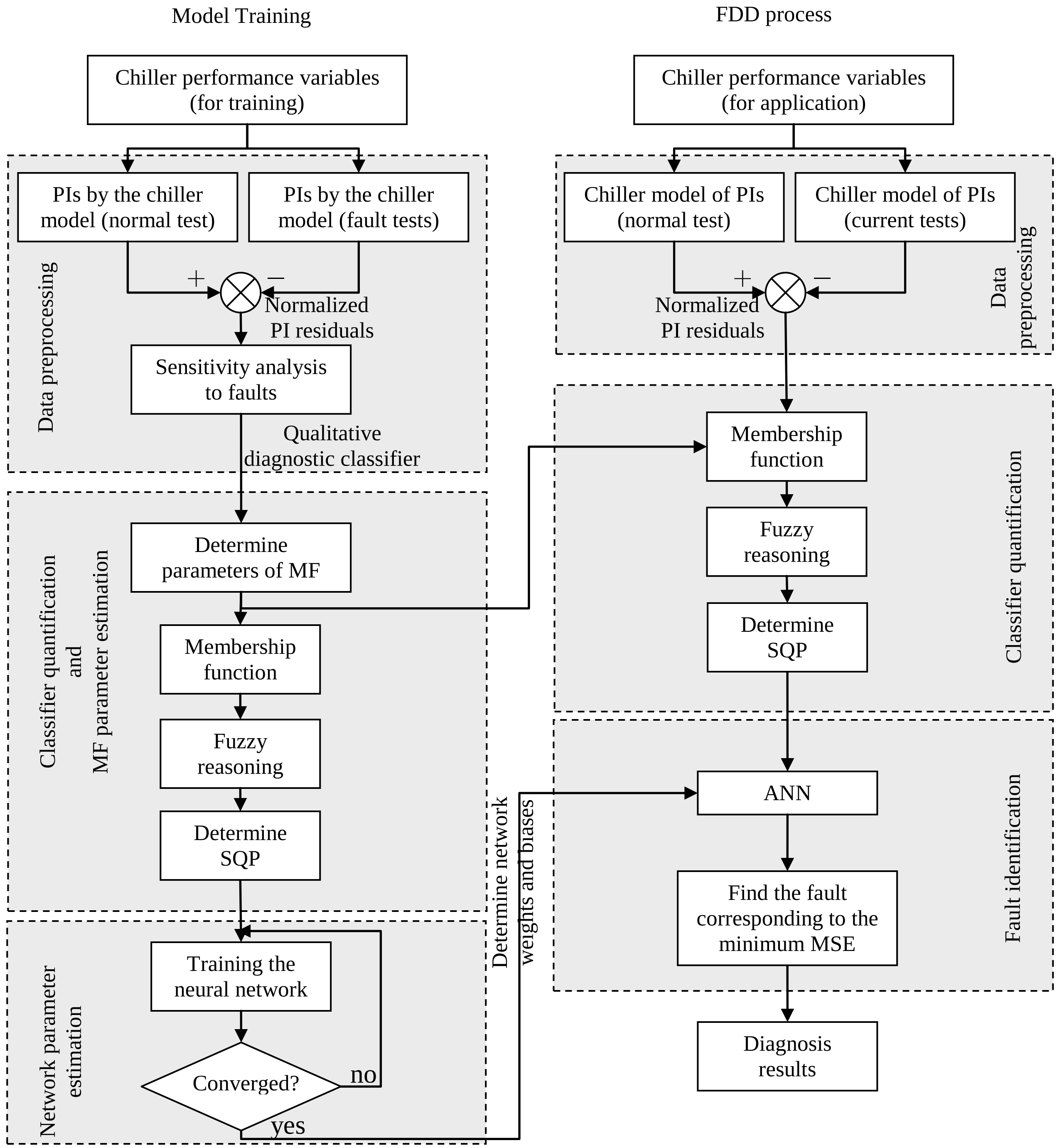

Figure 7.1 Flowchart of the FDD scheme for chiller systems

7.2 Introduction of Fuzzy Algorithm and ANN

Fuzzy theory and artificial neural network as artificial intelligence (AI) techniques have received considerable attention in recent years. They employ the computers as a tool to simulate the human's learning, thinking, understanding and even behavior. Applications of such artificial intelligences are widespread and abundant, such as some functions in air conditioners, refrigerators and medical machines. Fuzzy algorithm is very effective for handling the necessarily imprecise systems. Artificial neural network is very widely used as a recognition technique.

7.2.1 Fuzzy Algorithm

A fuzzy system is a nonlinear system. Usually a set of linguistic rules are used to describe the system behaviors. Based on Harris et al. (2002), a typical fuzzy system is described in Figure 7.2. A knowledge base composed of fuzzy sets and fuzzy operators is the benchmark to carry out fuzzy reasoning and fuzzy mapping. A fuzzifier fuzzifies real value inputs (classical sets) into fuzzy sets. An inference engine is the interface of a series of fuzzy operations between fuzzy inputs and fuzzy outputs. A defuzzifier transforms fuzzy sets into classical sets for use in traditional systems.

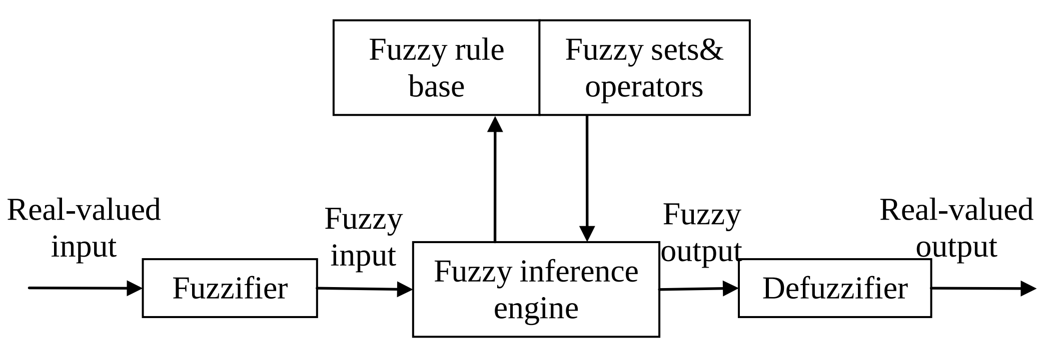

Figure 7.2 Basic components of a fuzzy system

a. Fuzzy membership function.

The rule base contains the knowledge in the form of *IF-THEN* production rules. Zadeh (1965) introduced the concept of a fuzzy set to represent rule antecedent and consequent parts. Unlike the binary or crisp set with membership of 0 or 1, a fuzzy set is allowed by the fuzzy membership function composed of elements, which are partial members of a set. The membership reflects the degree of uncertainty about the information. The fuzzy membership function of fuzzy set *A* is defined is on its universe of discourse *X*, $\mu_A(\bullet)$: $X \in [0,1]$. For an input, the output of the membership function represents the degree of membership of that set. Typical fuzzy membership functions with Gaussian basis functions are shown in Figure 7.3.

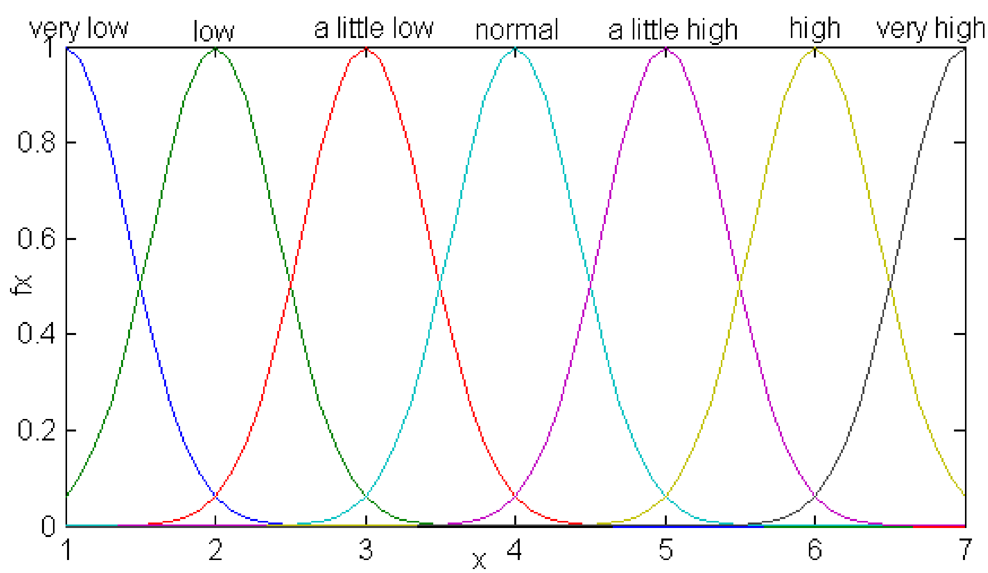

Figure 7.3 A typical set of membership functions with seven Gaussian functions

b. Fuzzy operators

The fuzzy operators are able to map data into fuzzy set memberships to fulfill the inference function in the fuzzy logic. A fuzzy production rule is formed using three typical operators: intersection (AND), union (OR) and implication (IF (•) THEN (•)).

The fuzzy intersection of two sets A and B can be expressed as $(x\ is\ A)\ AND\ (y\ is\ B)$. A new fuzzy membership function is deduced by the fuzzy intersection from the $X \times Y$ space.

$$\mu_{A \cap B}(x, y) = \mu_A(x) \hat{*} \mu_B(y) \tag{7.1}$$

Where, $\hat{*}$ is the T-operator which follows relationships of T-norms or triangular norms. Two popular T-norms provide a wide range of functions to execute the fuzzy intersection. Two of common T-operators are *min* and *product*.

Similarly, the fuzzy union of two sets A and B can be expressed as $(x\ is\ A)\ OR\ (y\ is\ B)$. The new membership function is

$$\mu_{A \cup B}(x, y) = \mu_A(x) \hat{+} \mu_B(y) \tag{7.2}$$

Where, $\hat{+}$ is the S-norm operator. The typical S-operators are *max* and *addition*.

Fuzzy implication is the interface to correspond an output set to an input set. For a a production rule in a fuzzy algorithm,

$$r_{ij} : IF\ (X\ is\ A^i)\ THEN\ (y\ is\ B^j), \quad c_{ij}$$

Where, r_{ij} is the *ij*th fuzzy production rule, c_{ij} is the rule confidence. The degree to which X is related to y is

$$\mu_{r_{ij}}(X, y) = \mu_{A^i}(X) \hat{\hat{*}} c_{ij} * \mu_{B^j}(y) \tag{7.3}$$

c. Fuzzification and defuzzification

Fuzzification is the process in which the real-valued signals are mapped into a fuzzy set using fuzzy membership function. The reverse process against the fuzzification is the defuzzification. Both of them are decided by what membership function is used for mapping the input and output. Two algorithms, i.e. the mean of maxima (MOM) and the center of gravity (COG) are commonly used in the defuzzification.

7.2.2 Artificial Neural Network

As a non-linear statistical data modeling tool, artificial neural networks (ANNs) are widely used in the pattern recognition or data classification between inputs and outputs in practical applications. They can be seen as the emulations of biological neural networks. Usually a neural network is composed of a number of interconnected artificial neurons to solve particular problems.

A neuron with a *t*-element input vector is shown in Figure 7.4. The neuron also has a bias *b* and weight matrix *W*. Σ is a sum operator. TF is a transfer function which can be hard-limit (threshold), linear or sigmoid.

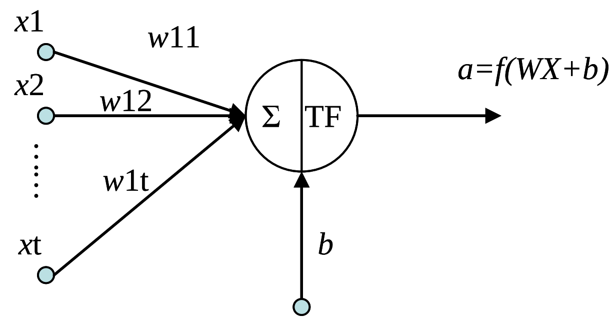

Figure 7.4 A neuron with the input number of t

Back propagation algorithm is usually used in neural networks for practical applications. This algorithm is composed of the Widrow-Hoff learning rule and nonlinear differentiable transfer functions. The ANN with backpropagation algorithm with a sigmoid layer, biases, and a linear output layer can approximate any function with a finite number of discontinuities. As a supervised learning method, the errors propagate backwards from the output nodes to the nodes before until the outputs reach to the desired values. The backpropagation algorithm of the error gradient modifies the connection weights and biases. A typical backpropagation network is necessarily composed of an input layer, one or more hidden layers and an output layer. This means they are multi-layer perceptrons. A training algorithm makes the weight move in the direction of the negative gradient..

7.3 Implementation of the Fuzzy Model and ANN in FDD

7.3.1 Fuzzy Model-Based Quantitative Diagnostic Classifier

As conventional qualitative or linguistic diagnostic classifiers based on the trend pattern of PIs residual percentage are ineffective in fault diagnosis especially when some type faults have the same symbolic rule pattern, a quantitative diagnostic classifier is developed based on fuzzy models to resolve this problem. A brief on the quantitative diagnostic classifier is given below.

Assuming input $x=[x_1,\ldots,x_m]^T$ and output $y=[y_1,\ldots,y_t]^T$, the structure of fuzzy network is shown in Figure 7.5. The inputs are the PI residual percentages obtained from the preprocessing step. The outputs are the standardized quantitative PIs (SQPs) which can be regarded as the standardized PI residual percentages. The network for fuzzy processing consists of four layers including input layer, fuzzification layer, layer of SQPs determination and output layer.

a. input layer

The inputs of the input layer are PI residual percentages as follows.

$$x = \frac{PI_{normal} - PI}{PI_{normal}} \tag{7.4}$$

Where, PI_{normal} is the PI estimation of chiller models based on the normal test. In the training process, PI is the estimation of chiller models based on the fault tests, while it is the estimation of chiller models based on the validation test in the validating process. The combination of different PI residual percentages can be used to constitute a linguistic (qualitative) diagnostic classifier to characterize different faults. How to evaluate the quantitative impact of PIs of different faults is disposed by fuzzy models.

b. fuzzification layer

The input (PI residual percentage) x is represented by a fuzzy set using membership functions (MF). MF can be implemented by many methods. The basis function used in the model is Gaussian membership function as Equation (7.5).

$$\mu_{A_i}(x) = \exp\left(-\frac{(x-c_i)^2}{2\sigma_i^2}\right) \tag{7.5}$$

Where, c_i and σ_i are the centre and width of the ith fuzzy set respectively.

The working range of PI residual percentages is divided into many intervals by membership functions. As long as the training data cover the range of possible operating conditions and the quantity of fuzzy sets is large enough to characterize the operating conditions of various faults, new operation data of tests for validation must be located in a range of one fuzzy set. Residual percentages of different PIs corresponding to those fuzzy sets can be used to characterize the operating status (normal or faulty and what fault).

c. layer of SQPs determination

To evaluate the quantitative impact of different faults on PIs, SQPs (i.e., standardized quantitative PIs) are used in this study rather than the exact PI residual percentages. Each interval of the working range of PI residual percentages is represented by an integral number named standardized quantitative PIs (SQPs). An SQP is corresponding to the largest membership of fuzzy sets of a PI residual percentage. SQPs can be regarded as the standardized PI residual percentages. More descriptions about SQPs are delivered in Section 7.5.3.

d. output layer

The output layer is composed of different SQPs to reflect the chiller status (normal or faulty and which fault). It can also be viewed as the input layer of a neural network.

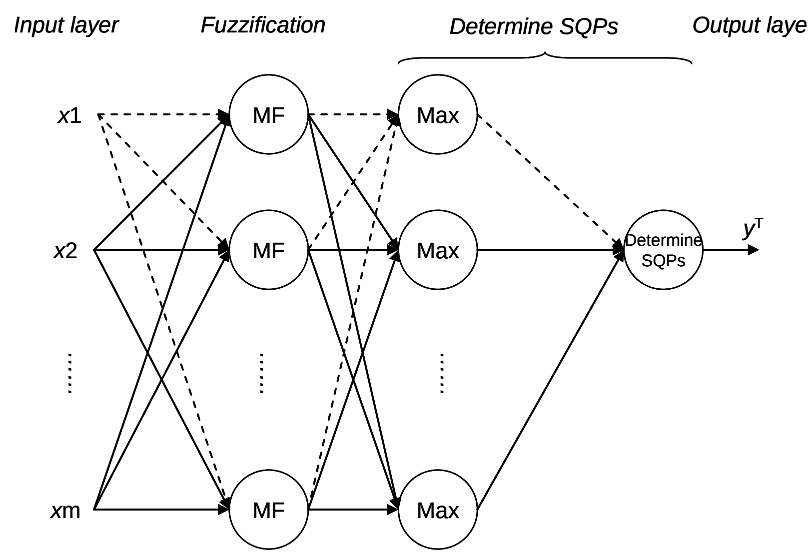

Figure 7.5 Fuzzy network structure

7.3.2 Neural Network-Based Fault Identification

The '*IF*' parts of the quantitative rule classifier are established using SQPs determined by fuzzy models. The '*THEN*' parts are the consequent parts of the rules. For each output of '*IF'* part, there is a corresponding specific '*THEN'* part (a specific fault). The whole rule set is accomplished if all '*IF*' parts and '*THEN*' parts are considered. Integration of '*IF*' parts and '*THEN*' parts is a process of fault diagnosis. The ANN is used to connect the '*IF*' parts and '*THEN*' parts.

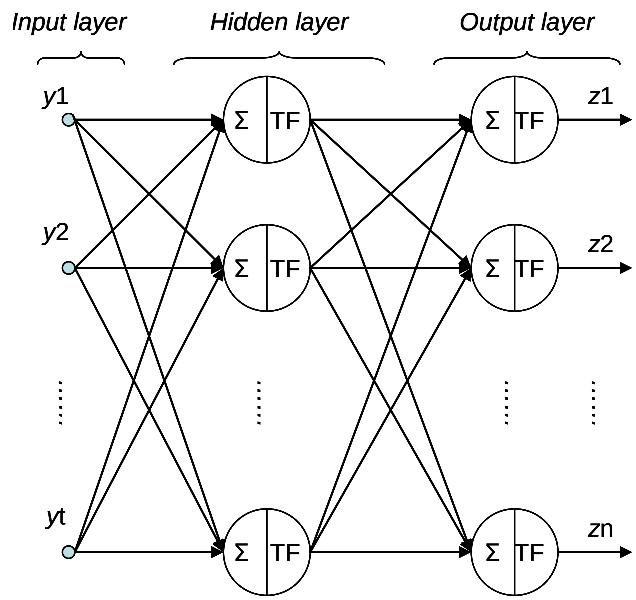

Figure 7.6 Neural network (BP) structure

The ANN used for fault identification has three layers, i.e., an input layer (the outputs of the fuzzy model), a hidden layer and an output layer (the whole fault set) as shown in Figure 7.6. The input layer of the ANN is SQPs, which are sensitive to an operating status (normal and fault category). The neuron number in the input layer is equivalent to the number of outputs in the fuzzy network. For the training process, the ANN shown in Figure 7.6 is one of the whole network, because ANNs are trained using the data at each load level and each fault severity level.

The output of the *j*th neuron of the hidden layer is given by:

$h_j = f(\sum \omega_{ji} x_i + \theta_j)$, where, ω_{ji} is the connection weight from *i*th input node to *j*th hidden layer node and θ_j is the bias of jth hidden layer node. The output of the *k*th neuron of the output layer is corresponding to a specific fault and given by:

$z_k = f(\sum \omega_{kj} x_j + \theta_k^{'})$, where, ω_{kj} is the connection weight from *j*th hidden layer node to *k*th output node and $\theta_k^{'}$ is the bias of *k*th hidden layer node.

Many transfer functions can be used in the layer connection. The tan-sigmoid and linear transfer functions are commonly adopted in the hidden layer and output layer respectively. The training is accomplished by minimizing the sum-of-squares error between the target values and the actual values. And the weights and biases are updated based on different algorithms (e.g. gradient descent function).

7.4 Test Facility for Chiller FDD

Fault tests can hardly be conducted in real building systems for studying chiller faults, since occupants or equipment are not going to tolerate/accept unpredicted situations. ASHRAE 1043 RP which is sponsored by ASHRAE is a meaningful attempt to accomplish a series of fault tests on a real centrifugal chiller. The data both in normal conditions and faulty conditions are very helpful to evaluate various FDD methods.

7.4.1 Laboratory Centrifugal Chiller

The chiller chosen for the various fault tests in RP 1043 is a 316-kW centrifugal chiller, which is installed in a lab. The outdoor air temperature is almost constant with 22℃.

A schematic diagram of the centrifugal chiller is shown in Figure 7.7. The chiller consists of an evaporator, a condenser, a centrifugal compressor, a throttle valve and sensors. There are two branches from the main refrigerant liquid line leaving the condenser. One carries refrigerant to the motor cavity to cool down the motor and oil. The other branch connects the main expansion valve regulated via the pilot valve. The evaporating refrigerant cools the return chiller water from the building, and is throttled across the expansion device under constant enthalpy. The cooled water usually from the cooling tower goes through the condenser and takes away the heat discharged by the condensing refrigerant. The supply chilled water temperature should be maintained at the set-point by regulating the inlet guide vane position.

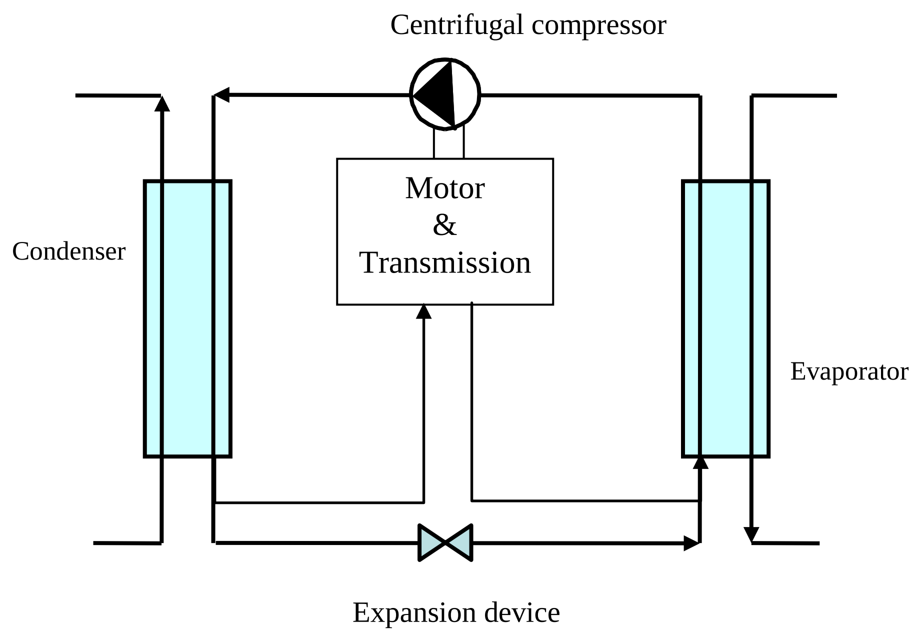

Figure 7.7 Schematics diagram of the centrifugal chiller

7.4.2 Test Stand Description

To substitute the real building and ambient load, the water-to-water and water-to-steam heat exchangers are used as described in Figure 7.8. The heat of the evaporator water is obtained from the heat rejection of condenser water and hot water. The heat of the condenser water is taken away by the city water through the heat exchanger and the evaporator water through the shared heat exchanger. The hot water obtains the heat from the steam.

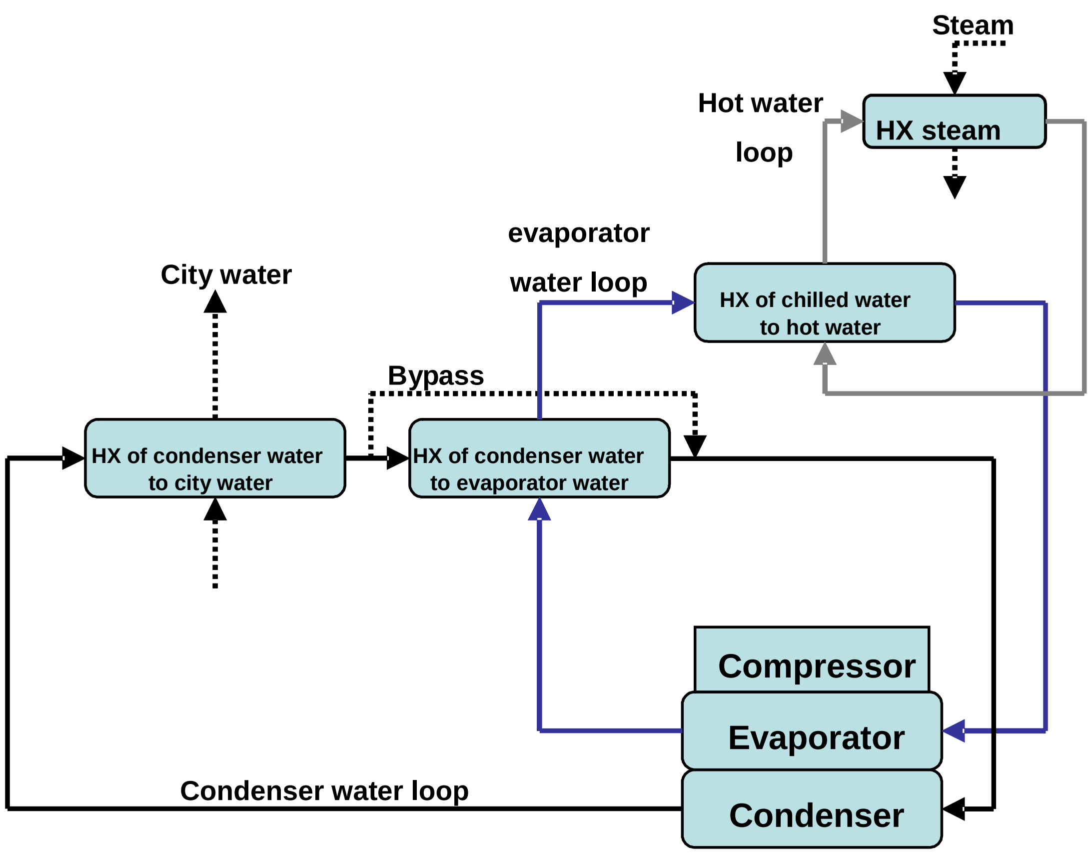

Figure 7.8 Schematics of the water system

A comprehensive suite of sensors is installed to monitor the chiller performance. A control interface of the test stand as shown in Figure 7.9 The sensor measurements are collected by the

Micotech controllers and sent to the computers. The test stand is controlled by three Johnson Controls Inc. Air Handling Unit controllers via RS-485 network. A converter is needed between RS-485 and RS-232. The control interface named VisSim is capable of handling real time data collection and analysis. The data are sampled at a 10-second interval.

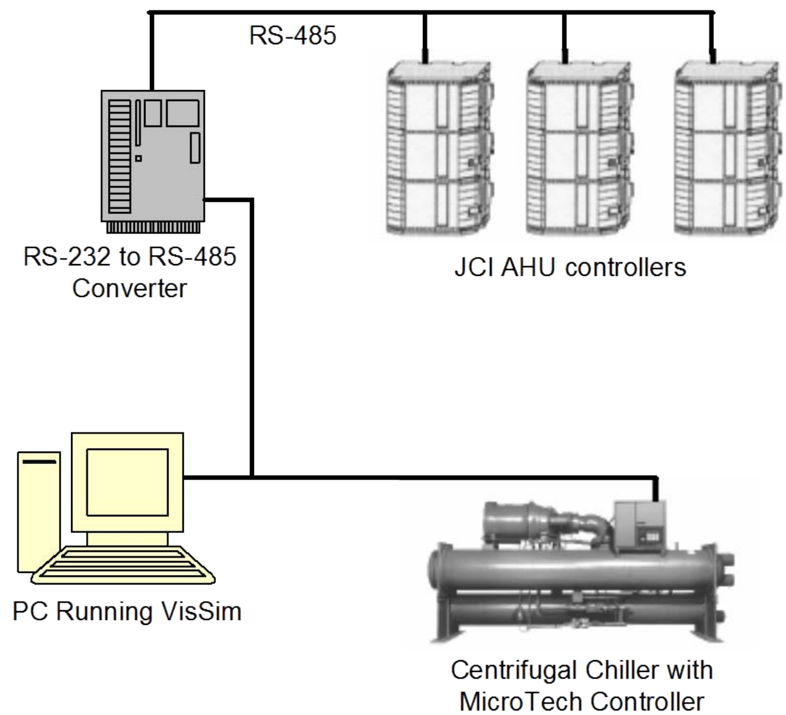

Figure 7.9 Schematic of the chiller test stand and its control interface

Among the sensor measurements, the ones related to this study are listed in Table 7.1 with uncertainties and sources.

Table 7.1 Sensor measurements and their uncertainties

Measurement	Source	Uncertainty
TRC_{sub}	Microtech	±0.54F
TCA	Microtech	±0.5F
PRC	Microtech	±0.5PSIG
TO_{sump}	Microtech	±0.2F
TEI-TEO	JCI AHU	±0.1F
TCO-TCI	JCI AHU	±0.1F

7.4.3 Fault Testing

To make the stand test follow the Air-Conditioning and Refrigeration Institute (ARI) Standard 550 for Centrifugal and Rotary Screw Water Chilling Packages as closely as possible, some particular cases are chosen. Three controlled variables are chilled water supply temperature, entering condenser water temperature and the cooling load. The chiller water supply temperature was controlled at three levels which are 40 F (4.4℃), 45F (7.2℃) and 50F (10℃). The entering condenser water temperature was controlled between two levels which are 60F (15.6℃) and 85F (29.4℃). The cooling load of the chiller was allowed to be varied from 25% to 100% of the rated cooling capacity. Using these three control variables with each one working at three levels, there are totally 27 different tests for each fault level. The test sequence is shown in Table 7.2.

Table 7.2 Test sequence in RP 1043

TEO (F)	TCI (F)	Capacity (%)
50	85	90-100
50	85	50-60
50	85	25-40
50	75	90-100
50	75	50-60
50	75	25-40
50	70	70-80
50	65	45-50
50	62	25-30
45	85	90-100
45	85	50-60
45	85	25-40
45	75	90-100
45	75	50-60
45	75	25-40
45	70	70-90
45	62	45-50
45	62	25-35
40	80	90-100
40	80	50-60
40	80	25-40
40	70	90-100
40	70	50-60
40	70	25-40
40	65	70-80
40	62	45-50
40	62	25-35

The complete data set was sampled at a ten-second interval. The interval was reduced to two minutes in a reduced data set which still contains transient behavior. Each of the 27 tests is allowed to run at least 30 minutes to reach steady state. The steady state is verified by the desired conditions. When an operating setpoint is changed, 5 to15 minutes are needed to reach a steady state according to the observation. So for each test, the steady state operation lasts about 15 to 25 minutes.

There are totally eight chiller faults introduced into the test stand. For each fault, four severity levels are considered by changing the magnitude of influencing factors. The eight chiller faults are defective pilot valve, reduced condenser water flow, reduced evaporator water flow, refrigerant leakage, refrigerant overcharge, excess oil, condenser fouling, and non-condensables in refrigerant. The faults at four severity levels and how to introduce them into the test stand are listed in Table 7.3. A normal test was performed before a category of fault tests to characterize the normal behavior of the chiller operation. If the test conditions were not satisfied in a normal test, it would be repeated. The data in the normal tests can be used as the benchmark or for the training purpose.

Table 7.3 Chiller faults at four levels and their characterization

Fault	Simulation approach	Nominal Value	Level 1	Level 2	Level 3	Level 4
Refrigerant leak	Reducing charge	300lb (136kg)	10% reduction in charge 270 lbs	20% reduction in charge 240 lbs	30%reduction in charge 210 lbs	40% reduction in charge 180 lbs
Refrigerant overcharge	Increasing charge	300lb (136kg)	10%increase in charge	20%increase in charge	30%increase in charge	40%increase in charge
Excess oil	Increasing oil	22lb(10kg)	14% increase in charge (25 lbs)	32% increase in charge (29 lbs)	50% increase in charge(33 lbs)	68% increase in charge (37 lbs)
Condenser fouling	Blocking condenser tubes	164 unblocked tubes	12% reduction in tubes 20 blocked tubes	20% reduction in tubes 33 blocked tubes	30% reduction in tubes 49 blocked tubes	45% reduction in tubes 74 blocked tube
Non-condensables	Adding nitrogen	No Nitrogen	0.10 pounds (1.0%)	0.16 pounds (1.7%)	0.22 pounds (2.4%)	0.54 pounds (5.7%)

7.5 Formulation of the Chiller FDD Scheme

7.5.1 Benchmark Models of Chiller PIs

The benchmark models of chiller performance indices of concern are needed as references for comparison for calculated (i.e., "measured") PIs by monitoring in faulty conditions. The residuals between the benchmark values and the measured values of PIs of concern are used in the chiller FDD scheme. To find the performance indices sensitive to the chiller faults, a chiller reference model as Equation (7.6) is used for predicting performance indices for benchmarking. The inputs of the model are chiller cooling load (Q_{EV}), entering condenser water temperature (T_{CI}), and chilled water supply temperature (T_{EO}). The outputs of the model are the performance indices as shown in Table 7.4.

$$\begin{aligned} Y &= f(Q_{EV}, T_{EO}, T_{CI}) + \varepsilon \\ &= b_0 + b_1 T_{EO} + b_2 T_{CI} + b_3 Q_{EV} + b_4 T_{EO} T_{CI} + b_5 T_{EO} Q_{EV} + b_6 T_{CI} Q_{EV} + b_7 Q_{EV}^2 + \varepsilon \end{aligned} \tag{7.6}$$

Where, the error term, $\varepsilon \sim N(0, \sigma^2)$, $b_0 \ldots b_7$ are constant, which are determined by linear regression techniques using the data in the normal test.

7.5.2 Qualitative Diagnostic Classifier - Linguistic Diagnostic Classifier

The data sets used in the study are provided by the ASHRAE research project, 1043-RP (Comstock and Braun 1999b) which aimed at chiller faults study and FDD evaluation. There were totally eight faults introduced into a 90-ton centrifugal water-cooled chiller with a cooling load range between about 25% and 100% of the rated cooling capacity. Only seven faults with four levels of severity were considered in this study, namely, reduced condenser water flow (by reducing water flow), condenser fouling (by plugging tubes in the condenser), refrigerant leakage (by charging less refrigerant), refrigerant overcharge (by charging more refrigerant), reduced evaporator water flow (by reducing water flow), non-condensables in refrigerant (by adding nitrogen into the refrigerant), and excess oil (by charging more oil). Steady-state data were used for chiller model training, and the reduced data after eliminating the steady-state data were used in the chiller model validation process. To know how to define the steady state and how to obtain the reduced data, please refer to Comstock and Braun (1999b).

Some previous papers illustrated how the performance indices were applied in the chiller fault diagnosis such as (McIntosh et al. 2000; Jia and Reddy 2003; Wang and Cui 2006). On the basis of impact of faults on the performance indices, the generic rules for chiller fault diagnostic classifier were formed in Table 7.4 which contains the most sensitive performance indices to the faults. This part of work can also be referred to Comstock et al. (2001) and Wang and Cui (2006). The detailed research of fault impact on the PIs and the meaning of PIs can be found in Comstock and Braun (1999a and 1999b) and Cui and Wang (2005). In the table, the sensor measurements, the characteristic quantities (CQs) and characteristic parameters (CPs) were used as the performance indices. CQs and CPs (refer to Reddy, 2007) are representative of physical properties of chiller operating states which are deduced from the basic sensor measurements. The signs ▲ and ▼ indicate the performance index increases and decreases when the fault severity increases and decreases respectively. The subscript '*1*' means that PI deviation of reference models using fault data from that of reference models using normal data is small, '*2*' means that the change trend of the PI deviation is not related to the fault severity in some tests. The columns of T_{sh_suc} and T_{EA} which only contain performance indices with subscript '*1*' and '*2*' can be neglected. Although

$LMTD_{EV}$ and $LMTD_{CD}$ have more physical meanings for chiller performance evaluation, they can totally be substituted with T_{EI}-T_{EO} and T_{CO}-T_{CI} respectively. That is because T_{EI}-T_{EO} was only sensitive to the fault of reduced evaporator water flow while $LMTD_{EV}$ also varied with the faults of reduced condenser water flow and refrigerant leakage. And T_{CO}-T_{CI} was not sensitive to the refrigerant leakage which could be distinguished using trend pattern of TRC_{sub} and T_{CA}. The *COP* with a deviation of only 4% was not sensitive to the faults at low severity level. The Eff_{moter} was only sensitive to the excess oil with maximum deviation of 6%, while this fault could be distinguished by the TO_{sump} with maximum deviation of 15% or TO_{feed} with maximum deviation of 11%. TO_{sump} was chosen as the performance index to characterize the fault of excess oil. Therefore, the rules of fault diagnostic classifier with a reduced PI number could be established in Table 7.5. As the reduced condenser water flow, refrigerant overcharge and non-condensables in refrigerant have the same rule pattern in Table 7.5, it is difficult to distinguish the fault from each other based on the linguistic rule pattern. But the quantitative impact of different faults at each severity level on the PIs is different. With regard to this consideration, the faults which have the same linguistic rule pattern can also be distinguished using the diagnostic classifier if it is quantified.

Table 7.4 Complete qualitative diagnostic rule table of fault diagnostic classifier

Fault	P_{RC}	TRC_{sub}	Tsh_{suc}	T_{EA}	T_{CA}	T_{EI}-T_{EO}	T_{CO}-T_{CI}	TO_{sump}	TO_{feed}	$LMTD_{EV}$	$LMTD_{CD}$	Eff_{motor}	COP
reduced condenser water flow (FWC)	▲	▲	-	▼2	▲2	-	▲	▲1	▲1	▲2	▲	-	▼
condenser fouling (CF)	▲	-	-	-	▲	-	▲	-	-	-	▲	-	▼
refrigerant leakage (RL)	▼1	▼	▼2	▼2	▼	-	-	-	-	▲2	▼	-	-
Refrigerant overcharge (RO)	▲	▲	▲2	▲2	▲		▲	▲1	▲1	-	▲	-	▼
reduced evaporator water flow (FWE)	-	-	▼2	▲2	-	▲	-	-	-	▲	-	-	▼2
non-condensables in refrigerant (NC)	▲	▲	-	-	▲	-	▲	▲1	▲1	-	▲	-	▼
excess oil (EO)	-	-	-	-	-	-	-	▲	▲	-	-	▼	▼1

Table 7.5 Qualitative diagnostic rule table of fault diagnostic classifier with reduced index number

Fault	CQ				measurement	
	TRC_{sub}	T_{CA}	T_{EI}-T_{EO}	T_{CO}-T_{CI}	P_{RC}	TO_{sump}
reduced condenser water flow	▲	▲2	-	▲	▲	▲1
condenser fouling	-	▲	-	▲	▲	-
refrigerant leakage	▼	▼	-	-	▼1	-
refrigerant overcharge	▲	▲	-	▲	▲	▲1
reduced evaporator water flow	-		▲	-	-	-
non-condensables in refrigerant	▲	▲	-	▲	▲	▲1
excess oil	-	-	-	-	-	▲

7.5.3 Quantitative Diagnostic Classifier

The original tests were conducted by controlling three variables (T_{EO}, T_{CI} and Q_{EV}) of the centrifugal chiller at three levels. These operating conditions in the test nearly cover all possible conditions in chiller operations. Only the seven operating conditions of 45F of T_{EO}, 75F of T_{CI}, and 30-90 tons of Q_{EV} with interval of 10 tons were considered both for training and validation in this study. The reason why these conditions are chosen as the operating conditions for the base of comparison is that these operating conditions are all covered by the training data and validation data. Conditions used as training and validation conditions can be selected artificially as long as they are within the range of working conditions of normal tests and fault tests. Since the parameters applied in the validation are all from the training process using some operating conditions, it is more reasonable to use the same operating conditions for validation. The PI residual percentages between the estimation of the regression models using the normal data and fault data are fuzzified by the Gaussian membership functions. The centers (c) and widths (σ) of the each fuzzy set *were* determined by the experiment data and expert experience as shown in Table 7.6. The PI residual percentages are divided into many intervals within the distribution range. The center is determined when the data scatter intensively in an interval. Usually the reliability is acceptable when the membership (as shown in Equation 7.5) is not less than 0.5. The widths are determined when the membership is 0.5. Every interval of the PI residual percentages is represented by a SQP listed in the first column of Table 7.6. This SQP can account for the quantitative impact of faults on the PI residual percentages. For example, 1 of SQP with regard to residual percentage of *TCA* means that the impact of faults on T_{CA} residual percentage is negatively large and 31 of SQP with regard to residual percentage of T_{CA} means that the impact on

T_{CA} residual percentage is positively large. 0 means the impact is very small. The membership functions of the selected performance indices were shown in Figure 7.10.

Using the experiment data (steady data) covering all operating conditions to calculate the SQPs for training, the final quantitative fault diagnostic classifier composed of SQPs was formed as the benchmark. As there were too many data contained, the quantitative diagnostic classifier for chiller faults at four severity levels and 50 tons and 80 tons was listed in Table 7.7. In this table, for each fault, there is a unique quantitative rule corresponding. For example, under a load of 50 tons, the rule for diagnosing reduced condenser water flow at severity 1 is represented as follows using associated standardized quantitative PIs.

IF

(P_{RC} is 4) AND (TRC_{sub} is 14) AND (T_{CA} is 10) AND (T_{EI}-T_{EO} is 1) AND (T_{CO}-T_{CI} is 14) AND (TO_{sump} is 2)

THEN

Fault is reduced condenser water flow at severity 1

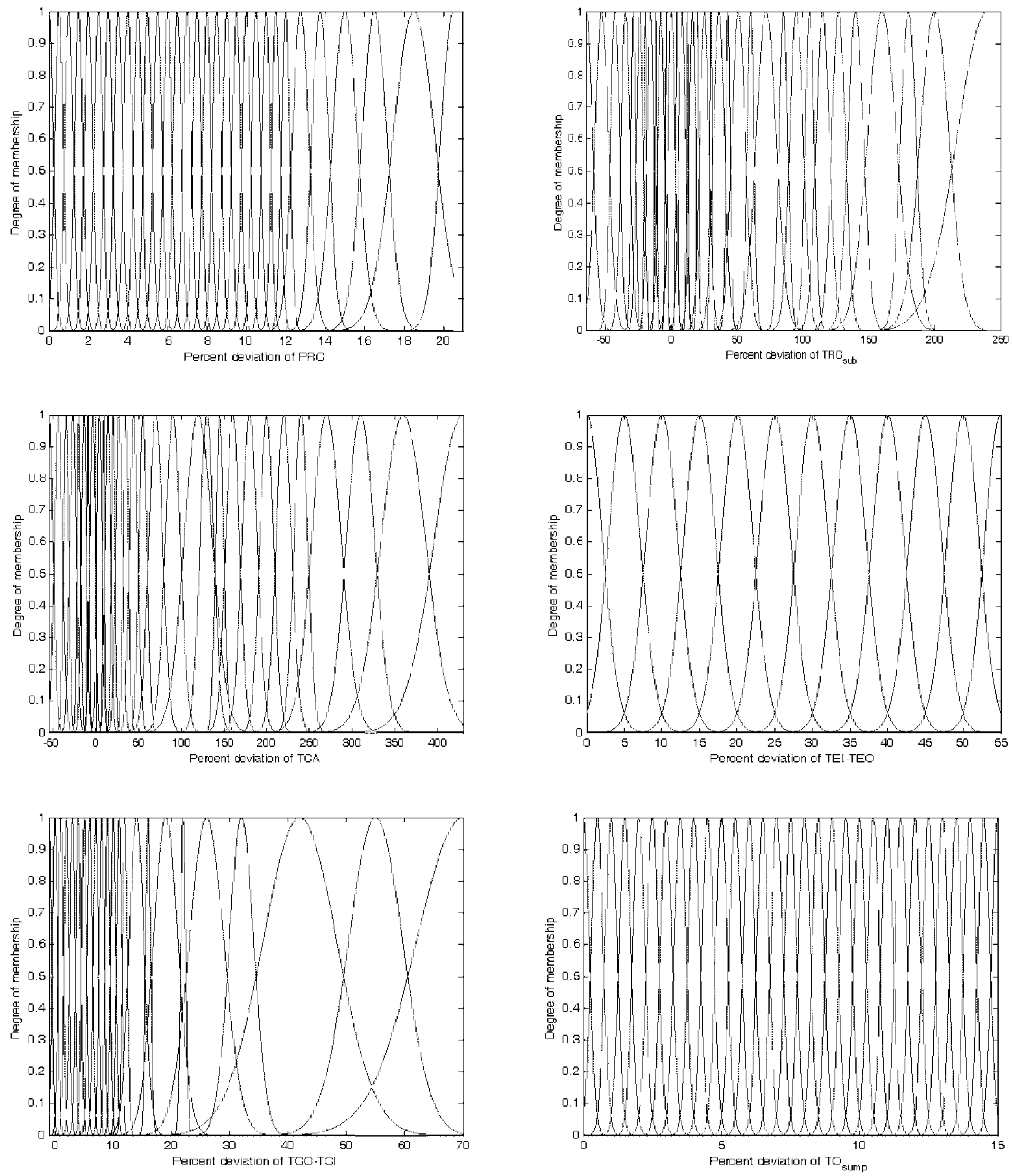

Figure 7.10 Membership functions of different PI residual percentages

Table 7.6 Centers of fuzzy set for the quantitative PI residual percentages

Standardized quantitative PIs	P_{RC}	TRC_{sub}	T_{CA}	T_{EI}-T_{EO}	T_{CO}-T_{CI}	TO_{sump}
1	0	-65	-55	0	-1	0
2	0.5	-53	-44	5	0	0.5
3	1	-43	-35	10	1	1
4	1.5	-35	-27	15	2	1.5
5	2	-29	-20	20	3	2
6	2.5	-24	-14	25	4	2.5
7	3	-20	-9	30	5	3
8	3.5	-16	-4	35	6	3.5
9	4	-12	0	40	7	4
10	4.5	-8	4	45	8	4.5
11	5	-4	9	50	9	5
12	5.5	0	14	55	10	5.5
13	6	4	20	-	11	6
14	6.5	8	27	-	12	6.5
15	7	12	35	-	14	7
16	7.5	16	44	-	16	7.5
17	8	20	55	-	19	8
18	8.5	25	70	-	22	8.5
19	9	30	90	-	26	9
20	9.5	36	120	-	32	9.5
21	10	43	130	-	42	10
22	10.5	51	145	-	55	10.5
23	11	60	160	-	70	11
24	11.5	72	180	-	-	11.5
25	12	85	200	-	-	12
26	12.75	95	220	-	-	12.5
27	13.75	105	240	-	-	13
28	15	115	270	-	-	13.5
29	16.5	127	310	-	-	14
30	18.5	140	360	-	-	14.5
31	20.5	160	430	-	-	15
32	-	180	-	-	-	-
33	-	200	-	-	-	-
34	-	240	-	-	-	-

Although there are some situations that the rules at two adjacent load levels are almost the same (e.g. two rules at 30% and 40% of load level for reduced condenser water flow), the rules for different faults at the same load level or two adjacent load levels are different significantly. It seems there are situations two faults are close with each other in terms of SQPs in Table 7.7 (e.g.

refrigerant overcharge at severity level 3 and 80 tons and non-condensables at severity level 1 and 80 tons). However, the PI residual percentages represented by SQPs of one fault vary much from those of another fault. The SQP of TRC_{sub} of refrigerant overcharge at severity level 3 and 80 tons is 24. Its corresponding PI residual percentage is 72%. However, this value is 51% for 22 of SQP of TRC_{sub} in the fault of non-condensables at the same condition. The traditional fault classifier is hard to distinguish the faults which have the same linguistic rule pattern (such as reduced condenser water flow, refrigerant overcharge and non-condensable in refrigerant in Table 7.5). However, the proposed quantitative diagnostic classifier can distinguish those faults effectively as it uses the numerical change trend of PI residual percentages rather than the change trend of the symbolic pattern. For example, the quantitative rules in Table 7.7 for diagnosing the reduced condenser water flow, refrigerant overcharge and non-condensable in refrigerant are totally different and unique from each other, while these faults cannot be distinguished by the conventional fault classifier as they have the same symbolic trend pattern.

Table 7.7 SQPs of faults at four severity levels and two load levels

fault	category of SQPs	severity level 1		severity level 2		severity level 3		severity level 4	
		50 tons	80 tons	50 tons	80 tons	50 tons	80 tons	50 tons	80 tons
reduced condenser water flow	P_{RC}	4	5	7	10	11	16	18	26
	TRC_{sub}	14	14	18	18	20	20	23	23
	T_{CA}	10	10	10	10	10	11	13	13
	T_{EI}-T_{EO}	1	1	1	1	1	1	1	1
	T_{CO}-T_{CI}	14	14	19	19	21	21	23	23
	TO_{sump}	2	2	2	3	3	5	5	7
condenser fouling	P_{RC}	2	4	3	3	5	6	8	14
	TRC_{sub}	12	13	12	12	13	12	12	12
	T_{CA}	10	12	12	11	13	13	16	17
	T_{EI}-T_{EO}	1	1	1	1	1	1	1	1
	T_{CO}-T_{CI}	3	3	5	5	6	5	9	9
	TO_{sump}	1	1	1	1	1	1	1	1
refrigerant leakage	P_{RC}	1	1	1	1	1	1	1	30
	TRC_{sub}	12	13	9	12	3	5	1	1
	T_{CA}	9	10	6	7	2	2	1	1
	T_{EI}-T_{EO}	1	1	1	1	1	1	1	1
	T_{CO}-T_{CI}	2	1	2	1	2	2	2	2
	TO_{sump}	1	1	1	1	1	1	1	1
refrigerant overcharge	P_{RC}	4	5	5	7	11	17	19	28
	TRC_{sub}	17	16	18	18	23	24	27	28
	T_{CA}	14	13	14	14	18	18	20	20
	T_{EI}-T_{EO}	1	1	1	1	1	1	1	1
	T_{CO}-T_{CI}	2	2	3	3	7	7	12	13
	TO_{sump}	1	2	1	2	3	3	5	6
reduced evaporator water flow	P_{RC}	1	1	3	1	1	1	1	1
	TRC_{sub}	12	12	12	12	12	12	12	12
	T_{CA}	8	8	10	8	9	9	10	9
	T_{EI}-T_{EO}	3	3	6	6	9	9	12	12
	T_{CO}-T_{CI}	3	2	3	2	3	2	4	2
	TO_{sump}	1	1	1	1	1	2	1	4
non-condensa bles	P_{RC}	17	17	21	22	25	26	30	31
	TRC_{sub}	24	22	26	24	28	25	32	29
	T_{CA}	21	19	23	20	25	21	29	26
	T_{EI}-T_{EO}	1	1	1	1	1	1	1	1
	T_{CO}-T_{CI}	4	3	5	3	6	4	8	4
	TO_{sump}	1	1	2	1	3	4	5	7
excess oil	P_{RC}	1	1	1	1	1	1	1	1
	TRC_{sub}	11	12	11	12	11	12	12	14
	T_{CA}	6	8	7	8	7	8	8	10
	T_{EI}-T_{EO}	1	1	1	1	1	1	1	1
	T_{CO}-T_{CI}	2	2	2	2	2	1	4	3
	TO_{sump}	5	5	14	14	21	21	29	31

The '*THEN*' parts of the diagnostic rules are quantified with identity matrix. Every column of the identity matrix represents a fault. All the quantified diagnostic rules including '*IF*' parts and '*THEN*' parts are used as the diagnostic classifier. This relationship mapping is realized by the backpropagation (BP) network. The training samples of the BP network at fault severity level 2 and load level of 50 tons are shown in Table 7.8.

Table 7.8 Example of data set for BP network training (at severity level 2, 50 tons)

Input						Output							fault	
y1	y2	y3	y4	y5	y6									
7	18	10	1	19	2	1	0	0	0	0	0	0	z1	FWC
3	12	12	1	5	1	0	1	0	0	0	0	0	z2	CF
1	10	6	1	1	1	0	0	1	0	0	0	0	z3	RL
5	18	14	1	2	1	0	0	0	1	0	0	0	z4	RO
1	12	10	5	3	1	0	0	0	0	1	0	0	z5	FWE
21	26	23	1	4	1	0	0	0	0	0	1	0	z6	NC
1	11	8	1	2	14	0	0	0	0	0	0	1	z7	EO

7.6 Summary

The chapter presents a FDD scheme for centrifugal chillers. This scheme is implemented at the component level.

There are totally seven typical chiller faults considered in the chapter. They are the reduced condenser water flow, reduced evaporator water flow, refrigerant leakage, refrigerant overcharge, excess oil, condenser fouling, and non-condensables in refrigerant. There are a number of performance indices to characterize the health status of the chiller. To benchmark the fault-free status of the operating performance, the reference models of the PIs are established using the polynomial regression technique. For a particular fault, a group of deviations of PI benchmarks from the PI measurements constitute a traditional classifier. However, the traditional classifier is difficult to describe quantitative impact of the severity level on the performance indices and difficult to distinguish the two faults which have the same rule pattern.

A quantitative diagnostic classifier using the fuzzy algorithm is developed to quantify the traditional diagnostic classifier. The standardized quantitative performance indices (SQPs) are used to indicate how much the fault has an impact on the PIs. Although two faults may have the same qualitative rule pattern, they may have various quantitative impacts on the same PIs. The artificial neural network is used to identify the fault by matching the input and output. The backpropagation network with three layers is deployed to fulfill this task. The scheme implementation is dependant on the data at normal and faulty operating conditions at a range of load level and fault severity level.

The component-level FDD method developed for the chiller in this chapter is validated in Chapter 8.

CHAPTER 8 VALIDATION OF THE CHILLER FDD SCHEME

The component-level FDD scheme for chillers is validated using the laboratory data provided by the ASHRAE RP 1043. Validation of PI benchmark models and discussion on main influencing factors affecting the chiller FDD performance are also included.

Firstly, the validation of these PI models for benchmarking in term of coefficient of determination is presented in Section 8.1. Then the validation of the FDD scheme is presented in Section 8.2, where seven typical chiller faults at four severity levels are evaluated. Section 8.3 is the summery.

8.1 Validation of Chiller PI Benchmark Models

The regression models of these chiller performance indices were trained using the complete data set after eliminating the reduced data and validated using the reduced data both from the normal test and seven fault tests at four severity levels. The validation results are summarized in Table 8.1 in terms of coefficient of determination (R^2). Most of the regression models showed good fitting with high R^2. As validation results for the regression models are similar for all the seven faults at four severity levels, only the results of validation for the reduced condenser water flow test at severity level 1 using the reduced data are shown in Figure 8.1.

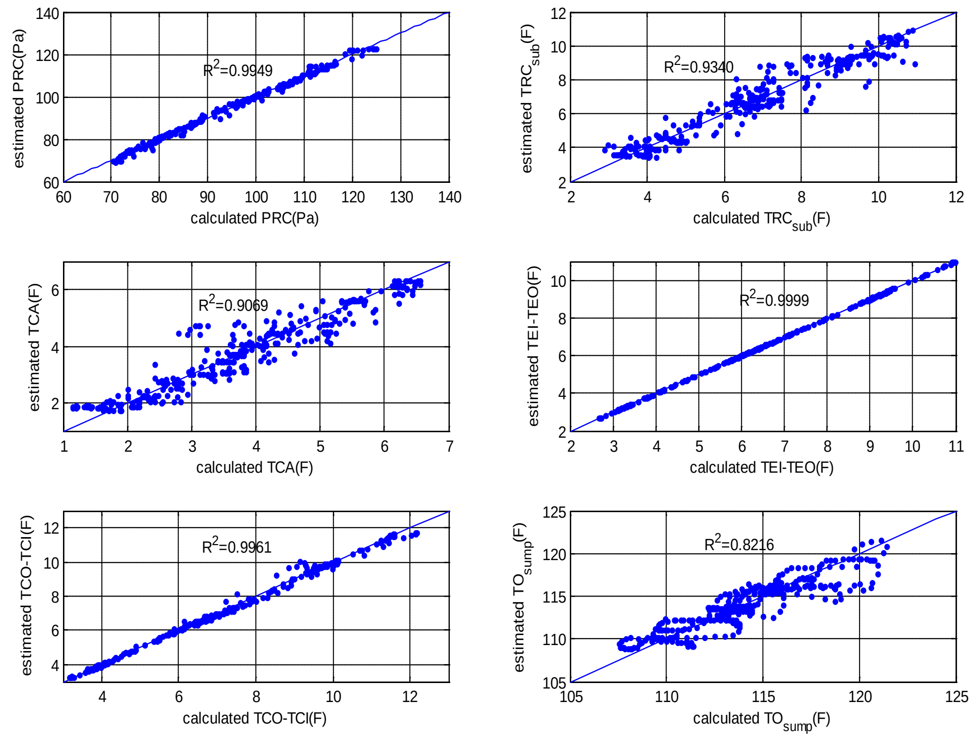

Figure 8.1 The estimated PIs vs the calculated PIs for the test with the reduced condenser water flow at severity level 1

Table 8.1 R^2 of PIs regressions of the normal test and fault tests at four severity levels

Test	severity level	P_{RC}	TRC_{sub}	TCA	T_{EI}-T_{EO}	T_{CO}-T_{CI}	TO_{sump}
Normal	-	0.9957	0.9204	0.8989	0.9999	0.9947	0.7530
Reduced condenser water flow	1	0.9949	0.9340	0.9069	0.9999	0.9961	0.8216
	2	0.9953	0.9425	0.8970	0.9999	0.9966	0.7772
	3	0.9940	0.9419	0.9150	0.9999	0.9967	0.7459
	4	0.9944	0.9418	0.9246	0.9999	0.9957	0.7300
Condenser fouling	1	0.9961	0.9306	0.9341	0.9999	0.9957	0.7322
	2	0.9942	0.8802	0.8720	0.9999	0.9960	0.7441
	3	0.9941	0.8873	0.9058	0.9999	0.9961	0.7620
	4	0.9937	0.8456	0.9069	0.9999	0.9962	0.7482
Refrigerant leakage	1	0.9950	0.9148	0.9274	0.9999	0.9957	0.7955
	2	0.9949	0.9078	0.8755	0.9999	0.9941	0.7958
	3	0.9957	0.8448	0.8437	0.9999	0.9951	0.7726
	4	0.9946	0.7605	0.7950	0.9999	0.9958	0.7493
Refrigerant overcharge	1	0.9946	0.9172	0.9073	0.9999	0.9957	0.7987
	2	0.9945	0.9338	0.9045	0.9999	0.9953	0.7828
	3	0.9934	0.9609	0.9430	0.9999	0.9931	0.7934
	4	0.9881	0.9437	0.9265	0.9999	0.9942	0.8237
Reduced evaporator water flow	1	0.9954	0.9239	0.8824	0.9999	0.9966	0.7633
	2	0.9972	0.9301	0.9225	0.9999	0.9969	0.7735
	3	0.9969	0.9274	0.9047	0.9999	0.9967	0.7459
	4	0.9953	0.9133	0.8841	0.9999	0.9972	0.7530
Non-condensables in refrigerant	1	0.9938	0.9237	0.9331	0.9999	0.9961	0.7829
	2	0.9926	0.8997	0.9020	0.9999	0.9945	0.7554
	3	0.9928	0.9113	0.9278	0.9999	0.9955	0.7750
	4	0.9947	0.8882	0.8977	0.9999	0.9913	0.9073
Excess oil	1	0.9928	0.9216	0.9106	0.9999	0.9956	0.7517
	2	0.9966	0.9409	0.9386	0.9999	0.9966	0.7582
	3	0.9966	0.9289	0.9530	0.9999	0.9958	0.7181
	4	0.9967	0.9168	0.9431	0.9999	0.9943	0.6668

8.2 Fault Diagnosis for Centrifugal Chillers

In the study, the diagnosis results were compared at the operating conditions in which supply chilled water temperature, condenser water entering temperature, and chiller cooling load are assumed to be 45F, 75F, the range of 30 to 90 tons with an interval of 10 tons. These conditions were chosen artificially since it covers the training data and validation data. The chosen conditions are the same as those in training process.

The fuzzy neural network was trained using the steady-state data at each load level of the normal test. The PI residual percentages of seven chiller faults from the regression models were fuzzified by the fuzzy network and parts of quantitative fuzzy rules composed of SQPs for fault diagnosis was formed as shown in Table 7.7. The main validation results of diagnosis for seven typical chiller faults were summarized in Table 8.2. The neuron number adopted in the hidden layer and the training method were 18 and resilient back propagation algorithm (Riedmiller and Braun, 1993) respectively. The SQP samples go through all the networks which have been trained using data of normal and fault tests. The fault corresponding to a network which has the least mean squared error (MSE) is isolated. The MSE of all samples is not more than 0.01. Diagnosis ratio 1 is the ratio of number of samples which are successfully diagnosed to the number (7 exactly) of samples at each severity level and seven load levels. The diagnosis ratio 1 includes the situations that although the fault severity level diagnosis failed, the final fault diagnosis is correct. It also can be deemed as a measure of how well a particular fault is diagnosed (over all load levels). Diagnosis ratio 2 is the diagnosis ratio 1 which has the successful fault diagnosis on severity level. It also can be deemed as a measure of how well a particular severity level of a particular fault is diagnosed (over all load levels). To find a complete set of rules which has the minimal number of PIs, the diagnosis results were compared using different numbers of PIs. 6 PIs contains all the PIs in the Table 7.5; 5 PIs do not contain P_{RC}. 4 PIs do not contain TRC_{sub} or T_{CA}. The diagnosis ratio 1 which is larger than 71.43% means two of the seven diagnosis output for a fault at a certain severity level failed. Although severity level diagnosis ratios (diagnosis ratio 2) for the chiller faults at some levels were lower, they did not impact the results much of fault category diagnosis (diagnosis ratio 1). Based on comparison in Table 8.2, the diagnosis ratios with 6 PIs are not improved compared with those using 5 PIs and 4 PIs for fault diagnosis of FWC, CF, RO, FWE and EO. Both diagnosis ratio 1 and 2 using the 4 PIs which has no TRC_{sub} are higher than those using other PIs. The ratios (diagnosis ratio 1) in the model validation are all 100% for all the faults diagnosis, and the diagnosis ratios 2 were improved further compared with those using other PIs. It may be due to the redundant information which affects the performance of ANN learning. And the random initial weights and biases in different tests may also contribute the uncertainty. From the comparison of diagnosis ratios of different faults, the excess oil with high diagnosis ratios is the easiest fault to be identified by using the proposed method.

Table 8.2 Comparison between diagnosis results using different number of PIs

<table>
<tr><th rowspan="2">Fault</th><th rowspan="2">severity level</th><th colspan="2">6 PIs</th><th colspan="2">5 PIs</th><th colspan="2">4 PIs (no TRC_{sub})</th><th colspan="2">4 PIs (no T_{CA})</th></tr>
<tr><th>diagnosis ratio 1 (%)</th><th>diagnosis ratio 2 (%)</th><th>diagnosis ratio 1 (%)</th><th>diagnosis ratio 2 (%)</th><th>diagnosis ratio 1 (%)</th><th>diagnosis ratio 2 (%)</th><th>diagnosis ratio 1 (%)</th><th>diagnosis ratio 2 (%)</th></tr>
<tr><td rowspan="4">Reduced condenser water flow</td><td>1</td><td>85.71</td><td>85.71</td><td rowspan="4">100</td><td>100</td><td rowspan="4">100</td><td>100</td><td rowspan="4">100</td><td>100</td></tr>
<tr><td>2</td><td rowspan="3">100</td><td>42.86</td><td>100</td><td>85.71</td><td>57.14</td></tr>
<tr><td>3</td><td>100</td><td>100</td><td>100</td><td>100</td></tr>
<tr><td>4</td><td>57.14</td><td>100</td><td>100</td><td>100</td></tr>
<tr><td rowspan="4">Condenser fouling</td><td>1</td><td rowspan="4">100</td><td>100</td><td rowspan="4">100</td><td>100</td><td rowspan="4">100</td><td>100</td><td rowspan="4">100</td><td>100</td></tr>
<tr><td>2</td><td>85.71</td><td>85.71</td><td>85.71</td><td>100</td></tr>
<tr><td>3</td><td>57.14</td><td>85.71</td><td>71.43</td><td>85.71</td></tr>
<tr><td>4</td><td>100</td><td>100</td><td>100</td><td>100</td></tr>
<tr><td rowspan="4">Refrigerant leakage</td><td>1</td><td rowspan="4">100</td><td>71.43</td><td rowspan="4">100</td><td>71.43</td><td rowspan="4">100</td><td>100</td><td>85.71</td><td>33.33</td></tr>
<tr><td>2</td><td>100</td><td>100</td><td>100</td><td>85.71</td><td>50</td></tr>
<tr><td>3</td><td>100</td><td>85.71</td><td>100</td><td rowspan="2">100</td><td>85.71</td></tr>
<tr><td>4</td><td>100</td><td>100</td><td>100</td><td>100</td></tr>
<tr><td rowspan="4">Refrigerant overcharge</td><td>1</td><td>85.71</td><td>28.57</td><td rowspan="4">100</td><td>28.57</td><td rowspan="4">100</td><td>85.71</td><td rowspan="4">100</td><td>14.29</td></tr>
<tr><td>2</td><td rowspan="3">100</td><td>71.43</td><td>85.71</td><td>85.71</td><td>71.43</td></tr>
<tr><td>3</td><td>100</td><td>85.71</td><td>100</td><td>100</td></tr>
<tr><td>4</td><td>100</td><td>100</td><td>100</td><td>100</td></tr>
<tr><td rowspan="4">Reduced evaporator water flow</td><td>1</td><td>85.71</td><td>85.71</td><td>85.71</td><td>85.71</td><td rowspan="4">100</td><td>85.71</td><td>85.71</td><td>100</td></tr>
<tr><td>2</td><td rowspan="3">100</td><td>100</td><td rowspan="3">100</td><td>14.29</td><td>42.86</td><td>71.43</td><td>100</td></tr>
<tr><td>3</td><td>100</td><td>100</td><td>100</td><td rowspan="2">100</td><td>85.71</td></tr>
<tr><td>4</td><td>100</td><td>100</td><td>100</td><td>100</td></tr>
<tr><td rowspan="4">Non-condensables in refrigerant</td><td>1</td><td rowspan="4">100</td><td>100</td><td rowspan="4">100</td><td>85.71</td><td rowspan="4">100</td><td>85.71</td><td rowspan="4">100</td><td>71.43</td></tr>
<tr><td>2</td><td>85.71</td><td>57.14</td><td>71.43</td><td>85.71</td></tr>
<tr><td>3</td><td>100</td><td>100</td><td>100</td><td>100</td></tr>
<tr><td>4</td><td>100</td><td>100</td><td>100</td><td>100</td></tr>
<tr><td rowspan="4">Excess oil</td><td>1</td><td rowspan="4">100</td><td>100</td><td rowspan="4">100</td><td>100</td><td rowspan="4">100</td><td>100</td><td rowspan="4">100</td><td>100</td></tr>
<tr><td>2</td><td>100</td><td>100</td><td>100</td><td>100</td></tr>
<tr><td>3</td><td>100</td><td>100</td><td>100</td><td>100</td></tr>
<tr><td>4</td><td>100</td><td>100</td><td>100</td><td>100</td></tr>
</table>

The results can also be affected by the number of neurons in the hidden layers and the training methods. Too few neurons can lead to underfitting in which the network fails to detect fully the signal in the training data set, whereas too many neurons can lead to overfitting, in which the network is so complex that it fits not only the signal but also the noise.

It is worth noticing several points. For different chiller systems, the working condition and range will be varied. This means centers and widths of the fuzzy set of the PI residual percentages will be varied. As the quantitative diagnostic classifier is determined by the centers and widths of the fuzzy set, it has to be rebuilt by selecting new membership functions for different chiller systems. The proposed approach was dependent on the normal (fault free) tests and fault tests at different fault severity. If only the data of limited test conditions can be obtained and/or the fault tests cannot run on the chillers due to practical limitation, a detailed physical chiller model is recommended to be developed for the use of simulating chiller faults at different load level and severity level, which can be calibrated using limited test data (see Wang et al. 2000). Some researchers developed the fault diagnosis method using fuzzy technique and ANN separately. However, the two techniques are utilized and combined in the scheme for chiller fault diagnosis in this article. Compared with the separate utilization of ANN and fuzzy models, the proposed method takes good advantage of these two AI techniques to fulfill different functions. The main purpose of fuzzy modeling utilization is to quantify the classical linguistic diagnostic classifier. This can make the classifier having the same rule patterns still valid for the fault identification. The purpose of using ANN is to establish the relationship between the input and output (fault isolation) because it is very effective in pattern reorganization practically.

8.3 Summary

The chapter presents the validation of the component-level FDD scheme for chillers by using the laboratory data. Seven typical chiller faults were considered in this scheme, i.e. reduced condenser water flow, reduced evaporator water flow, refrigerant leakage, refrigerant overcharge, excess oil, condenser fouling, and non-condensables in refrigerant. The performance of the chiller

FDD scheme is evaluated using diagnosis ratio 1 and diagnosis ratio 2. How to affect the results through the parameters of ANN and the fuzzy model is discussed. Recommendations on how to apply the scheme in other components are provided.

CHAPTER 9 IN-SITU IMPLEMENTATION OF THE BUILDING HVAC SYSTEM DIAGNOSIS STRATEGY

This chapter presents the in-situ implementation of the building system diagnosis strategy including three level diagnosis schemes. The software package of the building system diagnosis strategy is developed into a function module implemented in IBmanager. An introduction about how the diagnosis function module is integrated with other function modules for practical applications is briefed. The Intelligent Control and Diagnosis System for the commercial building named ICC working in the foreground of IBmanager is user-friendly to accomplish these functions.

Section 9.1 presents the introduction of IBmanager which is a customized and compatible platform integrating building automation systems and industrial automation systems. Section 9.2 presents the in-situ implementation of the diagnosis strategy in IBmanager. Section 9.3 presents main functions of the Intelligent Control and Diagnosis System for the commercial building ICC acting as an interface between the users and IBmanager. Section 9.4 is the summary.

9.1 IBmanager Introduction

An intelligent building systems integration and management system (IBmanager) is developed in the Research Center of Intelligent Building Control and Diagnosis, The Hong Kong Polytechnic University. It is a platform which integrates various building automation systems and industrial automation systems. The integration is supported by the middleware and web services technologies. IBmanager is composed of various sub-systems as described in Figure 9.1.

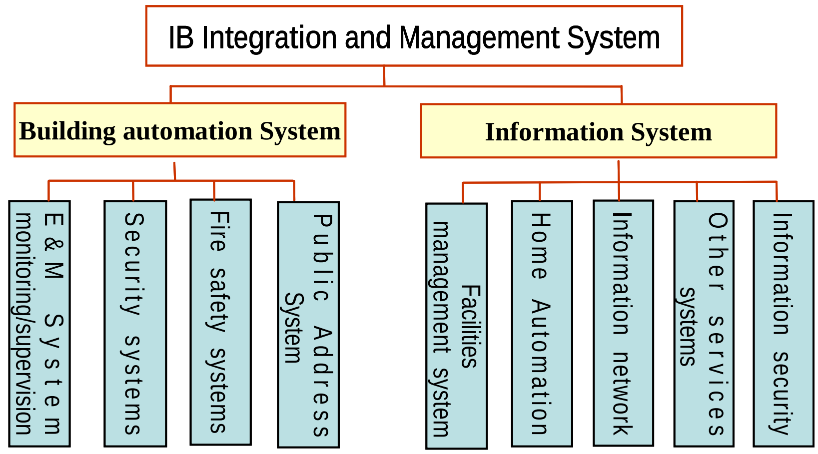

Figure 9.1 Structure of IBmanager

IBmanager is also a middleware platform which contains several components such as OLE for process control (OPC) servers, historical database, BMS function components, BMS human machine interface (HMI), web services server and building management web server. Various interfaces connection and functions blocks in IBmanager are shown in Figure 9.2. BMS function components executes the tasks of the six functions including the intelligent diagnosis module. This module is the main work of the thesis. BMS HMI realizes the building automation functions in the local area network (LAN). Web services server converts the COM/DCOM interfaces to web services interfaces. The user access interface is provided by the kits of active service pages (asp) and dynamic link library (.dll). They are the interface between the building management web server and web services server.

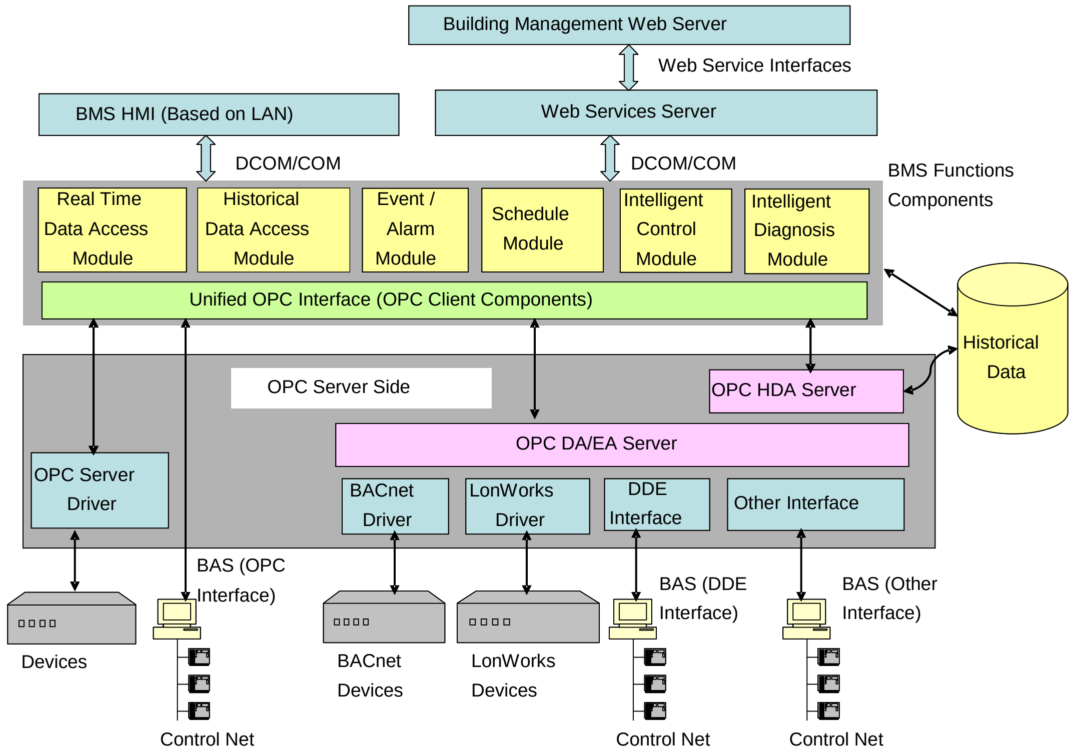

Figure 9.2 Function blocks of IBmanager

The main features and functions of IBmanager are listed below.

a. *Core technologies*: Windows distributed internet applications Architecture (DNA) and Web Services technologies. Client/server architecture and web application development based on windows DNA. Supervise and monitor the automation systems via Intranet or Internet based on web Services technologies

b. *Flexible three-tiers distributed architecture*: It is flexible network configuration, convenience in system updating and extension without interruption.

c. *User-friendly platform for customized applications development*: Simple and standard accessing different BA systems, fast Web-style data point definition and system configuration tools, rich professional controls and display interface library.

d. *Accommodating various protocols*: Support most popular protocols, such as BACnet、LonWorks、ProfiBus、OPC、web services, etc. Other protocols can get support conveniently also by adding relevant drivers.

e. *Rich high-end functions*: Provide on-line configuration of linkage action management, schedule management, user authority setting, alarm configuration, historical database configuration, real time monitoring, on-line building system performance evaluation and diagnosis and historical data log.

f. *Powerful integration capabilities*: Convenient in integrating with mainstream building automation systems, such as Honeywell, Johnson controls, Siemens, Trend; Fire security sub-systems such as Siemens, Simplex.

g. *Integration with Management Information System (MIS)*: Provides XML and ODBC interfaces for integration with MIS.

9.2 Implementation Architecture of the Software Package of the Building System Diagnosis Strategy

The software package of the building systems diagnosis strategy is developed in Matlab. The package consists three independent function blocks. They are the building-level diagnosis package, system-level FDD package for the HVAC systems and component-level FDD package for chillers. These programs are compiled in independent DLL modules for convenient use in IBmanager. They are supposed to be used in the real building systems in ICC briefed in Chapter 5.

The in-situ implementation architecture of the building system diagnosis software package for ICC is shown in Figure 9.3. The communication interface between the software package and the bottom control system is provided by the contractors. The software package is implemented as a function module of IBmanager. IBmanager is interfaced with the BMS via network automation engine (NAE). The data needed for the building-level diagnosis module includes total cooling load, indoor air temperature, etc. The data needed for the system-level FDD module includes evaporator inlet water temperature, condenser inlet water temperature, pump power consumption, etc. The data needed for the component-level FDD module includes refrigerant sub-cooling temperature, condensing pressure, oil temperature in sump, etc. The feedbacks of the software package to the BMS are diagnosis results, fault alarms, improvement recommendations, etc.

In Figure 9.3, automatic temperature control (ATC) system is used in ICC project. It plays the role of BMS in terms of main functions. IBmanager is also compatible with common BMS and bottom control systems.

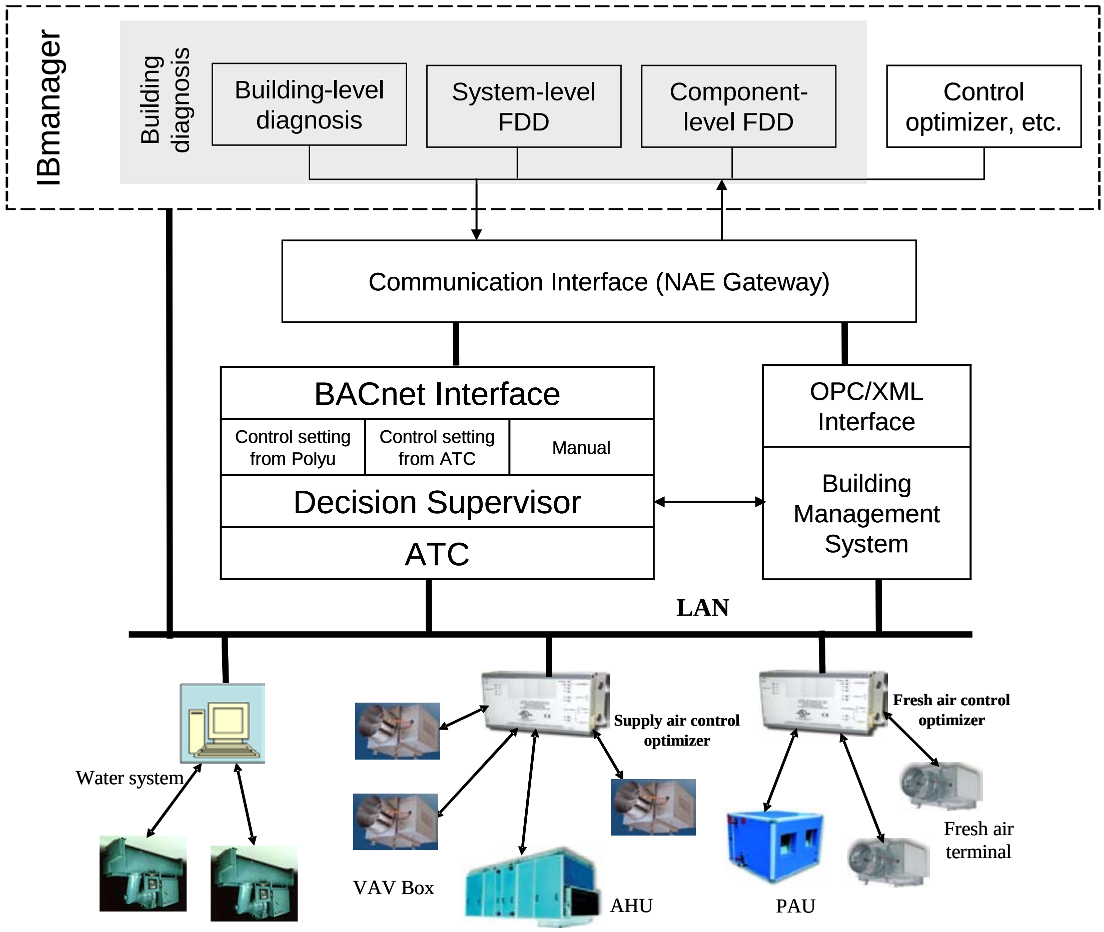

Figure 9.3 In-situ implementation architecture of the on-line building system diagnosis strategy

9.3 Overview of the Intelligent Control and Diagnosis System

Corresponding to IBmanager working in the background of the working station, foreground processing and interface are developed as shown in Figure 9.4 for ICC. The Intelligent Control and Diagnosis System for ICC consists of six functions modules, i.e. access management, history data storage, system setting, system configuration, system maintenance and real-time monitoring.

Access Management provides logging in using different authorities. *History Data Storage* is to record the monitoring data from BMS into the database in IBmanager. *System Setting* is to select the proper protocols to link various building automation systems. *System Configuration* is to configure the parameters decided by different control strategies. *System Maintenance* contains server log, event recording and authority control. *Real-time Monitoring* is to monitor the operating status of the systems and components on-line via a friendly human machine interface (HMI).

Figure 9.4 The cover page of the ICDS for ICC

Human machine interfaces (HMI) of various HVAC sub-systems are snapped as shown in Figure 9.5, 9.6 and 9.7 together with the monitoring data. The operation data displayed on the screen are convenient for building operators to monitor and evaluate the status of the components of concern. These operation data together with some operation data collected in the background are used as inputs of the system-level diagnosis package for HVAC systems. Figure 9.8 is the HMI of Chiller 1 for performance monitoring. These monitored operation data together with some operation data collected in the background are used as the inputs of the component-level FDD package for chillers.

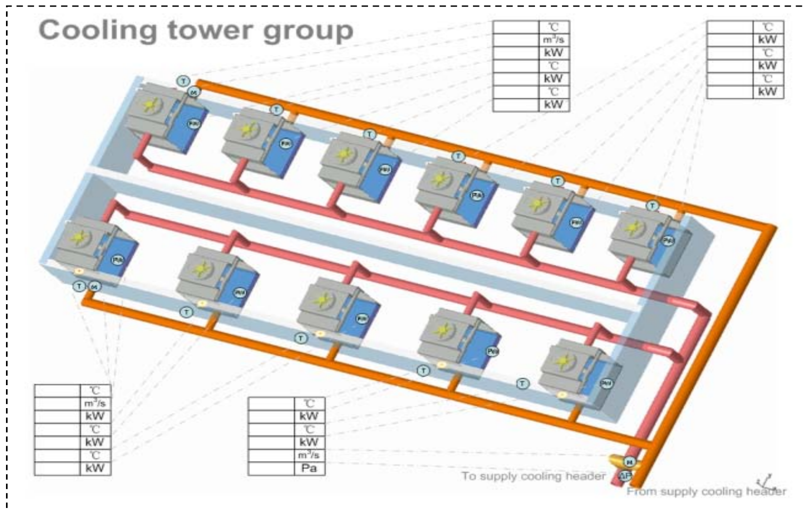

Figure 9.5 HMI of the operation of the cooling tower system

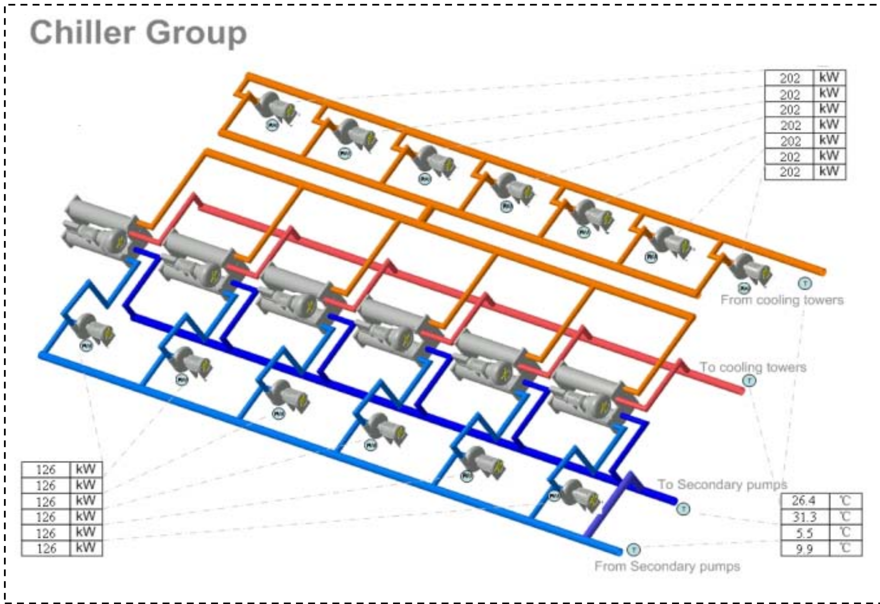

Figure 9.6 HMI of the operation of the chiller system

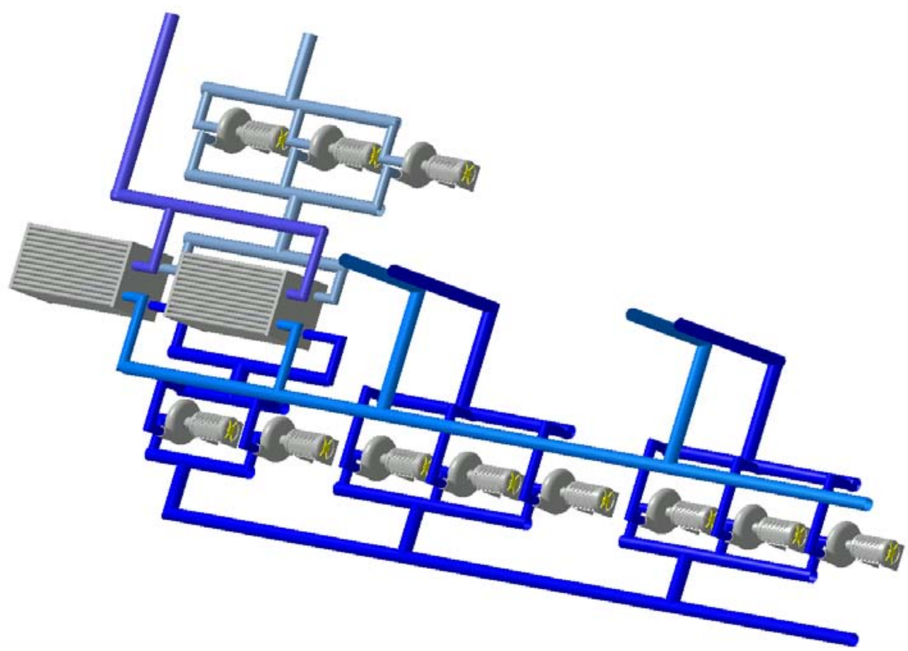

Figure 9.7 HMI of the operation of the heat exchanger system, SCHWP systems before and after heat exchangers

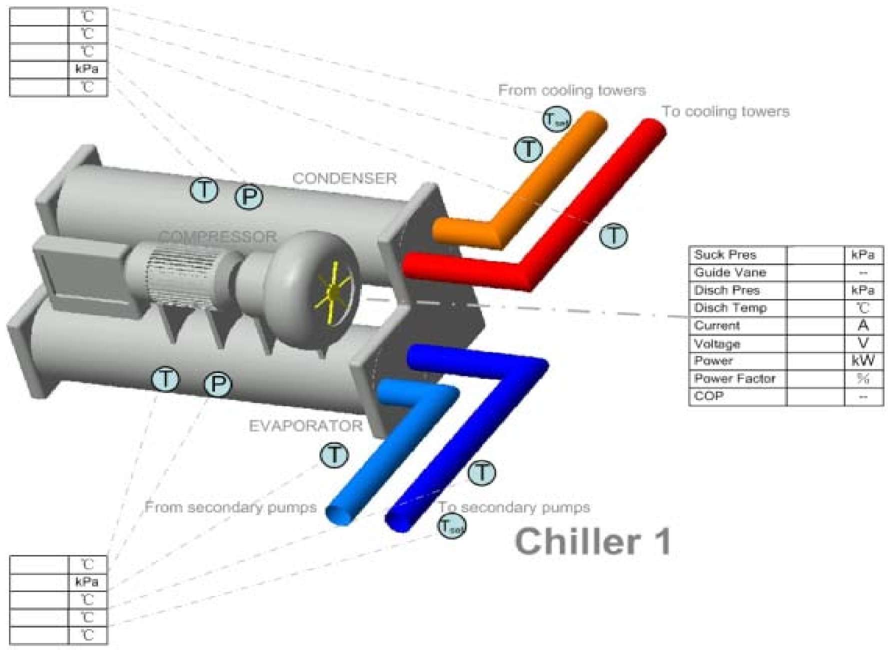

Figure 9.8 HMI of the operation of Chiller 1

9.4 Summary

The building system diagnosis strategy is packaged and implemented in-situ in IBmanager. This package as a module in IBmanager is to detect unhealthy conditions of building system and identify faults automatically. The building system diagnosis package is supposed to be a useful and powerful tool for building operators to improve the building system performance. The Intelligent Control and Diagnosis System working in the foreground and IBmanager working in the background for ICC are being tested and shaped simultaneously with the progress of the building construction.

CHAPTER 10 CONCLUSIONS AND RECOMMENDATIONS

A diagnosis strategy for building HVAC system is developed at three levels, i.e. building-level diagnosis based on building load estimation, system-level FDD for the HVAC systems, component level FDD for the chiller. This strategy may help in saving energy, prolonging equipment life and satisfying IAQ requirement. The contributions and recommendations are presented as follows.

<u>Summary on Main Contributions</u>

The main contributions of the thesis are listed as below.

i. A structure of the three-level building HVAC system diagnosis strategy is proposed. The software package of the building system diagnosis is developed and incorporated into the IBmanager as a function module. As the interface between the user and IBmanager, the Intelligent Control and Diagnosis System for ICC is being tested via the BMS in the ICC building. The software package loaded by the integrated intelligent building management system is being tested as well and is supposed to enhance the building system operating performance, prolong the equipment life and save the energy cost.

ii. The building-level diagnosis is implemented by comparing the actual cooling load measurement with load estimation. The building load estimation/forecast scheme adopts the thermal network model using thermal resistance and capacitance to represent the building envelope and internal mass. In the building load forecast scheme, the weather prediction modules are introduced into the thermal network model. One is outdoor air temperature and relative humidity prediction module based on the grey dynamic model. The other is the solar radiation prediction module based on cloud amount and maximum/minimum temperature forecast from the observatory.

iii. The system-level FDD for HVAC systems is developed to be effective in diagnosing the sensor faults and isolating the faulty sub-system. The sensor FDD&E based on the PCA method is implemented prior to the use of the system FDD. It is capable not only to identify the faulty sensor, but also to recover the sensor bias. Using the normal or corrected sensor measurements, the performance indices are more reliable to evaluate the health of various HVAC sub-systems.

iv. A novel FDD scheme at the component-level is developed for the chiller. It is competent to identify the typical chiller faults and even the faults which have the same rule pattern. For the latter situation, the traditional fault classifier based on the rule pattern of PI trends becomes weak and even incapable. The quantitative diagnostic classifier based on the fuzzy model quantifies the PI residuals so that the standardized quantitative PI (SQPs) can use the sensitive intervals to interpret the faults even if they have the same rule pattern of PI residuals. The artificial neural network is deployed to identify the particular fault by matching the SQPs with the faulty categories.

Summary on In-situ Implementation of the Building System Diagnosis Strategy

The building system diagnosis strategy is developed into a software package including three sub-modules corresponding to the three-level diagnosis methods. The software package is included in the IBmanager as a function module to fulfill the task of performance evaluation and fault diagnosis for the building systems. The IBmanager working in the background of the working station is highly compatible with various network protocols and building automation systems. The Intelligent Control and Diagnosis System for ICC working in the foreground of the working station provides the users with a user-friendly interface to realize the supervision and performance monitoring. The intelligent building management system is an effective platform for the building system diagnosis software package to provide the useful information from BMS and feedback the diagnosis results and recommendations to building operators automatically.

Conclusive Remarks on Building-level Diagnosis

The accurate building load estimation, as the performance benchmark, plays an important role in the building-level diagnosis scheme. It takes advantage of the basic thermal network model to represent the heat transfer through the building envelope and internal mass. The roof and exterior walls are representative of the three thermal resistances and two thermal capacitances (3R2C). The internal mass is representative of 2R2C. In the building load forecast scheme for optimal settings of HVAC control strategies, two weather prediction modules are introduced into the thermal network model for building load prediction. One is the outdoor air temperature/relative humidity prediction module based on the grey dynamic models. The other is the solar radiation prediction module based on the cloud amount and maximum/minimums temperature forecast from the observatory. The weather prediction modules and building load estimation/forecast model are validated using the field data. The building-level diagnosis based on the load prediction model is proved to be effective to detect the considerable performance degradation of the building systems.

Conclusive Remarks on System-level FDD for HVAC Systems

The system-level FDD for HVAC systems is to identify the faulty sub-system among various HVAC sub-systems, rather than the specific fault category of the system or the faulty component. The PCA-based sensor FDD&E is an effective method to diagnose the faulty sensor and recover the sensor bias prior to the use of system FDD module. The PCA matrix is established based on the heat balance and sensitivity to the bias. There are totally twelve sensor measurements selected as the variables in the PCA matrix. Five HVAC sub-systems are investigated, i.e. the cooling tower system, the chiller system, the secondary chilled water pump systems before and after HX, and the heat exchanger system. One or more PIs are selected to characterize the health status of each sub-system. The on-line adaptive threshold is used to judge whether the PI residuals deviate from the normal range. The sensitivity analysis of how the system fault affects the sensor FDD&E is conducted. It is proved that the sensor FDD&E scheme is still valid in most cases especially when the fault severity is high. The sensitivity analysis of how the corrected sensor measurements affect the system-level FDD scheme is conducted as well. It is proved that the system-level FDD for HVAC systems involving sensor faults is valid by using the simulation data.

Conclusive Remarks on Component-level FDD for the Chiller

As the chiller is a main power-consuming component in the HVAC system, it is very necessary to implement a FDD scheme for it. The component-level FDD scheme for the chiller is based on two artificial intelligent (AI) techniques, i.e. fuzzy algorithm and artificial neural network (ANN). Seven typical chiller faults at four severity levels are considered, i.e. reduced condenser water flow (by reducing water flow), condenser fouling (by plugging tubes in the condenser), refrigerant leakage (by charging less refrigerant), refrigerant overcharge (by charging more refrigerant), reduced evaporator water flow (by reducing water flow), non-condensables in refrigerant (by adding nitrogen into the refrigerant), and excess oil (by charging more oil). A number of PI residuals are selected to form a qualitative diagnostic classifier to indicate the health of the chiller performance. The PI residuals are quantified using the fuzzy model to form a quantitative diagnostic classier with elements named standardized quantitative PI (SQPs). The SQPs covering the full range of operating conditions are the intervals which are continuous along the operating conditions. The backpropagation network is used to identify the fault by mapping the SQPs and the fault categories. The FDD scheme for the chiller is validated using the laboratory data provided by the AHSRAE RP 1043.

Recommendations for Future Work

The thesis proposes a systematic building system diagnosis strategy of three levels, i.e. the building-level diagnosis based on the cooling load estimation, the system-level FDD for the HVAC systems and the component-level FDD for the chiller. Furthermore, the building load forecast scheme for optimal settings of HVAC system control strategies is also proposed. More efforts are needed to make the research work more applicable and desirable.

i. The software package of the building system diagnosis strategy is needed to be tested and shaped according to the practical situations to be more applicable and convenient for the building operators to use. The interface including auto-alarm, auto-report generating and auto-graph generating is needed to be included in the diagnosis strategy for the user-friendly purpose. Up to this time, the IBmanager and Intelligent Control and Diagnosis System for ICC working in the background and foreground respectively of the working station have started to be tested and retrieve the data from the in-situ BMS of the ICC building. Intensive efforts are still needed to commercialize the software package of the building system diagnosis strategy.

ii. In the structure of the building system diagnosis strategy, the three-level diagnosis methods are independent with each other. It is recommended to fuse the three-level methods using the logical connections such as expert rules. That is because the component-level fault may cause the system-level performance degradation, and the system-level fault may cause the building-level performance degradation. A hierarchical logic is needed to distinguish the level which the fault belongs to. The up-to-now strategy does not incorporate the diagnosis for non-HVAC systems, air-side HVAC systems and other components besides the chiller. To make the diagnosis strategy more comprehensive and powerful for improving the performance of the building systems, intensive efforts are needed to consider these systems and components. The recommendations are,

a. The building electricity consumption model is needed for the building-level diagnosis. This can consider the performance of HVAC systems as well as the non-HVAC systems such as lightings, appliances. Although the building load estimation method is satisfactory in terms of accuracy for the building-level diagnosis, the diagnosis validation is still needed on site for the real application.

b. A method is needed to predict the energy consumption of the non-HVAC systems for the system-level diagnosis. The non-HVAC system is usually schedule-fixed with a fixed profile of power consumption. Some mathematical models are competent for this task, such as the Fourier model and regression model.

c. Component-level FDD methods are needed to evaluate the performance and to identify the faults of other components besides the chiller. Although the proposed chiller FDD method is suitable for other components, efforts are still needed in investigating the corresponding typical faults and sensitive performance indices. For a component which can provide rich data at normal and faulty conditions within a wide range of operating conditions, the scheme can be used to diagnose the investigated faults occurring on the same type of component. For a component which cannot provide the extensive data for training, especially when two or more faults occur simultaneously, a detailed physical component model is recommended to be developed for the use of simulating chiller faults at different load level and severity level.

REFERENCES

Ahn, B.C., J.W. Mitchell and I.B. McIntosh. 2001. Model-based fault detection and diagnosis for cooling towers. *ASHRAE Transactions*, 107(1):839–846.

Barker, H.W. 1992. Solar radiative transfer through clouds possessing isotropic variable extinction coefficient. *Quarterly Journal-Royal Meteorological Society*, 118:1145-1162.

Braun, J.E. 1988. Methodologies for the design and control of central cooling plant, PhD thesis, University of Wisconsin, Madison.

Braun, J.E., and N. Chaturvedi. 2002. An inverse gray-box model for transient building load prediction. *HVAC&R*, 8(1):73-99.

Bristow, K.L., and G.S. Campbell. 1984. On the relationship between incoming solar radiation and daily maximum and minimum temperature. *Agric. Forest Meteorol*, 31:159-166.

Chen Y., X. Hao, G. Zhang, and S.W. Wang. 2006. Flow meter fault isolation in building central chilling systems using wavelet analysis. *Energy Conversion and Management*, 47(13-14):1700-1710.

Comstock, M.C., and J.E. Braun. 1999a. Development of Analysis Tools for the Evaluation of Fault Detection and Diagnostics in Chillers, ASHRAE Research Project 1043-RP. Report # HL 99-20. Purdue University, Ray W. Herrick Laboratories, West Lafayette, IN.

Comstock, M.C., and J.E. Braun. 1999b. Experimental data from fault detection and diagnostic studies on a centrifugal chiller, ASHRAE Research Project 1043-RP. Report # HL 99-18. Purdue University, Ray W. Herrick Laboratories.

Comstock, M.C., J.E. Braun, and E.A. Groll. 2001. The sensitivity of chiller performance to common faults. *HVAC&R*, 7(3):263-279.

Crawley, D., L.K. Lawrie,.C.O. Pedersen, and F.C. Winkelmann. 2000. EnergyPlus: Energy simulation program. *ASHRAE Journal*, 42(4):49-56.

Cui, J.T., and S.W. Wang. 2005. A model-based online fault detection and diagnosis strategy for centrifugal chiller systems. *International Journal of Thermal Science*, 44:986-999.

Davies, J.A., and D.C. McKay. 1988. Estimating radiation from incomplete cloud data. *Solar Energy*, 41:15-18.

Deng, J.L. 1989. Introduction to grey system theory. *The Journal of Grey System*, 1(1):1-24.

Dexter, A.L., and D. Ngo. 2001. Fault diagnosis in air-conditioning systems: a multi-step fuzzy model-based approach. *HVAC&R*, 7(1):83-102.

Dhar, A., T.A. Reddy, and D.E. Claridge. 1999a. Generalization of the Fourier series approach to model hourly energy use in commercial buildings. *Journal of Solar Energy Engineering*, 121 (1):54-62.

Dhar, A., T.A. Reddy, and D.E. Claridge. 1999b. A Fourier series model to predict hourly heating and cooling energy use in commercial buildings with outdoor temperature as the only weather variable. *Journal of Solar Energy Engineering*, 121:47-53.

DOE. 2007. 2007 buildings energy data book. Office of Energy Efficiency and Renewable Energy, U.S. Department of Energy.

Ed Kidd et al. 2001. DOE-2 Program Documentation, Energy Science & Technology Software Center, Oak Ridge, http://gundog.lbl.gov/dirsoft/d2getdoc.html

Jackson, J.E. 1991. A user’s guide to principal components. New York: John Wiley & Sons

Jackson, J.E., and G.S. Mudholkar. 1979. Control Procedures for Residual Associated with Principal Component Analysis. *Technometrics*, 21(3):341-349

Ehnberg, J.S.G., and M.H.J. Bollen. 2005. Simulation of global solar radiation based on cloud observations. *Solar Energy*, 78:157-162.

EMSD. 2005. Hong Kong energy end-use data. The Energy Efficiency Office, Electrical & Mechanical Services Department, Hong Kong.

EMSD. 2007. Hong Kong energy end-use data. The Energy Efficiency Office, Electrical & Mechanical Services Department, Hong Kong.

Forrester, J.R., and W.J. Wepfer. 1984. Formulation of a load-prediction algorithm for a large commercial-building. *ASHRAE Transactions*, 90(2):536–551.

Gertler, J.J. 1998. Fault detection and diagnosis in engineering systems, Marcel Dekker, Inc.

Giebler, T., M. Liu, and D. Claridge. 1998. Evaluation of energy conversion measures by model simulation. The eleventh symposium on improving building systems in hot and humid climates proceedings, June 1-2, Fort Worth, Texes.

Gordon, J.M., and K.C. Ng. 1995. Predictive and diagnostic aspects of a universal thermodynamic model for chillers. *International Journal of Heat and Mass Transfer,* 38(5):807-18.

Grimmelius, H.T., J.K. Woud, and G. Been. 1995. On-line failure diagnosis for compression refrigerant plants. *International Journal of Refrigeration*, 18(1):31-41.

Hargreaves, G.L., G.H. Hargreaves, and P. Riley. 1985. Irrigation water requirement for the Senegal River Basin. *Journal of Irrigation and Drainage Engineering ASCE*, 111:417-421.

Hashimoto, M., H. Kawashima, T. Nakagami, and F. Oba. 2001. Sensor fault detection and identification in dead-reckoning system of mobile robot: interacting multiple model approach. *Intelligent Robots and System*, 3:1321-1326.

HK-BEAM. 2003. An environmental assessment for new building developments, HK-BEAM, Version 2003, HK-BEAM Society, Kowloon, Hong Kong.

Hou, Z., Z. Lian, Y. Yao, and X. Yuan. 2006. Data mining based sensor fault diagnosis and validation for building air conditioning system. *Energy Conversion and Management*, 47 (15-16):2479-2490.

House, J.M., and G.E. Kelly. 1999. An overview of building diagnostics. Diagnostics for Commercial Buildings: Research to Practice, Organized by Pacific Energy Center, San Francisco, CA.

Hsu, L.C. 2003. Applying the Grey prediction model to the global integrated circuit industry. *Technological Forecasting and Social Change*, 70 (6):563-574.

Inatsu, H., H. Matsuo, K. Fujiwara, K. Yamada, and K. Nishizawa. 1992. Development of Refrigerant Monitoring Systems for Automotive Air-Conditioning Systems. *SAE Transactions*, 101(6):165-175.

Jia, Y., and T.A. Reddy. 2003. Characteristic physical parameter approach to modeling chillers suitable for fault detection, diagnosis and evaluation. *ASME Journal of Solar Energy Eng*., 125: 258-265.

Jiang, Y., Y. Yao., S. Deng., and Z. Ma. 2004. Applying grey forecasting to predicting the operating energy performance of air cooled water chillers. *International Journal of Refrigeration*, 27(4):385–392.

Jolliffe, I.T. 2002. Principal Component Analysis, 2nd Edition, Springer, New York.

Katipamula, S. and M.R. Brambley. 2005a. Methods for fault detection, diagnostics and prognostics for building systems- A review, Part I. *HVAC&R Research*, 11 (1):3-25.

Katipamula, S. and M.R. Brambley. 2005b. Methods for fault detection, diagnostics and prognostics for building systems- A review, Part II. *HVAC&R Research*, 12 (2):169-187.

Kawashima, M., C.E. Dorgan, and J.W. Mitchell. 1995. Hourly thermal load prediction for the next 24 hours by ARIMA, EWMA, LR, and an artificial neural network. *ASHRAE Transactions*, 101(1):186-200.

Klein, S.A., P.J. Hughes, and W.A. Beckman et al. 1990. TRNSYS – A Transient Simulation Program, User Manual Version 13.1. Madison: Engineering Experimentation Station, University of Wisconsin.

Khan, J.U.R., and S.M. Zubair. 2004. A study of fouling and its effects on the performance of counter flow wet cooling towers. *Proceedings of the Institution of Mechanical Engineers Part E Journal of Process Mechanical Engineering*, 218(1):43-51.

Kresta, J., J.F. MacGregor, and T.E. Marlin. 1991. Multivariable Statistical Monitoring Of Process Operating Performance. *Can. J. Chem. Eng*, 69(1):35-47.

Lee, W.Y., C. Park, and G.E. Kelly. 1996a. Fault detection of an air-handling unit using residual and recursive parameter identification methods. *ASHRAE Transactions*, 102(1):528-539.

Lee, W.Y., J.M. House, C. Park, and G.E. Kelly. 1996b. Fault diagnosis of an air-handling uni using artificial neural networks. *ASHRAE Transactions*, 102(1):540-549.

Lee, W.Y., J.M. House and D.R. Shin. 1997. Fault diagnosis and temperature sensor recovery for an air-handling unit. *ASHRAE Transactions*, 103(1):621–633.

Lee, W.Y., J.M. House and N.H. Kyong. 2004. Subsystem level fault diagnosis of a building's air-handling unit using general regression neural networks. *Applied Energy*, 77(2):153-170.

Li, H., and J.E. Braun. 2007. A methodology for diagnosing multiple simultaneous faults in vapor-compression air conditioners. *International Journal of Heating, Ventilating, Air Conditioning and Refrigerating Research*, 13(2):369-395.

Liu, M, D. Claridge, and L. Song. 2002. Draft report-potential of on-line simulation for fault detection and diagnosis in large commercial buildings with built-up HVAC systems, submitted to California Energy Commission. June, 2002.

Luo, R., M. Misra, D.M. Himmelblau. 1999. Sensor Fault Detection via Multiscale Analysis and

Dynamic PCA. *Ind. Eng. Chem. Res*., 38(4):1489–1495.

Ma, Z.J. 2008. Online supervisory and optimal control of complex building central chilling system, PhD thesis, The Hong Kong Polytechnic University, Hong Kong.

Ma, Z.J., S.W. Wang, X.H. Xu, and F. Xiao. 2008. A supervisory control strategy for building cooling water systems for practical and real time applications. *Energy Conversion and Management*, 49(8):2324-2336.

MacArthur, J.W., A. Mathur, and J. Zhao. 1989. On-line recursive estimation for load profile prediction. *ASHRAE Transactions*, 95(1):621-628.

Martens, H., and T. Naes. 1989. Multivariate calibration. New York: John Wiley & Sons

McIntosh, I.B.D. 1999. A Model-Based Fault Detection and Diagnosis Methodology for HVAC Subsystems. Ph.D. Thesis, University of Wisconsin, Madison.

McIntosh, I.B.D., J.W. Mitchell, and A. Beckman. 2000. Fault detection and diagnosis in chillers part I: Model development and application. *ASHRAE Transactions*, 106(2):268–282.

Mehranbod, N., M. Soroush, and C. Panjapornpon. 2005. A method of sensor fault detection and identification. *Journal of Process Control*, 15(3):321-339.

Mehranbod, N., M. Soroush, M. Piovoso, and B.A. Ogunnaike. 2003. Probabilistic model for sensor fault detection and identification. *AIChE Journal*, 49(7):1787-1802.

Mohandes, M. 2002. Support vector machines for short term electrical load forecasting. *International Journal of Energy Research*, 26(4):335-346.

Morita, H., T. Kase, Y. Tamura, and S. Iwamoto. 1996. Interval prediction of annual maximum demand using grey dynamic model. *International Journal of Electrical Power & Energy Systems*, 18(7):409-413.

Ngo, D., and A.L. Dexter. 1999. A robust model-based approach to diagnosing faults in air-handling units. *ASHRAE Transactions*, 105(2): 1078-1086.

Norford, L.K., J.A. Wright, R.A. Buswell, D. Luo, C.J. Klaasen, and A. Suby. 2002. Demonstration of fault detection and diagnosis methods for air-handling units (ASHRAE 1020-RP). *International Journal of Heating, Ventilating, Air Conditioning and Refrigerating Research*, 8(1):41-71.

NTIS. 1986. HVACSIM+ Building Systems and Equipment Simulation Program Reference

Manual. Washington, DC: National Technical Information Services, U.S. Department of Commerce 1986.

Peitsman, H.C., and V. Bakker. 1996. Application of black-box models to HVAC systems for fault detection. *ASHRAE Transactions*, 102(1):628-640.

Persin, S., and B. Tovornic. 2005. Real-time implementation of fault diagnosis to a heat exchanger. *Control Engineering Practice*, 13(8):1061-1069.

Prescott, J.A. 1940. Evaporation from a water surface in relation to solar radiation. Trans. R. Soc. Austr. 64:114-118.

Qin, J.Y., and S.W. Wang. 2005. A fault detection and diagnosis strategy of VAV air-conditioning systems for improved energy and control performances. *Energy and Buildings*, 37(10):1035-1048.

Reddy, T.A. 2007. Application of a generic evaluation methodology to assess four different chiller FDD methods (RP-1275). *HVAC&R Research*, 13(5):711-729.

Riedmiller, M., and H. Braun. 1993. A direct adaptive method for faster backpropagation learning: The rprop algorithm, Proc. IEEE Int. Conf. Neural Networks San Francisco, CA, Apr, 586-591.

Rossi, T.M., and J.E. Braun. 1997. A statistical, rule-based fault detection and diagnostic method for vapor compression air conditioners. *International Journal of Heating, Ventilating, Air Conditioning and Refrigerating Research*, 3(1):19-37.

Roumeliotis, S.I., G.S. Sukhatme, and G.A. Bekey. 1998. Sensor fault detection and identification in a mobile robot. *Intelligent Robots and Systems*, 3:1383-1388.

Schein, J., and S.T. Bushby. 2006. A hierarchical rule-based fault detection and diagnostic method for HVAC systems. *HVAC&R Research*, 12(1):111-126.

Seem, J.E., and J.E. Braun. 1991. Adaptive methods for real-time forecasting of building electrical demand. *ASHRAE Transactions*, 97(1): 710-721.

Stylianou, M. 1997. Classification functions to chiller fault detection and diagnosis. *ASHRAE Transactions* 103(1):645-648.

Stylianou, M., and D. Nikanpour. 1996. Performance monitoring, fault detection and diagnosis of reciprocating chillers. *ASHRAE Transactions*, 102(1):615-627.

Supit, I and R.R. Van Kappel. 1998. A simple method to estimate global radiation. *Solar Energy*, 63(3): 147-160.

Thornton, P.E., and S.W. Running. 1999. An improved algorithm for estimating incident daily solar radiation from measurements of temperature, humidity, and precipitation. *Agricultural and Forest Meteorology*, 93(4):211-228.

Upadhyayaa, B.R., and E. Eryurekb. 2006. Degradation monitoring of industrial heat exchangers. Proceedings of the 1st World Congress on Engineering Asset Management (WCEAM), 504-215.

Wang, S.W., J.B. Wang, and J. Burnett. 2000. A mechanistic model of centrifugal chillers for HVAC system dynamic simulation. *Building Services Engineering Research and Technology*, 21(2):73-83.

Wang, S.W., and J.Y. Qin. 2005. Sensor fault detection and validation of VAV terminals in air-conditioning systems. *Energy Conversion and Management* 46(15-16):2482–2500.

Wang, X.M., Z.K. Chen, C.G. Yang, and Y.M. Chen. 1999. Gray predicting theory and application of energy consumption of building heat-moisture system. *Building and Environment*, 34(4):417-420.

Wang, S.W., and X.H. Xu. 2006. Simplified building model for transient thermal performance estimation using GA-based parameter identification. *International Journal of Thermal Sciences*, 45(4):419-432.

Wang, S.W. 1998. Dynamic simulation of a building central chilling system and evaluation of EMCS on-line control strategies. *Building and Environment*, 33(1):1-20.

Wang, S.W., and F. Xiao. 2004. AHU sensor fault diagnosis using principal-component analysis method. *Energy and Buildings*, 36(2):147–160.

Wang, S.W., and J.B. Wang. 1999. Law-based sensor fault diagnosis and validation for building air-conditioning systems. *HVAC&R Research*, 5(4):353-378.

Wang, S.W., and J.B. Wang. 2002a. Automatic Sensor Evaluation in BMS Commissioning of Building Refrigeration Systems. *Automation in Construction*, 11(1):59-73.

Wang, S.W., and J.B. Wang. 2002b. Robust Sensor Fault Diagnosis and Validation in HVAC Systems. *Transactions of the Institute of Measurement and Control*, 24(3):231-262.

Wang, S.W., and J.T. Cui. 2005. Sensor fault detection, diagnosis and estimation for centrifugal chiller systems using principal-component analysis method. *Applied Energy*, 82(3):197-213.

Wang, S.W., and J.T. Cui. 2006. A robust fault detection and diagnosis strategy for centrifugal chillers, *HVAC&R Research*, 12(3):407-428.

Weyer, E., G. Szederkenyi, and K. Hangos. 2000. Grey box fault detection of heat exchangers. *Control Engineering Practice*, 8(2):121-131.

Wise, B.M., N.L. Ricker, D.J. Velkamp, and B.R. Kowalski. 1990. A theoretical basis for the used of principal component models for monitoring multivariate processes. *Process Control and Quality*, 1(1):41-51

Xiao, F., S.W. Wang, X.H. Xu, and G.M. Ge. 2008. An isolation enhanced PCA method with expert-based multivariate decoupling for sensor FDD in air-conditioning systems. *Applied Thermal Engineering*, 29(4):712-722.

Xu, X.H. 2005. Model-based building performance evaluation and diagnosis, PhD thesis, The Hong Kong Polytechnic University, Hong Kong.

Xu, X.H., F. Xiao, and S.W. Wang. 2007. Enhanced chiller sensor fault detection, diagnosis and estimation using wavelet analysis and principal component analysis methods. *Applied Thermal Engineering*, 28(2-3):226-237.

Yoshida, H., and S. Kumar. 1999. ARX and AFMM model-based on-line real-time data base diagnosis of sudden fault in AHU of VAV system. *Energy Conversion & Management*, 40(11):1191-1206.

Yoshimura, M., and N. Ito. 1989. Effective diagnosis methods for air-conditioning equipment in telecommunications buildings. INTELEC 89: The Eleventh International Telecommunications Energy Conference, October 15–18, 1989, Centro dei, Firenze, 21:1-7.

Yu, D.L., J.B. Gomm, and D. Williams. 1999. Sensor fault diagnosis in a chemical process via RBF neural networks. *Control Engineering Practice*, 7(1):49-55.

Zadeh, L.A. 1965. Fuzzy sets. *Information and Control*, 8 (3) 338-353.